2D indoor localization system with an UWB multistatic radar

Nour Awarkeh

To cite this version:

Nour Awarkeh. 2D indoor localization system with an UWB multistatic radar. Electromagnetism. Université Paris Saclay (COmUE), 2019. English. NNT : 2019SACLT041 . tel-02505477

HAL Id: tel-02505477
https://theses.hal.science/tel-02505477v1

Submitted on 11 Mar 2020

université
PARIS-SACLAY

TELECOM
ParisTech

NNT: 2019SACLT041

2D Indoor Localization System with an UWB Multistatic Radar

Thèse de doctorat de l'Université Paris-Saclay
préparée à Télécom ParisTech

École doctorale n° 580 "Sciences et Technologies de l'Information et de la Communication" (STIC)
Spécialité de doctorat: Réseaux, Information et Communications

Thèse présentée et soutenue à Paris, le 30 Octobre 2019, par

Nour AWARKEH

Composition du jury:

Genevieve BAUDOIN
Professeur, ESIEE Paris — Présidente
Julien SARRAZIN
Maître de Conférences (HDR), Sorbonne Université — Rapporteur
Davy GAILLOT
Maître de Conférences (HDR), Université de Lille — Rapporteur
Elizabeth COLIN
Enseignante-Chercheuse, EFREI Paris — Examinatrice
Alain SIBILLE
Professeur, Télécom Paris — Examinateur
Nel SAMAMA
Professeur, Télécom SudParis — Directeur de thèse
Jean-christophe COUSIN
Maître de Conférences, Télécom Paris — Encadrant de thèse
Muriel MULLER
Maître de Conférences, Télécom SudParis — Encadrante de thèse

Thèse de doctorat

Acknowledgments

I would like to express my full appreciation to the people who helped, encouraged and supported me throughout my thesis. A big apology to those I will forget, but I will still try to do my best.

Firstly, I would like to express my deep gratitude to Professor Nel SAMAMA, Dr. Jean-Christophe COUSIN and Dr. Muriel MULLER, my research supervisors, for the continuous support of my Ph.D study, for their patience, enthusiastic encouragement and vast knowledge. Their advice helped me throughout the research and writing of this thesis.

I would like to thank the members of my thesis committee, starting with M. Julien SARRAZIN, associate professor at Sorbonne University and M. Davy GAILLOT, associate professor at the University of Lille, for the precious time they have given me by agreeing to be *rapporteurs* for this thesis. Their careful and meticulous reviews were a great help to me and I am very grateful to them. I would also like to thank M. Genevieve BAUDOIN, full professor at ESIEE Paris, Mme Elizabeth COLIN, associate professor at EFREI Paris and M. Alain SIBILLE, full professeur at Télécom Paris, for having agreed to examine this thesis. In general, I sincerely thank all the members of the jury for their feedback both on the manuscript and on my defense, which impressed me a lot.

Many thanks to my friends and colleagues for all the good times together.

Last but not least, I would like to thank my family who have supported me spiritually all along the writing of this thesis and my life as a whole.

Abstract

Nowadays, the ability to track objects and people is crucial for a huge number of applications, such as medical applications (monitoring of patients) or independent applications that require a very high accuracy and resolution in the positioning process.

Therefore, the main scientific objective of this thesis is to develop a tracking system using an Ultra Wide Band (UWB) multistatic radar system to provide real-time 2D location of transponders or active tags. The localization is carried out in polar coordinates (distance and azimuth angle) by merging the interferometry and goniometry principles, assuming a propagation channel with a direct path, or Line of Sight (LoS) between the station and the target. The designed Indoor Localization System (ILS) incorporates a hybrid technique by combining the duplex UWB and the Phase Correlation methods for the radial-distance and the azimuth angle estimates.

The proposed ILS consists of two main components, a transmitter /receiver (transceiver) station serving as a Localization Base Station (LBS) and an Active Tag (AT). The LBS has one transmitting channel and two identical and independent receiving channels. The localization is performed by sending UWB pulses towards the AT which acts as an active transponder and retransmits in turn the received signal back to the LBS upon delaying it.

This designed ILS is expected to offer, under LoS conditions, a position estimation with high accuracy and resolution while maintaining low system complexity. The system works with a single anchor, and simultaneously addresses indoor challenges such as multipaths, strong signal attenuations, reflections, etc.

Contents

List of Acronyms and Abbreviations

ADC Analog-to-Digital Converter

AP Access Point

API Application Program Interface

AoA Angle of Arrival

AR Axial Ratio

AT Active Tag

BLE Bluetooth Low Energy

BP Break-Point

BPF Band-Pass Filter

CDMA Code Division Multiple Access

CIR Channel Impulse Response

CMOS Complementary Metal Oxide Semiconductor

CPU Central Processing Unit

CRLB Cramer-Rao lower bound

CSS Chirp Spread Spectrum

CST Computer Simulation Technology

CW Continuous Wave

DC Direct Current

DFP Davidon Fletcher-Powell

DIP Dual In-Line Package

DME Distance Measuring Equipment

DoA Direction of Arrival

DoP Dilution of Precision

ECC Electronic Communications Committee

ED Energy Detection

EIRP Effective Isotropic Radiated Power

FCC Federal Communications Commission

FH Frequency Hopping

FMCW Frequency Modulated Continuous Wave

GPR Ground Penetration Radar

GPS Global Positioning System

ID Identification

IL Insertion Loss

ILS Indoor Localization System

IP Internet Protocol

IPS Indoor Positioning System

IR Infrared

IR-UWB Impulse Radio - UWB

ISM Industrial, Scientific and Medical

LAN Local Area Network

LBM Location-Based Marketing

LBS Localization Base Station

LEDs Light Emitting Diodes

LHCP Left Hand Circular Polarization

LNA Low Noise Amplifier

LO Local Oscillator

LPR Local Position Radar

LoS Line of Sight

MES Maximum Energy Selection

MES-SB Maximum Energy Selection with Search-Back

MESS Maximum Energy Sum Selection

MF Matching Filtering

ML Maximum Likelihood

MM Method of Moments

MU Mobile User

NFA Near Field Approximation

NIC Network Interface Card

NLoS Non Line of Sight

PC Phase Correlation

PCB Printed Circuit Board

PCs Personal Computers

PDAs Personal Digital Assistants

PDF Probability Density Function

PDP Power Delay Profile

PHY Physical

PSDs Power Spectral Densities

PWC Plane Wave Condition

RF Radio Frequency

RFID Radio Frequency Identification

RHCP Right Hand Circular Polarization

RL Return Loss

RMSE Root Mean Square Error

RSS Received Signal Strength

RToF Round Time of Flight

SDK Software Development Kit

SMA SubMiniature version A

SNR Signal-to-Nosie Ratio

SR Stored-Reference

SRD Step Recovery Diode

SV Saleh-Valenzuela

TC Threshold Comparison

TDC Time to Digital Converter

TDoA Time Difference of Arrival

TDSC Time Delayed Sampling and Correlation

TH Time Hopping

ToA Time of Arrival

ToF Time of Flight

TR Transmitted-Reference

TR-UWB Transmitted Reference UWB

TWR Two-Way Ranging

U.S. United States

USB Universal Serial Bus

UWB Ultra Wide Band

VAT Value-Added Tax

VCO Voltage-Controlled Oscillator

VNA Vector Network Analyzer

WiFi Wireless Fidelity

WLAN Wireless Local Area Network

WPANs Wireless Personal Networks

Introduction

Indoor positioning is defined as the process of locating people or objects within a closed infrastructure, such as an airport, hospital or any other type of building. The applications and services offered by indoor localization are diverse and their number keeps growing. Among the various fields, we can mention industrial surveillance and control, security, information services, health services, etc. For instance, it plays a significant role in medical applications to follow patients, small children and elderly people. This location-based application and countless others have therefore become very relevant and contribute significantly to our daily lives.

However, this proliferation of position-based applications is accompanied by an increasing demand for accurate, robust and high-resolution indoor positioning systems. Despite the fact that Global Positioning System (GPS) offer high coverage with an accuracy of a few meters outdoors, their applicability is considerably limited indoors due to their low signal reception power. For this reason, the research of alternative solutions for internal positioning has attracted enormous attention in recent years. Designing such a system is challenging and should consider an appropriate balance between complexity and performance.

To this end, various technologies (infrared, ultrasound, Wireless Fidelity (WiFi), Bluetooth, etc.) have been proposed to develop a low-cost, accurate and robust Indoor Localization System (ILS). Nevertheless, most of these technologies can be severely affected by multipath propagation as a result of the narrow bandwidth, which reduces the accuracy of the overall ILS. Hence, a rising interest in Ultra Wide Band (UWB)-based ILS is emerging due to its high bandwidth allowing accurate localization with high resolution. Traditional UWB ILSs are based on the constellation principle [1]. This approach is strictly related to the measurement of the distance between the object to be located and a certain number of anchors fixed at known positions (3 anchors for a 2D localization and 4 anchors for a 3D localization), followed by the application of the trilateration technique. These systems have the drawback of prior knowledge of at least three anchors that must be synchronized with each other. To overcome this problem, another state-of-the-art ILS using a Frequency Modulated Continuous Wave (FMCW) signal is proposed in [2] with a single anchor and four interrogators to locate a target in 3D, by combining distance and angle measurements.

Although this system has performed well, it is important to point out that an FMCW radar requires additional signal to carry out the localization since this type of signal is not implemented in current communication systems. In addition, it has some difficulties in managing the Voltage-Controlled Oscillator (VCO), which requires the frequency variation to be as linear as possible. Finally, it can be severely affected by multipath propagation, which in turn reduces the accuracy of the system.

At this stage, UWB technology seems to be the most promising solution to address these limitations and meet the requirements of future applications. It is already deployed in existing communication systems and has many features including large bandwidth, immunity to interference, high ability to dissociate multiple target responses directly in the time domain and robustness to perturbations.

Therefore, the main objective of this thesis is to design and implement a novel ILS using the UWB multistatic radar system to provide a more robust and accurate real-time 2D location of an Active Tag (AT). Thanks to UWB technology, our proposed system is able to locate the AT with a high resolution making it capable of distinguishing even close positions, thus achieving a high accuracy of a few centimeters. This thesis is composed of 4 chapters.

In Chapter 1, the different techniques used for position estimation are presented and compared them to select the most appropriate technique for each technology. Next, the different technologies that use an appropriate technique to locate a target in an indoor environment are compared. This gives a good knowledge of the advantages and disadvantages of each technology in order to choose the one we are interested in terms of accuracy, resolution, coverage and cost to ILS. Afterwards, a brief overview of the state of the art of both commercial and experimental UWB localization systems is provided. Finally, depending on the application requirements, an ILS based on UWB technology is proposed.

In Chapter 2, the essential elements of the UWB including the Federal Communications Commission (FCC) definition, regulation and characterization of channels in an indoor environment are illustrated. The Cramer-Rao lower bound (CRLB) study for Time of Arrival (ToA) estimation shows that UWB signals are particularly suitable for ToA measurement. For this reason, different state-of-the-art UWB-based approaches are identified. Next, a hybrid technique combining duplex UWB and Phase Correlation (PC) methods is proposed. The first method is used to estimate the distance while the second one is used to estimate the angle.

In Chapter 3, the localization algorithm of a constellation-based ILS is presented. Next, the architecture of our proposed UWB ILS for 2D positioning is described. This positioning requires two identical antennas used as interrogators (receivers) separated by a single anchor in the center. To this end, the characterization of the different Radio Frequency (RF) components such as antennas, filters and amplifiers is presented and detailed. The concept of the system is validated by conducting some experiments in a controlled environment. The constraints associated with the proposed design are also mathematically validated to better understand the system's performance. Finally, the power levels at the different stages of the developed ILS are also discussed and interpreted.

In Chapter 4, the performance of the proposed UWB-based ILS is studied. The angular resolution is validated using the PC method in simulations and experimental setups. Then, the distance resolution is validated using the duplex UWB method in the CM3 channel model (office Line of Sight (LoS)) of IEEE.802.15.4a. The accuracy and resolution of the 2D position estimation are validated using both distance and angular measurement. The results are discussed and explained taking into account both LoS and Non Line of Sight (NLoS) cases. Finally, the conclusion of thesis work is presented along with some future work plans such as the extension of the prototype to 3D position estimation.

Bibliography

[1] P. Gulden, S. Roehr, and M. Christmann, “An Overview of Wireless Local Positioning System Configurations,” IEEE International Microwave Workshop on Wireless Sensing, Local Positioning, and RFID, pp. 1–4, September 2009. Cited page 1

[2] R. Kumar, “Indoor Localisation pour Telemonitoring,” Ph.D. dissertation, Telecom Paristech, Electronique et Communications, Paris, France, 2014. Cited page 1

Chapter 1

State-of-the-art Characteristics of Indoor Localization Systems

1.1 Introduction

Location data of a user or device in a given space appeared a few years ago and has since become an essential element of contextual information. This has been largely influenced by the widespread use of wireless connection, making it easier to obtain more and more information of this type. For instance, the location information has attracted a lot of attention in marketing for both consumers and advertisers. On one hand, brands and advertisers uses Location-Based Marketing (LBM) strategies to attract consumers by displaying relevant messages on their mobile phones based on their geographic location. One of the main objectives of this new marketing method is to prevent consumers from escaping to e-commerce sites. On the other hand, this information helps the consumer and assist him from his place to the shopping center, guides him inside and allows him to reach his destinations more easily. Similarly, many airports, train stations, congress and exhibition centers are using these technologies to help users by providing them with useful information.

The relevance of localization is not limited to these applications, but also extends to other areas and services such as medical surveillance, assistance to the elderly and disabled people in their daily lives, monitoring children in their activities, etc. Therefore, the goal of the Indoor Localization System (ILS) is to determine the position of objects or people in an internal space of a structure (buildings, houses, industry, $\cdots$).

This chapter is dedicated to present an overview of existing ILS. The different techniques used within an ILS are presented in Section 1.2. Section 1.3 describes the famous trilateration algorithm used to estimate a tag's position. Various positionning technologies are described in Section 1.4. Section 1.5 is devoted to compare the different technologies described in Section 1.4. Some solutions based on Ultra Wide Band (UWB) technology are discussed in Section 1.6. Our proposed system is described in Section 1.7. Finally, the chapter ends with a conclusion in Section 1.8.

1.2 Position Estimation Techniques

In general terms, the location estimation consists of a three-tiered algorithm. The first stage involves measuring the characteristics of the signal. These measurements are used in the second stage to estimate the direction of the object to be located and its distance from the localization device. Finally, these distance or direction estimates are combined to estimate the exact position in the last stage. The combination method is different from one system to another and could be achieved using several techniques [1,2].

The position estimates may be obtained from a variety of measurements such as Time of Arrival (ToA), Time Difference of Arrival (TDoA), Angle of Arrival (AoA) and Received Signal Strength (RSS). This section presents the different measurement techniques used to locate a user/object in an indoor environment.

1.2.1 Time of Arrival

As its name suggests, the ToA provides a measurement of the arrival time of a received signal at a reference anchor. It depends on the signal Time of Flight (ToF), which is defined as the propagation time of a signal traveling from a target to a reference anchor. Therefore, the knowledge of the exact emission time t_m of the target signal and its exact arrival time t_i at the reference anchor i are required to apply ToA technique. The distance d_i between the reference anchor i and the target is then computed easily using

$$d_i = c.(t_i - t_m) \tag{1.1}$$

where c is the speed of light.

Once the distance d_i is obtained, all possible target locations can be determined. From a multilateration point of view [3], ToA defines circles around the reference anchors as shown in Figure 1.1. So if the anchor i is located at (x_i, y_i), the target coordinate (x, y) must satisfy

$$d_i{}^2 = (x_i - x)^2 + (y_i - y)^2 \tag{1.2}$$

To estimate the 2D position, this measurement must take place at a minimum of three reference anchors, and the exact position of the target will be then the intersection of the obtained three circles. This scheme can be extended for 3D localization by using at least

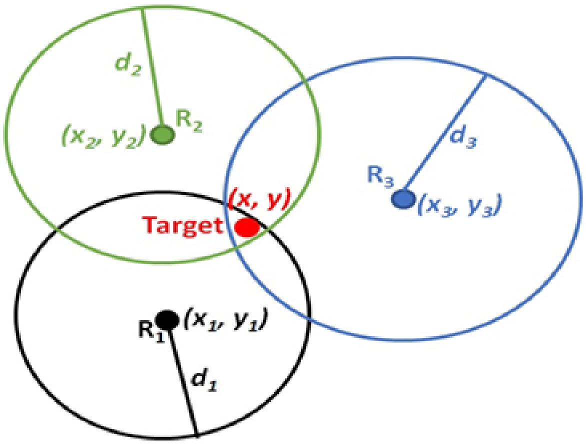

Figure 1.1 – ToA principle.

four reference anchors.

This technique achieves high accuracy in locating the position of a target even if the distance between the reference anchor and the target increases. However, this can only be accomplished when the target and all the reference anchors in the system are properly synchronized. As such, low time synchronization, multipath propagation and low Signal-to-Nosie Ratio (SNR) are major sources of error in this method.

1.2.2 Time Difference of Arrival

Sometimes the emitting time t_m of the target signal is unknown, so the usage of the ToA technique is not possible anymore. In this case, the distance estimation can still be done using another technique known as TDoA. Like ToA, this technique uses the travel time of a signal from the target to the reference anchor, but instead of using the target's emission time, which is now unknown, it uses the difference in travel times from each reference anchor to estimate the distance to each one of them. Thus, knowing the time of transmission in no more required, and the time difference is now sufficient to estimate the distances [4].

Once a signal is received by two reference anchors i and j, the difference in arrival times Δt_{ij} is used to calculate the difference in distances Δd_{ij} between the target and the two reference anchors using

$$\Delta d_{ij} = c.\Delta t_{ij} \qquad i \neq j \tag{1.3}$$

Assuming that the two reference anchors i and j are located respectively at (x_i, y_i) and (x_j, y_j), the target at (x, y) must lie on a hyperboloid with a constant range difference between the two reference anchors for each TDoA measurement as shown in Figure 1.2. The equation of the hyperboloid is given by

$$\Delta d_{ij} = \sqrt{(x_i - x)^2 + (y_i - y)^2} - \sqrt{(x_j - x)^2 + (y_j - y)^2} \qquad i \neq j \tag{1.4}$$

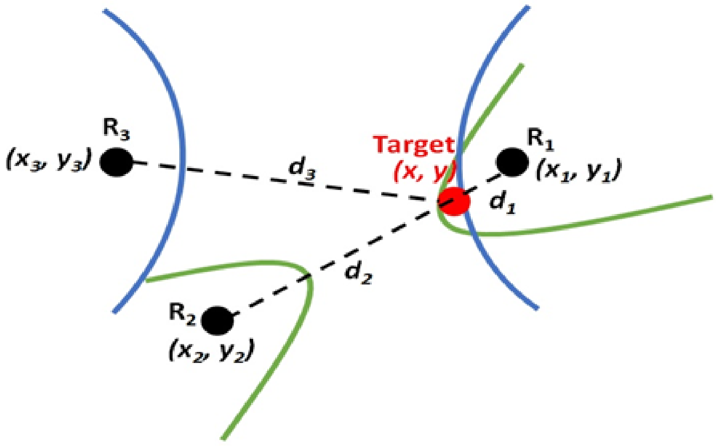

Figure 1.2 – TDoA principle.

To locate a target in 2D, TDoA measurements (for instance, Δt_{12} and Δt_{13} in the example shown in Figure 1.2) must be made at three fixed reference anchors to form two hyperbolas whose intersection determines the target position.

Similar to ToA or any other time-based method, the accuracy is affected by multipath propagation and low SNR. Furthermore, synchronization between devices is mandatory to obtain accurate measurements. However, the synchronization in TDoA is only required between the reference anchors, since the target is located based on their time/distance difference. The target does not need to be synchronized with the reference anchors because the distance between them is not taken into account in the TDoA calculation.

1.2.3 Angle of Arrival

AoA, also known as Direction of Arrival (DoA), provides a measurement of the angle at which a signal is received by a reference anchor [5]. Using this angle, the reference anchor defines a straight line from its position that indicates the different possible positions of the target. The exact position of the target will thus be the intersection of several lines from several reference anchors.

Assume that the target at (x, y) transmits a signal to the i-th reference anchor R_i located at (x_i, y_i). As shown in Figure 1.3, the straight line connecting these two entities makes an angle θ_i with the axis (R_i, R_j). The angle of arrival θ_i is therefore obtained by the triangulation principle

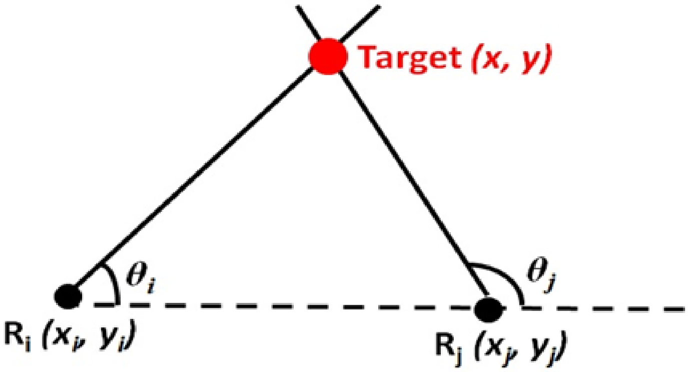

Figure 1.3 – AoA principle.

$$\tan \theta_i = \frac{y - y_i}{x - x_i} \tag{1.5}$$

To find the 2D position of the target, AoA methods use at least two known reference anchors, R_i and R_j. The exact position of the target will be then the intersection of the two lines of direction θ_i and θ_j. Following the same approach, 3D positioning is also possible using at least three reference anchors.

Unlike ToA and TDoA methods, AoA method does not require synchronization between the target and the reference anchors. Moreover, the minimum number of reference anchors needed to locate the target is reduced (two in 2D and three in 3D). However, besides the large and complex material requirements, the accuracy of the position estimation decreases as the distance between the target and the reference anchors increases. In fact, this method works well in situations with Line of Sight (LoS), but accuracy decreases too when there are signal reflections and multiple paths. Thus, it is not suitable for indoor environments unless combined with other techniques forming a hybrid ILS system.

1.2.4 Received Signal Strength

The RSS is the field intensity of a signal measured at the reception point. In this approach, the power level of a received radio signal is used to estimate the position of a remote target using multilateration technique while applying either signal propagation models [6] or fingerprint method [7].

Based on a path loss model, the distance d_i between the target and the i-th reference anchor can be obtained using

$$\frac{P_i}{P_0} = \left(\frac{d_0}{d_i}\right)^n \tag{1.6}$$

where P_i is the received power at the reference anchor i, P_0 is the received power at the reference distance d_0, and n is the path loss exponent of the environment under consideration.

However, path loss models are not always applicable due to shadowing and severe multipath fading. Therefore, it is difficult to apply these models to the received signal, which is continuously affected by the complex nature of the indoor environment.

One way to overcome this problem and avoid complex modelling of signal propagation is by using the fingerprint method. This method comprises two phases: training and position determination. The first phase consists of determining the RSS values at each point using offline measurement campaigns to build a database, also called a radio map. Then, the position of a target can be estimated in the second phase by comparing the RSS observations with the values already recorded in the radio map using proximity matching algorithms.

In 2D, at least three reference anchors are required to estimate the target position, while in 3D, at least four reference anchors are needed.

The RSS method provides high accuracy in short-range and LoS environments. Unlike ToA and TDoA, this method does not need any time synchronization between the system anchors. However, the dynamic nature of the indoor environment requires a continuous updating of the radio map affecting the system's performance.

Table 1.1 outlines the main characteristics of the different techniques described above. This comparison allowed us to choose the most appropriate technique for each technology used in localization systems. A detailed description of these technologies, including the technique adopted for each one, is presented in the following section.

Table 1.1 – Comparison between different ILS techniques

Criteria		**ToA**	**TDoA**	**AoA**	**RSS**
Position Estimation		The time taken by the signal to move from the target anchor to several reference anchors.	The time difference between the arrival of the signal at multiple reference anchors.	The intersection of several pairs of angle direction lines.	The signal strength received at the target anchor from several reference anchors.
Number of reference anchors	**2D**	At least three.	At least three.	At least two.	At least three.
	3D	At least four.	At least four.	At least three.	At least four.
Synchronization		All transmitters and receivers in the system must be perfectly synchronized.	Only the reference anchors should be synchronized.	Less synchronization and clock precision requirements.	Not required.
LoS Vs. NLoS				Requires a clear LoS between transmitter and receiver.	Favours LoS to reduce multipath effects.
Issues		Relative clock shift between transmitter and receiver.	Lower accuracy than ToA with the same system geometry.	A small error in the angle measurement has a big impact on the accuracy. Requires large and expensive antenna arrays.	Sensitive to channel inconsistency. Requires short distances between anchors.

The measurements obtained by the techniques mentioned above are used to estimate a target's position through a series of algorithms such as the trilateration algorithm, which will be detailed in the next section.

1.3 Trilateration-based ILS

ILSs based on trilateration have fixed anchors at known positions that form a well-defined constellation. To find the 2D location of the tag, at least 3 anchors or alternatively 3 reference nodes are required. The system uses trilateration technique to estimate the tag position T by calculating the distance to each anchor R_i ($i = \{1,2,3\}$), as shown in Figure 1.4. Therefore, the algorithm requires the coordinates (x_i,y_i) of all the anchors to predict the location of the tag by calculating the distance d_i between the latter and each anchor.

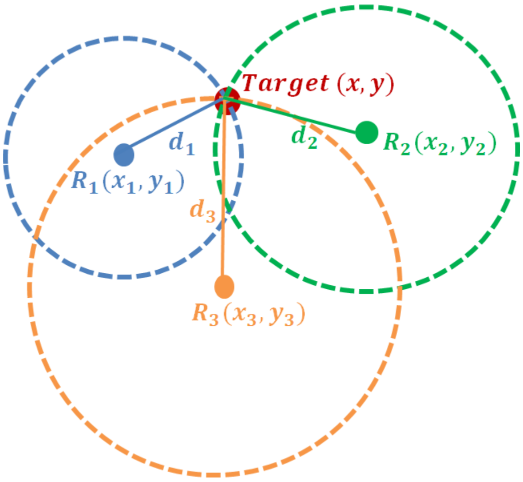

Figure 1.4 – Trilateration estimation.

The distances d_i are given by the following equation

$$\begin{cases} {d_1}^2 = (x_1 - x)^2 + (y_1 - y)^2 \\ {d_2}^2 = (x_2 - x)^2 + (y_2 - y)^2 \\ {d_3}^2 = (x_3 - x)^2 + (y_3 - y)^2 \end{cases} \tag{1.7}$$

Solving this system of equation reveals the tag position (x,y) as follows

$$x = \frac{Ay_{32} + By_{13} + Cy_{21}}{2(x_1 y_{32} + x_2 y_{13} + x_3 y_{21})} \tag{1.8}$$

$$y = \frac{Ax_{32} + Bx_{13} + Cx_{21}}{2(y_1 x_{32} + y_2 x_{13} + y_3 x_{21})} \tag{1.9}$$

where

$$\begin{cases} A = {x_1}^2 + {y_1}^2 - {d_1}^2 \\ B = {x_2}^2 + {y_2}^2 - {d_2}^2 \\ C = {x_3}^2 + {y_3}^2 - {d_3}^2 \end{cases} \tag{1.10}$$

and

$$\begin{cases} x_{32} = x_3 - x_2 \\ x_{13} = x_1 - x_3 \\ x_{21} = x_2 - x_1 \end{cases} \tag{1.11}$$

$$\begin{cases} y_{32} = y_3 - y_2 \\ y_{13} = y_1 - y_3 \\ y_{21} = y_2 - y_1 \end{cases} \tag{1.12}$$

Figure 1.5 highlights a new problem or limitation of this method. In fact, the accuracy of the localization is strongly affected by the geometry of the anchors. This well-known problem in the field of localization is reflected in the definition of *Dilution of Precision (DoP)*. This concept has been mathematically derived and proved in [4] and has long been used in GPS tracking systems as an indicator of anchor positioning. As we can see, the geometry of the anchor failed to accurately locate the AT, and merely provided a surface of uncertainty in which the AT can occupy any position. When this area is narrow, which is equivalent to a small DoP value, the estimation error is also small. However, this error increases for large areas, corresponding to a high DoP value.

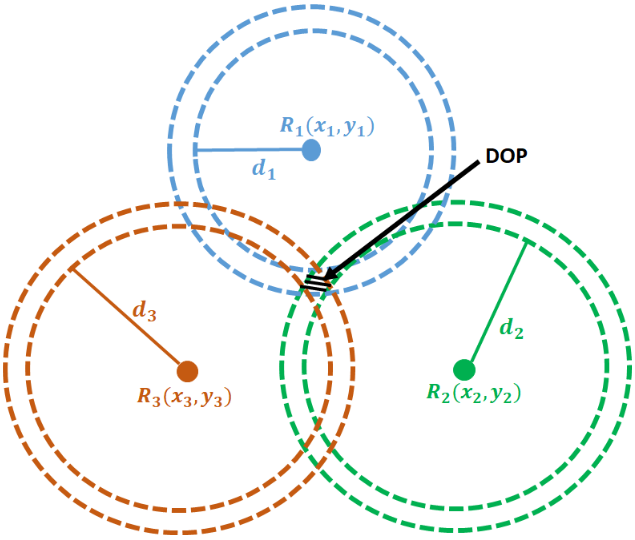

Figure 1.5 – Anchors Geometry Problem.

1.4 Positioning Technologies

Positioning technologies have a major influence on the performance, reliability and confidentiality of location-based services, systems and applications [8]. Therefore, this section is devoted to presenting the different technologies that utilize the aforementioned techniques to locate a target in an indoor environment.

1.4.1 Global Positioning System

Global Positioning System (GPS) is the most popular and widespread radio navigation system for finding the location and position of objects, especially for the outdoor environment. The fundamental aspect of positioning using this technology is the measurement of the distance between the satellites and the receiver. To do this, satellites send messages containing the sending time, their exact orbits and other useful information. The receiver processes this information and measures the time differences of these signals to find its position as shown in Figure 1.6. In this scenario, at least four satellites are required to determine the 3D position.

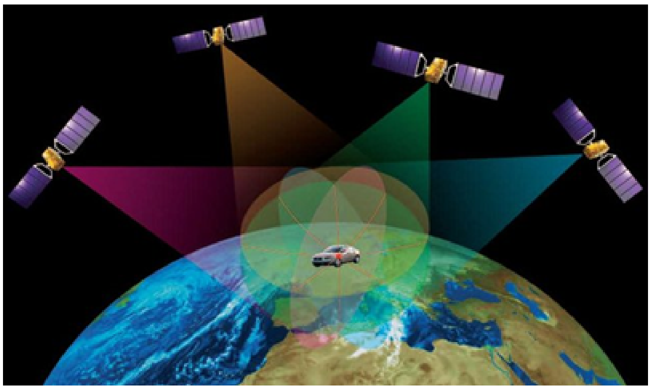

Figure 1.6 – GPS methodology [9].

However, the presence of obstacles that block the line of sight between the satellite and the receiver as well as the attenuation and dispersion of electromagnetic waves by buildings and external obstacles, make GPS a technology not suitable for indoor environments [10].

To solve this problem, several positioning systems based on conventional GPS are proposed [11]. An example of such a system is the pseudo-sattelites, also known as pseudolites. A pseudolite is a device that generates and transmits GPS-type signals. These signals are similar to real GPS signals but using different carrier frequencies or containing different navigation data [12]. Therefore, this method estimates the position by simulating the constellation of real satellites through several pseudolites located at different corners of the building. Nevertheless, this method has several disadvantages, such as the cost of modifying receiver equipment to be compatible with pseudolites, clock synchronization problems and multi-path and near-far effects. These problems can be addressed by using GPS repeaters.

Another example of these systems is GPS repeaters [13]. This approach uses several switching modules to amplify and retransmit high quality GPS signals from an outdoor antenna to the indoor environment. To avoid the interference problem, the transmission of the modules is done in a sequential way, i.e. only one module will be active and transmits signals at a time. The switching period of the signal received by the indoor terminal corresponds to the TDoA between two successive repeaters. Therefore, using at least four TDoA measurements, this method allows a standard receiver to provide indoor position.

Although these methods can provide a reasonable estimate of the indoor position, most of them are costly and require additional infrastructure for the building. User terminals still need hardware modifications and interference between the outdoor and indoor antennas cannot be completely mitigated. All these weaknesses of GPS technology have highlighted the need to find a better solution for indoor localization that offers good performance at a low cost.

1.4.2 Infrared

Infrared (IR) positioning systems are one of the most common positioning systems that use wireless technology [14] and AoA technique. A simple infrared system consists of a diode that emits an infrared signal in the form of non-visible light flashes, and a receiving photodiode that detects and captures the light pulses, which will then be processed to extract the information [15]. IR localization can be used in active or passive configurations.

IR technology is adopted by several systems to perform position detection. For instance, the Active Badge System [16, 17] is one of the first indoor badge positioning systems that covers the area inside a building and provides symbolic information on the location of each active badge. This system can therefore locate people in its coverage area by estimating the location of their active badges. In this system, an active badge transmits a globally unique IR signal every 15 seconds. These signals are detected by one or more sensors connected by wires and fixed in each localized place. The information provided by the latter makes it possible to determine the position of the active badges, which will be transmitted and saved in a central server.

Infrared systems provide very accurate positioning estimates. They are used in Wireless Personal Networks (WPANs) because they are a short-range beam with a narrow transmission angle, suitable for aiming and selective signal reception. IR emitters are small, lightweight and easy to transport. The system architecture is simple and does not require time-consuming installation and maintenance.

In contrast, indoor infrared positioning systems have some drawbacks, such as security and privacy issues. In addition, infrared signals are sensitive and the location determination is affected by interference from fluorescent light and sunlight [18]. Moreover, IR waves cannot penetrate opaque materials, so the system no longer works if the IR device is covered. Although IR emitters are not expensive, the entire system using a camera array and connected by special wires is expensive compared to its limited coverage area. Another limitation of IR systems is the need for a transmitter or receiver in each location, i.e. each room in a building must be equipped with at least one IR device to locate whether or not the persons or target devices are in the room.

1.4.3 Ultrasonic

Ultrasonic location-based systems [19, 20] use sound frequencies beyond the audible range (above 20 KHz) to determine the user's position through the time required for an ultrasonic signal to move from a transmitter to a receiver. Ultrasonic technology uses the TDoA technique, and the ranging is mainly done using the reflective distance method through the triangulation positioning algorithm to determine the location of objects.

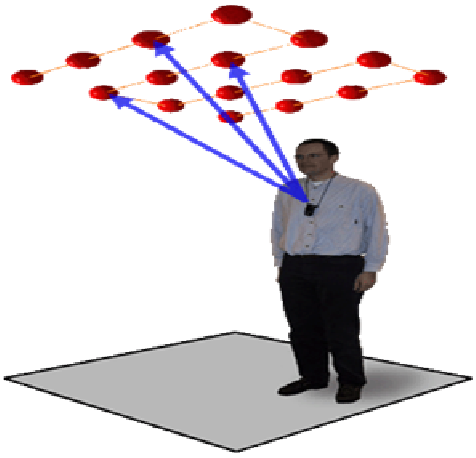

Figure 1.7 – Active Bat system [22].

The Active Bat system is an example of systems that use ultrasonic technology to determine the position of an ultrasonic tag, or "bat", being carried by a person. To do this, a tag periodically broadcasts a short ultrasonic pulse, which is then received by a matrix of receivers mounted on the ceiling at known positions, as shown in Figure 1.7. The distances between the tag and the receivers can be measured through ultrasonic waves and the position of the tag is determined by the triangulation method. Active Bat positioning system [21,22] provides 3D position and orientation information of the tracked tags using at least three receivers according to the principles of multilateration.

However, from the user's point of view, deploying a large number of ceiling sensors in each room is a time-consuming task, which impacts the system's scalability. Receivers must also be placed accurately, which results in a complex and costly installation. Moreover, these systems have a lower measurement accuracy (several centimetres) than IR-based systems (several millimetres). They also suffer from air flows, reflected ultrasonic signals and other noise sources such as the jangling of metal objects, crispy packages, etc.

1.4.4 Wireless Local Area Network

Wireless Local Area Network (WLAN), also known as "Wireless Fidelity (WiFi)", transmits and receives data using electromagnetic waves, providing wireless connectivity within its coverage area. WLAN technology is very popular and has been implemented in public places such as hospitals, stations, universities, etc. This widespread use of WiFi technology has motivated researchers to utilize it in designing localization systems inside buildings [23]. To determine the location, this system converts the detected electromagnetic signals into measurable metrics such as distance and angle, using the signal strength and SNR available from the WLAN Network Interface Card (NIC). It triangulates the 2D position of an object within a building using empirical data or mathematical model of indoor radio propagation.

In indoor localization, it is necessary to go beyond the mere identification of the Access Point (AP) in order to achieve higher precision. Therefore, three approaches have been proposed to locate a user using WLAN technology and RSS technique:

- The propagation model of a known antenna is used to calculate the distance to a known base [24].
- The relative strength of several known WiFi bases is used to determine the position by a multilateration method.
- Fingerprinting is used to match a pattern of known WiFi bases along with their relative strengths, to a database of known patterns associated with the locations [25]. Of course, building the database requires extensive pre-mapping activity and storing WiFi patterns for each mapped point.

A famous example of an indoor position tracking system that uses existing WLAN technology is the RADAR system [26], proposed by a Microsoft research group. The RADAR system can provide 2D absolute position information using signal strength and SNR with triangulation location technique, and thereby enable location-based applications for users. In [26], the RADAR system was tested on a floor inside a building, which is a typical indoor environment. The authors used three Personal Computers (PCs) serving as APs to track the target object represented by a laptop computer. The three APs measure the signal strength of the target's Radio Frequency (RF) signals. These measurements are used to determine a 2D position of the object. The main advantage of the RADAR system is that it uses the existing indoor WLAN infrastructure, eliminating the need to deploy new equipment. In addition, position detection requires few base stations, making RADAR a system that is easy to set up. However, this system can only locate objects equipped with WLAN technology, which is difficult for some light and energy-limited devices. In addition, this system does not take into account privacy issues, i.e. a person using a device with a WLAN interface can be easily tracked, even without their permission. Also, the RADAR system suffers from the limitations of the RSS positioning methodology [27].

Generally speaking, WLAN-based indoor positioning is an example of a low-cost positioning technology that uses existing infrastructure in indoor environments. WLAN technology is widely used and integrated in various wireless devices such as Personal Digital Assistants (PDAs), laptops, mobile phones, etc. Thus, WLAN-based indoor positioning systems can also reuse these wireless devices to track people, by measuring certain signal parameters provided by each wireless card.

Nevertheless, the accuracy of location estimations based on the signal strength of WLAN signals is affected by various sources of the indoor environment [28] such as movement and orientation of the human body, overlapping APs, walls, doors, etc. In some situations, it may be important to have a large number of APs to confront the high attenuation of the WiFi signal, especially if the signal passes through walls. Ideally, using at least one AP per room helps to limit the distance for the received signal from a particular access point, and thus minimizes the estimated position errors. Moreover, using stored information and fingerprinting techniques is complex and costly if the number of users of the indoor positioning system increases significantly.

1.4.5 Bluetooth

Bluetooth technology is a low-power, short-range wireless transmission technology that uses short-wave radio communications to send and receive data (audio, video, etc.) between devices such as mobile devices, computers, PDAs, etc. It uses the Frequency Hopping (FH) technique to protect its signals against other technologies using the same Industrial, Scientific and Medical (ISM) band. In Bluetooth-based positioning systems [29], several Bluetooth devices are grouped together to form a positioning infrastructure or what is called a cluster. A Bluetooth mobile device is then located using other mobile devices in the same cluster. In fact, a Bluetooth indoor positioning system uses the RSS technique to determine a user's position as long as he/she is equipped with a mobile device having Bluetooth technology and has activated this feature in it. Like any other Bluetooth device, a Bluetooth tag, which is a small transceiver, is identified by its unique Identification (ID). This ID can be used to locate the Bluetooth tag [30].

The Topaz location system [31] uses Bluetooth technology to locate tags in indoor environments. The architecture and the different components of this indoor localization system are shown in Figure 1.8. In this system, Bluetooth servers receive the measured signal strength and forward the raw data to the location server, whose role is to calculate the location of the tags. Bluetooth servers, location servers and location clients are connected via Local Area Network (LAN). This Bluetooth-based location system can only provide 2D location information with an error range of about 2 m, which is not sufficient to achieve high accuracy in an indoor environment with multiple obstacles.

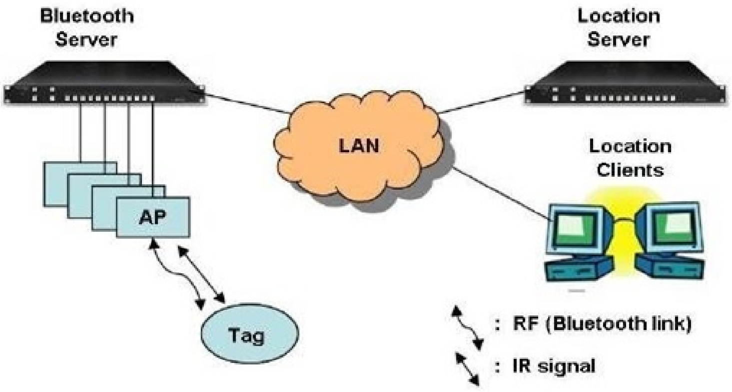

Figure 1.8 – System architecture of Topaz [31].

Bluetooth technology is mainly intended to facilitate communications between mobile devices and those with fixed devices, in order to eliminate the need for cables and connectors (e.g. when using wireless headsets), and to simplify the synchronization of data between personal devices [32]. Bluetooth devices are small in size and easy to integrate into the various electronic devices, so it is easy to popularize. Moreover, Bluetooth technology is reusable, i.e. it uses infrastructures that have already built-in Bluetooth chips. It is cost-effective and consumes a small amount of energy during operation.

However, a disadvantage of the Bluetooth-based positioning system is the delay time it takes to calculate the position of a tag. This delay of about 10 to 30 seconds is considered quite long compared to the operational range (2 to 3 m) of such a system. Moreover, the frequency hopping technique makes the impulse response of the propagation channel barely constant in the ISM band, which in turn causes a variation in the power of the received signal at each frequency hopping. Thus, this technique is the origin of different attenuation, thereby complicating the analysis of the received power measurements, and limiting the effectiveness of positioning systems based on Bluetooth RSS measurements [33]. Bluetooth positioning systems also suffer from the drawbacks of RF positioning technology in complex and changing indoor situations [30]. In addition, the stability of the Bluetooth system is affected in a complex spatial environment due to noise signal interference.

1.4.6 Radio Frequency Identification

Radio Frequency Identification (RFID) is a mechanism to store and retrieve data via electromagnetic transmission to an RF-compatible integrated circuit [34]. This technology uses radio waves to trigger a specialized circuit into producing a response containing a unique identifier, which can be used to identify people, animals or objects using RSS technique. An RFID system consists of RFID readers and RFID tags. The RFID reader is responsible for retrieving data from RFID tags. RFID tags or "transponders" are equipped with a microchip and a printed circuit board. This card acts as an antenna and allows the tag to transmit radio signals containing useful information, mainly the tag's unique ID [35]. The tags can be classified into "passive" or "active" depending on the energy source they use to respond to an RFID reader. On one hand, a passive RFID tag operates without a battery. It responds to an RFID reader by using only the small amount of energy emitted by the reader, which is collected using a small antenna. It reflects the RF signal received from the reader and adds information by modulating it. Passive RFID tags are mainly used to replace traditional barcode technology. They are much lighter, smaller in volume and less expensive than active tags. However, their reading range is very limited (1-2 m), and the cost of readers is relatively high. On the other hand, active RFID tags have their own power supply. They are small transceivers, which can actively transmit their ID (or other additional data) in response to a query. The advantages of active RFID are a smaller antenna and a much longer range (several tens of meters).

RFID technology has many applications and areas of use, such as personal/vehicle access control, department store security, equipment tracking, luggage, fast food establishments, logistics, medical equipment, etc [36]. In addition, RFID systems have been used for localization, especially when the user's position is not requested at all times, but only when passing through important control points, like entrance doors. In these cases, the user's location is often given in a logical form rather than in a coordinate system, e.g. "before the door", "in the waiting room", etc.

Two variants of user positioning are possible: in the first, the user carries the tag, and the readers are fixed in the infrastructure. In the other option, the user carries a reader, and many tags are incorporated in key locations in a given area. The first option was the most popular because the tags are cheaper and very lightweight, while the readers are bulky and very expensive.

LANDMARC (Location Identification based on Dynamic Active RFID Calibration) is a pioneering RFID system [34]. It belongs to the category of systems in which the tag is attached to the object or person to be located. LANDMARC needs information on the signal intensity of each tag reader to calculate the position of RFID tags using the *k*-Nearest Neighbour algorithm (*k*-NN). Although the authors claim an accuracy of 1 meter, the main limitation of this system is that the reader does not directly provide the signal strength; rather it reports only if the tag is "detectable" or "undetectable". LANDMARC must periodically scan power levels to estimate the signal strength of the tag, which produces latency in the localization. An additional problem is the wide variation in the behaviour of RFID tags due to the battery's loss of energy. Another indoor positioning system using RFID is called SPOT ON [37]. It is a new tagging technology for 3D location detection based on RSS measurements. These measurements, provided by several base stations, are sent and stored in the server. The server processor maps the RSS values and determines the exact position of the objects using the triangulation technique. Once the position is known, a virtual 3D display of the indoor environment can be built to show the location of the tags.

RFID technology is not only intended for indoor positioning applications, but also provides many potential services to meet user demands. They are cost-effective, their RF tags can be read in any environment, and can work at high speeds even if the line-of-site is not available. In addition, the RFID positioning system has lightweight and small tags that can be carried by the people to be tracked. Therefore, the RFID system can only identify equipment and people equipped with a tag. However, proximity and absolute positioning techniques require the installation and maintenance of many infrastructure components in the working area of an RFID positioning system [14]. In addition, their range is quite limited and the cost of readers is relatively high in the case of passive tags.

1.4.7 Ultra Wide Band

UWB is a technology based on the transmission of electromagnetic waveforms composed of a sequence of very short pulses, a shown in Figure 1.9a, using a very large bandwidth (greater than 500MHz) [38]. This radio technology uses a very large part of the radio spectrum to transmit, but at the same time consumes very small amounts of energy during operation, as shown in Figure 1.9b. UWB has many applications and areas of use: radar and imaging, security applications, medical applications, vehicle radar systems, high-penetration radar systems, location and tracking, etc [39, 40]. UWB can be used for accurate indoor positioning, such as finding the location of soldiers on the battlefield, tracking the movement of a robot. Therefore, UWB technology was selected for deployment in indoor positioning systems because it offers different advantages in terms of accuracy of time-of-flight measurement, multipath immunity and low power consumption for extended operation [41]. To determine the distance between the target and a reference point, two different measurements can be used in a UWB positioning system : ToA and TDoA, regardless of the used modulation scheme.

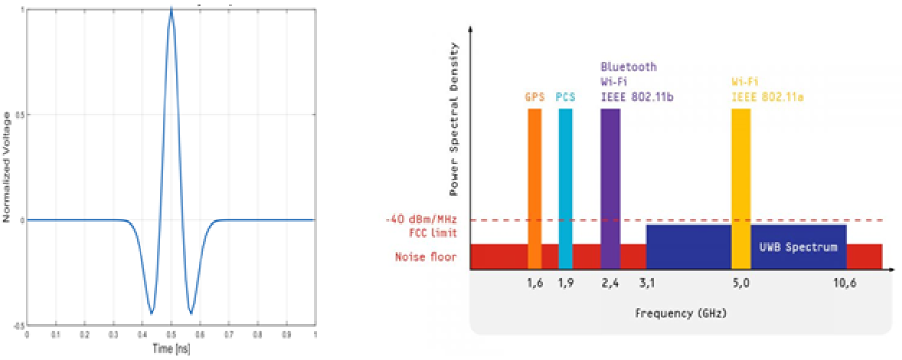

(a) (b)

Figure 1.9 – (a) UWB pulse [42] and (b) UWB spectrum [43]

.

Ubisense is an example of a new real-time positioning system based on UWB technology [44]. It uses the triangulation localization technique, which takes advantage of both the TDoA and AoA techniques, to provide a flexible position detection capability. This system consists of three parts: sensors, tags and the Ubisense software platform. The active tags transmit UWB pulses. These pulses are received by the sensors, fixed at known locations. Next, the tag location data is forwarded via existing Ethernet links from these sensors to the Ubisense software platform, which analyzes and displays the tag location. The software platform consists of two parts: the location engine and the location platform. Location Engine is an execution component that allows to configure the sensors and tags. Location Platform collects location data from location-aware applications. Once the visualization of the location of the tags is provided, absolute, relative and proximity information can be extracted and sent to various location-aware applications. Ubisense sensors are arranged in cells. In each cell, there are at least four sensors, covering an area of up to 400m^2. Thus, the coverage by infrastructure element is important and the system is scalable with respect to a large position monitoring area. Tracked tags in this system are wireless, easy to wear, lightweight (45 g) and equipped with a long life battery (about 1 year). Ubisense provides high precision (a few tens of centimetres) in indoor positioning, because it is based on both measurements of signal angles and arrival time differences, and it is not affected by complex indoor environments, including walls and doors [43]. With this high accuracy, the price of this system remains significantly high, limiting its use on a large scale.

UWB localization exploits the temporal synchronization characteristics of UWB communication to obtain a very high indoor localization accuracy (20 cm). It is therefore suitable for high-precision real-time 2D and 3D localization. 3D positioning can be performed using two different measuring techniques: TDoA, which measures the difference in arrival time of a UWB pulse at several sensors, and AoA. Using both techniques at the same time allows to reduce the required sensor density compared to systems that use only TDoA, because a location can now be determined with only two sensors. Furthermore, UWB technology offers various advantages over other positioning technologies used in the ILS, such as no line-of-sight requirement, no multipath distortion, less interference, high penetration ability, etc. In addition, UWB sensors are cheap, making the positioning system a cost-effective solution. Finally, the large range of each sensor allows the UWB positioning system to be scalable.

1.5 How to choose the Indoor Localization System ?

Indoor localization has lately gained interest due to the vast range of services it can offer. As discussed in the previous sections, different techniques, wireless technologies and mechanisms have been developed in the literature to provide indoor location and improve services offered to users. So the main question that arises now is, how to choose the indoor positioning system ?

Unfortunately, there is no unique answer to this question because the different use cases impose specific requirements for the indoor localization system. Generally speaking, there are several aspects that help to characterize an ILS system and distinguish it from other systems. Among these aspects, we are interested in [45]:

- **Accuracy:** It is roughly referred to the difference between the estimated and the actual positions. In the UWB case, very accurate measuring can be easily achieved due to the short pulse duration. In this case, the diffuse multiple path is well separated from the LoS, so that neither amplitude fading nor pulse distortion impairs the received signal. This is not the case for the narrow band where amplitude fading occurs and complete diffuse multipath propagation interferes with the LoS component.
- **Resolution:** It is the minimum ToA or TDoA that the system can measure. These measurements will then be used to derive the distance and angular resolutions which are the minimum required values to distinguish one target from another depending on the radio waves' bandwidth. In particular, the large bandwidth of UWB signals can be conveyed to a high resolution in the pulse arrival time.
- **Coverage:** It is the territorial extension in which the system can locate a user or object. Some technologies may provide extensive coverage in an ideal environment,

but when used indoors, their coverage may be limited due to environmental factors. An ILS can locate a person or object within a range of several meters or even on different levels in a building.

- **Cost:** It is the amount of resources invested in the installation and operation of a positioning system. Systems that reuse existing technology in indoor environments (e.g. WiFi APs) or those that are carried by the user (e.g. mobile devices), require a small investment for installation and maintenance and a low cost for user service. However, in the case of indoor positioning systems based on technologies that use special devices and specialized infrastructure (e.g. sensor networks, readers), installation and maintenance costs are high.

With this in mind, this section aims to compare the different ILS technologies taking into account different aspects and characteristics of each one of them.

Compared to outdoor environments, indoor environments are more complex because there are various objects (such as walls, equipment and people) that reflect, cause high attenuation and diffusion of signals, and subsequently lead to multipath and delay problems. Indoor environments are then forced to rely on Non Line of Sight (NLoS) propagation where the signal cannot move directly in a straight line from a transmitter to a receiver, causing inconsistent delays at the latter. Typically, indoor positioning applications require higher accuracy and precision than outdoor positioning applications to be able to deal with relatively small areas and existing obstacles. In this sense, GPS has poor performance in dense urban areas compared to rural areas. In particular, the low coverage of the satellite signal in the indoor environment reduces its accuracy and makes it unsuitable. In addition, GPS has a large infrastructure to support location measurement, which is expensive and complex.

Infrared is a near foolproof way to ensure room-level accuracy. It uses light instead of radio waves, which cannot pass through walls - if the system says that an asset is in room 4B, it is undoubtedly in room 4B. Radio-based systems cannot provide such certainty, as radio waves can sometimes be captured by other readers through walls and subsequently cause positioning errors. However, in non-segmented rooms, infrared positioning would be a challenge - if three receivers read a light pulse, it is impossible to know from which receiver the tag is closest, because it is difficult to measure the relative strength of the infrared signal. In this case, radio technologies work better generally.

Most existing smartphones, laptops and other portable devices are WiFi compatible, making WiFi an ideal solution for indoor localization without the need to deploy additional infrastructure. However, the positioning accuracy that this technology can provide remains subject to uncontrolled interference in the ISM band. Compared to Bluetooth, WiFi provides lower accuracy (5-10 meters) and is a bit expensive. In addition, it consumes much more energy than UWB.

Bluetooth technology is considered as a competitor to WiFi in indoor positioning systems, particularly since the widespread adoption of Bluetooth Low Energy (BLE), due to its high availability (it is supported by most modern smartphones), low cost and very low power consumption, which allows fixed transmitters to run on batteries for several months or even years [46]. Bluetooth operates in the 2.4 GHz ISM band. Compared to WLAN, the gross bit rate is lower (1 Mbps) and the range is shorter (typically $10 - 15$ m). In addition, apart from the variations in the indoor environment that affect the RSS measurement, the latter is also influenced by the type of FH modulation. Despite all of this, Bluetooth remains a "lighter" standard, very ubiquitous and supports several other network services in addition to Internet Protocol (IP).

Regarding RFID technology, passive RFID is the most commonly used and finds its applications at airport security checkpoints for baggage tracking or as an anti-theft measure in libraries, etc. because of their ability to identify items with just a quick scan. RFID is not a feasible option for live tracking due to its small range and large size. In addition, it is also not a preferred option for the medical industry due to the high presence of RF energy. It is therefore obvious that with its low accuracy, current RFID technology is not the right choice for an ILS.

Ultrasonic ILS can reach even subcentimeter accuracies in still air conditions [47]. However, ultrasonic systems are limited in range (about 10 m) and cannot penetrate walls, making their coverage dependent on the number of installed beacons and the partitioning of the building. Moreover, the propagation properties of sound waves in indoor environments present a challenge for accurate position estimation. Environmental elements such as furniture, walls and their salient edges can create echoes. The appearance of such echoes can lead to inaccurate location [48, 49].

UWB technology is a great option for Indoor Positioning System (IPS) and has a high anti-interference capability, but it is expensive and requires more infrastructure. This technology has many advantages over traditional narrow-band systems, such as high penetration power, low energy consumption, resistance to multi-path effects, high security, low complexity, very precise positioning, etc. Short pulse waveforms permit to determine accurately the ToA of a burst transmission. UWB signals pass easily through walls, equipment and clothing, but are affected by metallic and liquid materials that cause interference. This problem can be avoided by using more UWB readers strategically placed in the infrastructure. In general, RF positioning systems suffer from multipath distortion of radio signals reflected by walls or any other obstacle in indoor environments.

This problem is overcomed with UWB pulses because they allow to filter the reflected signals from the original one. In this way, the system can offer higher accuracy compared to traditional wireless technologies such as RFID and WLAN. This is clearly reflected in the Ubisense system, which achieves an accuracy of about 15 cm in 3D, considered very high compared to other RF positioning systems. The delay time of the position estimates is short and the sensing rate can reach 20 times per second. Unlike conventional RFID systems, which operate on a single band of the radio spectrum, UWB transmits a signal over several frequency bands simultaneously, from 3.1 to 10.6 GHz. UWB signals are also transmitted for a much shorter time (less than 1 ns) than those used in conventional RFID. In addition, UWB tags consume less energy than conventional RF tags and can operate over a wide range of frequencies. UWB can be used in the immediate vicinity of other RF signals without causing or experiencing interference due to differences in signal types and the radio spectrum used. So using UWB technology in positioning systems has been a popular way to improve positioning accuracy. Therefore, UWB technology can be applied to fixed or moving indoor objects and people tracking and navigation, and can provide very high positioning accuracy.

For active RF location and positioning applications, short-pulse UWB techniques offer distinct advantages in terms of accurate time-of-flight measurement, multipath immunity for leading edge detection and primary energy consumption for extended-operation RFID tags [50]. For this reason, the UWB technology is considered a promising solution for ILS.

Table 1.2 shows the main advantages and disadvantages of different technologies used in ILS. Among the different technologies, UWB has met the aforementioned aspects that interest us. In the following section, some existing UWB systems will be presented.

Table 1.2 – Comparison between different ILS technologies

Technologies	Techniques	Advantages	Disadvantages
IR	AoA	Cheap for user	Sunlight interfernce Limited range
Ultrasonic	TDoA	High accuracy	Interference Limited range Low penetration Air flow
WLAN	RSS	Low cost Large range	High variance signal High power consumption Continuous update of the radio map
Bluetooth	RSS	Low cost Low power consumption	Intrusive Limited range FH
RFID	RSS	Very low cost with passive tags	Limited accuracy Limited range with passive tags
UWB	TDoA/ToA	High accuracy High resolution Immune to interference	High cost

1.6 UWB Indoor Localization system

In general, there are two types of UWB indoor localization systems based on the TDoA measurement:

1. The first type refers to systems in which the tag sends its user-specific information sequence, encoded by UWB pulses. In this case, the tag will be localized by a Central Processing Unit (CPU), responsible for synchronizing all receivers and collecting time measurement data.

2. The second type refers to systems in which the receivers are used exclusively as repeaters. Thus, the tag receives back the transmitted signal, also containing the information (coordinates) of the receiver that it has sent it. In this case, the tag must calculate its own position using the relative distance information to the receivers. This is based on the Two-Way Ranging (TWR) measurement principle.

These two approaches are adopted in different literature systems, although the majority favour the first one. Therefore, a brief overview of the state of the art of both commercial and experimental UWB localization system is provided in this section.

In [51], a complete UWB indoor location demonstrator is presented. The system includes several interconnected APs to ensure synchronization and an autonomous Mobile User (MU) equipped with an UWB tag to transmit the pulses. In this scenario, the signals propagate over different physical paths (channels) and reach the AP. The received signals from all APs are forwarded to the time measurement unit - Time to Digital Converter (TDC) - via the synchronization network. The obtained positioning results show an original average accuracy of 9 cm. This accuracy is improved to 2.5 cm by including the influences of the antenna and signal detection threshold level.

In [52], an example of a UWB indoor localization and tracking system is presented. The transmitted signal is a sequence of short pulses that propagate through the media and are received by the four receivers placed at known positions. The architecture of this system is illustrated in Figure 1.10. As one can see, the receivers of this system are interconnected by two networks: the clock network which provides a reference clock to all receivers, and the data network which is used for communication between the receivers and the computer. The role of the latter is to process the received data to analyze the ToA of the receiver pulses and then determine the position of the transmitter. The location error was below 30% for 95% of all position estimates.

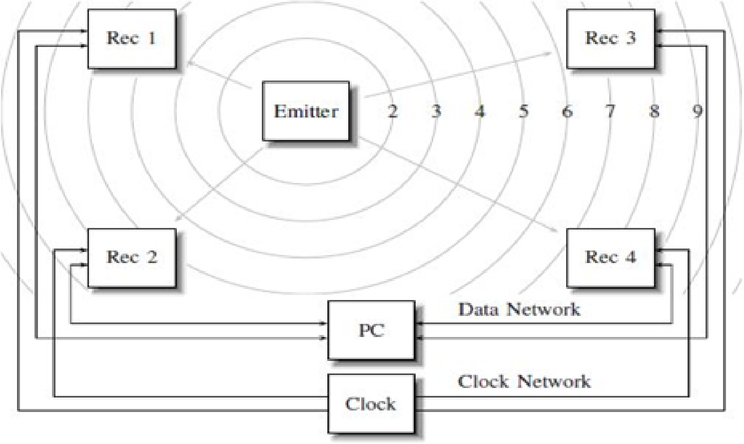

Figure 1.10 – UWB indoor localization system [52]

.

In [53], an ILS based on UWB is presented. The considered system is composed by four fixed transmitters, synchronized using a time division scheme. Each transmitter sends an UWB signal to some mobile users. The location of the latter is easily estimated using a triangulation method based on TDoA measurements between transmitters and receivers.

In [54], a performance comparison between ten impulse-radio UWB localization systems is described. Nine of them are laboratory setup that use an oscilloscope or squarer/comparator to acquire the received signals and estimate the ToA or the TDoA. The obtained results show that the system using the squarer/comparator and the TDoA method achieved the best accuracy of 3.4 cm in 2D.

Despite the accuracy that the above-mentioned systems can achieve, they nevertheless suffer from the synchronization constraint between receivers (or AP). Therefore, an additional synchronization circuit is required, which increases the overall complexity and cost of the system.

So far, several UWB commercial location systems have been fielded [55].

Ubisense [56] is one of the first companies to commercialize UWB technology for localization services. It was founded in 2002 in Cambridge, United Kingdom and has become a leader in the field of business location solutions. It has offices in Europe (Cambridge, Paris and Düsseldorf), the United States, Canada and Japan. The Ubisense positioning system consists of a network of sensors, installed at fixed positions, and UWB tags whose position is to be estimated. The sensors contain an array of antennas connected to the UWB radio receiver. They estimate the location of Ubisense tags using the UWB signals received from each of them. Each sensor independently determines the azimuth and elevation AoA of the UWB signal, providing a bearing for each tag. The TDoA information is determined between each sensor pairs connected by a synchronization cable. The company points out that combining AoA and TDoA measurement techniques provides a flexible, powerful and robust localization system, capable of determining a precise location with just one sensor and a precise 3D location using two sensors. Thus, the integration of AoA and TDoA makes it possible to minimize infrastructure and installation costs and improve the reliability and robustness of the system. UWB systems operate in the $6-8$ GHz band and employ an additional narrow-band telemetry channel (2.4 GHz) to provide bidirectional control and telemetric communications with Ubisense tags (monitoring battery, button, Light Emitting Diodes (LEDs), etc.). The tag updating rate can be adjusted between 0.1 and 20 Hz. According to the manufacturer, the maximum operating range of the Ubisense 7000 system is over 160 m and the resulting accuracy does not exceed 15 cm in 3D. A kit with six sensors and ten tags costs $26,900$ Euros (including Value-Added Tax (VAT) and shipping).

BeSpoon [57] is a French start-up that has developed a miniature IR-UWB system. They were the first manufacturer to prove that UWB technology can be successfully integrated into a smartphone. Their "SpoonPhone" prototype has been used by hardware manufacturers and software developers to conduct research and evaluation. This phone along with 6 tags costs 1699 euros (VAT and shipping included). Now, this company has changed its sales strategy and their products are sold in the form of general purpose modular kits (UM100) to design customized solutions for each customer. These modules use UWB channel 2 (3.99 GHz) and offer the possibility to obtain good precision (down to 10 cm), large coverage (up to 880 m in line of sight) with a receiver sensitivity down to −118 dBm. The UWB radio can be activated in the SpoonPhone in the same way as the WiFi/BLE radio is enabled in a phone, i.e. by activating it through a menu. The UWB antenna is also used for WiFi communication and is located at the top left of the phone screen. A Software Development Kit (SDK) Application Program Interface (API) is available to programmers to access in real time the telemetry data of the various miniature tags on the phone. The average range measurement rate is 2.5 Hz.

DecaWave DW1000 modules [58] are fully integrated low power Complementary Metal Oxide Semiconductor (CMOS) chips that comply with the IEEE 802.15.4−2011 UWB standard. They allow to perform distance measurements with an accuracy of ± 10 cm using TWR (ToF) measurements. This system is capable of estimating the real-time position of a moving tag with an accuracy of about ± 30 cm in X and Y directions, using either TWR (ToF) measurements or one-way TDoA approaches. A maximum measurable range of 300 m is possible under ideal conditions. This company provides the TREK1000 development kit for US$ 925 (plus import customs fees). This kit contains four fully functional UWB anchors, which consist of a DW1000 UWB ranging chip, an STM32F105 ARM Cortex M3 processor and an omnidirectional antenna. The anchors are able to interconnect and estimate the distance between them. An external device (computer) can connect to any available anchor via Universal Serial Bus (USB) to collect all inter-anchor ranges. Each UWB anchor can be configured by changing the Dual In-Line Package (DIP) switches on the Printed Circuit Board (PCB) board, to toggle between the anchor and tag function. These switches can also be used to choose between two channel options (2 and 5), which correspond to the central frequencies 3.99 and 6.48 GHz, and data rates 110 kb/s and 6.8 Mb/s respectively. By default, the system uses the 4 GHz central frequency and a data rate of 110 kb/s. This configuration is recommended for maximum distance measurement. According to the manufacturer, the updating rate of a moving tag must be 3.5 Hz. This frequency is reduced when the number of tags increases because they are multiplexed over time.

The performance of these three systems (Ubisense, BeSpoon and DecaWave) is compared in [59]. It has been shown that these systems reach even subcentimeter accuracies under still air conditions. However, they require a prior knowledge of at least three anchors, which implies synchronization between them. Therefore, anchor clock drifts, RF and Analog-to-Digital Converter (ADC) front-end delays and their long-term variations are the main factors limiting the performance of these systems.

In the following, a system attempting to mitigate this problem while ensuring good accuracy, resolution, coverage and a reasonable price will be presented.

1.7 Proposed UWB Indoor Localization System

As already outlined in Section 1.4, there are several wireless technologies in the literature used for indoor positioning. The design methodology and the selected technology are critical factors affecting ILS performance. Among the different technologies, ultra-wideband indoor positioning systems have offered highly accurate solutions, in situations where other radio frequency technologies such as RFID, WiFi or Bluetooth cannot provide these levels of accuracy.

The choice of a positioning method depends on the intended specific application. In general, a positioning system using UWB technology aims to locate one or more targets (e.g. MU) in an indoor environment, such as offices or industrial halls. In such scenario, an UWB system only requires prior knowledge of the reference anchor (e.g. APs) positions to be able to find the location.

Depending on the selected positioning method, synchronization between reference anchors and targets may or may not be necessary. In the ToA method, all reference anchors and targets in the system must be perfectly synchronized. However, in applications where no information on the target is given, only relative time methods such as the TDoA or the AoA are applicable. The TDoA method requires information on the signal propagation time from the target (transmitter) to all reference anchors (receivers). For 3D anchor positioning, at least four reference anchors are required. In the AoA approach, each reference node is equipped with an antenna array linked to an UWB receiver and the difference in receive times is measured. For 3D localization, a minimum of two reference anchors is required, where each anchor must be composed of at least three elements.

For future applications, it is recommended to combine TDoA and AoA techniques to obtain synergistic effects [60]. For example, in the Ubisense positioning system, the combination of AoA and TDoA measurement techniques provides a flexible, powerful and robust localization system that can determine a precise 2D location with just one sensor and an accurate 3D location using two sensors.

It is worth recalling that the short pulse waveforms of UWB technology make it possible to accurately determine the ToF. For this reason, the TDoA technique is extensively used in conventional commercial and experimental indoor UWB localization systems, as described in Section 1.6. In these systems, different algorithms such as triangulation, multilateration or received data processing are applied to TDoA measurements in order to determine the position of the target. This is achievable only if synchronization between the reference anchors and prior knowledge of at least three reference anchors in multilateration or triangulation methods are ensured.

From the knowledge acquired in the above study, our proposed ILS is based on UWB technology operating in the European $3-4$ GHz band. This band is used as a proof of concept, before moving to the $6-10$ GHz band. This work is in line with the one developed by R. Kumar [61] in which a Frequency Modulated Continuous Wave (FMCW) signal is used. Thus, the main scientific objective is to implement a tracking system using the UWB multistatic radar system to provide real-time 2D location of transponders or active tags. This system includes a base station having 2 co-located UWB radars (to overcome time constraints) and UWB tags. The location is done in polar coordinates (distance and azimuth angle) by combining the principles of interferometry and goniometry, assuming a propagation channel with a direct path, or LoS between the station and the badge.

The proposed indoor location system consists of two main components, a transmitter/receiver (transceiver) station acting as a Localization Base Station (LBS) and an Active Tag (AT). The LBS has one transmitting channel and two identical and independent receiving channels. UWB pulses covering a bandwidth of 4 GHz ($0-4$ GHz) will be generated by a pulse generator and placed in the available bandwidth of the antenna ($3-4$ GHz) before being transmitted to the AT. The AT is used as an active transponder in which a delay τ will be applied to the received UWB pulse. The use of such a delay is very important because it helps the system to separate the LBS signal from the backscattered signals of an indoor environment. The intended signal and the broadcast ones will therefore have a different arrival time as in the ground stations of Distance Measuring Equipment (DME) systems dedicated to air navigation [62]. Finally, the delayed signal will be received by the receiver antennas of the LBS, and the position will be estimated using the duplex UWB method for distance estimation and the phase correlation method for azimuth angle estimation. The method and the full setup will be detailed in Chapter 2 and Chapter 3, respectively.

The objective of the proposed solution is to improve the accuracy, the angular and distance resolutions of the ILS under LoS conditions compared to conventional systems, without prior knowledge of the anchors' position and therefore no synchronization is required between them.

1.8 Conclusion

In this chapter, we have presented a detailed description of the different indoor localization techniques (ToA, TDoA, AoA and RSS) and technologies (GPS, IR, Ultrasonic, WiFi, Bluetooth, RFID and UWB). Taking into account the most relevant aspects of an ILS (accuracy, coverage and cost), we have compared the different technologies used in the literature, and have shown the importance of UWB in current localization systems and its significance in the research and development of future systems that aim to provide better accuracy while maintaining simple complexity and low cost. This motivated us to adopt it in the work of this thesis to design a low complexity microwave system that can accurately locate people inside a building in 3D. As a first step, we have proposed an UWB system for 2D indoor localization based on radial distance and Azimuth angle measurements. In the next chapter, the main elements of UWB technology required for its implementation in the ILS will be presented along with a detailed description of the proposed methods for achieving high precision and resolution of the position estimation.

Bibliography

[1] D. Munoz, F. B. Lara, C. Vargas and R. Enriquez-Caldera, "Position Location Techniques and Applications," Academic Press, 2009. Cited page 8

[2] J. Hightower and G. Borriello, "Location Sensing Techniques," IEEE Computer, vol. 34, no. 8, pp. 57–66, 2001. Cited page 8

[3] A.M.H. Khalel, "Position Location Techniques in Wireless Communication Systems," Thesis, Blekinge Institute of Technology, Department of Electrical Engineering, 2010. Cited page 8

[4] B.O'Keefe, "Finding Location with Time of Arrival and Time Difference of Arrival Techniques," ECE Senior Capstone Project, 2017. Cited page 9

[5] H. Liu, H. Darabi, P. Banerjee and J. Liu, "Survey of Wireless Indoor Positioning Techniques and Systems," IEEE Transactions on Systems, Man and Cybernetics Part C: Applications and Reviews, vol. 37, no. 6, pp. 1067-1080, 2007. Cited page 10

[6] J. Zhu and G.D. Durgin, "Indoor/Outdoor Location of Cellular Handsets Based on Received Signal Strength," Vehicular Technology conference, vol. 1, pp. 92–69, 2005. Cited page 11

[7] B. Li, "Terrestrial Mobile User Positioning Using TDOA and Fingerprinting Techniques," PhD thesis, School of Surveying & Spatial Information Systems, University of New South Wales, 2006. Cited page 11

[8] D. Mohapatra and S. B. Suma, "Survey of Location Based Wireless Services," IEEE International Conference on Personal Wireless Communications (ICPWC), pp. 358–362, January 2005. Cited page 16

[9] `http://www.esa.int/Our_Activities/Navigation/How_satellite_navigation_works`. Cited page 16

[10] F. Seco, A. R. Jimenez, C. Prieto, J. Roa and K. Koutsou, "A Survey of Mathematical Methods for Indoor Localization," IEEE International Symposium on Intelligent Signal Processing (WISP), pp. 9–14, August 2009. Cited page 16

[11] H. Huang, "Post Hoc Indoor Localization Based on RSS Fingerprint in WLAN," Thesis, University of Massachusetts Amherst, Electrical and Computer Engineering, China, 2014. Cited page 16

[12] J. Rapinski, S. Cellmer and Z.Rzepecka, "Modified GPS/Pseudolite Navigation Message," The Journal of Navigation, vol. 65, pp. 711–716, 2012. Cited page 16

[13] N. Jardak and N. Semama, "Indoor Positioning Based on GPS-Repeaters: Performance Enhancement Using an Open Code Loop Architecture," IEEE Transactions on Aerospace and Electronic Systems, vol. 45, no. 1, pp. 347–359, 2007. Cited page 17

[14] Y. Gu, A. Lo and I. Niemegeers, "A Survey of Indoor Positioning Systems for Wireless Personal Networks," IEEE Communications Surveys and Tutorials, vol. 11, no. 1, pp. 13–32, 2009. Cited pages 17 and 23

[15] A. Rogalski, "Infrared Detectors: an Overview," Infrared Physics and Technology, vol. 43, no. 3–5, pp. 187–210, 2002. Cited page 17

[16] J. H. Oh, D. Kim and B. H. Lee, "An Indoor Localization System for Mobile Robots Using an Active Infrared Positioning Sensor," Journal of Industrial and Intelligent Information, vol. 2, no. 1, March 2014. Cited page 17

[17] R. Want, A. Hopper, V. Falcao and J. Gibbons, "The Active Badge Location System," ACM Transactions on Information Systems, vol. 10, no. 1, pp. 91-102, January 1992. Cited page 17

[18] X. Fernando, S. Krishnan, H. Sun and K. Kazemi-Moud, "Adaptive Denoising at Infrared Wireless Receivers," SPIE, 2003. Cited page 18

[19] A. Runge, M. Baunach and R. Kolla, "Precise Self-Calibration of Ultrasound Based Indoor Localization Systems," International Conference on Indoor Positioning and Indoor Navigation (IPIN), September 2011. Cited page 18

[20] C. Medina, J. C. Segura and S. Holm, "Feasibility of Ultrasound Positioning Based on Signal Strength," International Conference on Indoor Positioning and Indoor Navigation (IPIN), pp. 1–9, November 2012. Cited page 18

[21] M. Hazas and A. Hopper, "A Novel Broadband Ultrasonic Location System for Improved Indoor Positioning," IEEE Transactions on mobile Computing, vol. 5, no. 5, May 2006. Cited page 18

[22] `http://www.cl.cam.ac.uk/research/dtg/attarchive/bat`. Cited page 18

[23] P. Bahl and V. N. Padmanabhan, "User Location and Tracking in an In-Building Radio Network," Microsoft Research Technical Report: MSR-TR-99-12, February 1999. Cited page 19

[24] H. L. Bertoni, “Radio Propagation for Modern Wireless Systems,” Prentice Hall, 2000. Cited page 19

[25] P. Jiang, Y. Zhang, W. Fu, H. Liu and X. Su, “Indoor mobile localization based on Wi-Fi fingerprint’s important access point,” International Journal of Distributed Sensor Networks, Article ID 429104, 2015. Cited page 19

[26] P. Bahl and V. Padmanabhan, “RADAR: An in-Building RF Based User Location and Tracking System,” IEEE International Conference on Computer Communications (INFOCOM), vol. 2, pp. 775-784, March 2000. Cited page 19

[27] K. Kaemarungsi and P. Krishnamurthy, “Properties of Indoor Received Signal Strength for WLAN Location Fingerprinting,” International Conference on Mobile and Ubiquitous Systems: Networking and Services (MobiQuitous), pp. 14-23, August 2004. Cited page 20

[28] Y. Wang, X. Jia and H. K. Lee, “An Indoor wireless positioning system based on wireless local area network infrastructure,” International Symposium on Satellite Navigation Technology Including Mobile Positioning and Location Services, 2003. Cited page 20

[29] S. Kawakubo, A. Chansavang, S. Tanaka, T. Iwasaki, K. Sasaki, T. Hirota, H. Hosaka and H. Ando, “Wireless Network System for Indoor Human Positioning,” International Symposium on Wireless Pervasive Computing, pp. 1-6, 2006. Cited page 20

[30] P. Prasithsangaree, P. Krishnamurthi and P. K. Chrysanthis, “On indoor position location with wireless LANs,” IEEE International Symposium on Personal, Indoor and Mobile Radio Communications, vol. 2, pp. 720–724, September 2002. Cited pages 21 and 22

[31] A. A. Khudhair, S. Q. Jabbar, M. Q. Sulttan and D. Wang, “Wireless Indoor Localization Systems and Techniques: Survey and Comparative Study,” Indonesian Journal of Electrical Engineering and Computer Science, vol. 3, no. 2, pp. 392–409, August 2016. Cited page 21

[32] C. Bisdikian, “An Overview of The Bluetooth Wireless Technology,” IEEE Communications Magazine, vol. 39, no. 12, pp. 86–94, 2001. Cited page 21

[33] R. Faragher and R. Harle, “An Analysis of the Accuracy of Bluetooth Low Energy for Indoor Positioning Applications,” International Technical Meeting of the Satellite Division of the Institute of Navigation, 2014. Cited page 22

[34] L. M. Ni and Y. Liu, “LANDMARC: Indoor Location Sensing Using Active RFID,” IEEE International Conference on Pervasive Computing and Communications, pp. 407-416, 2003. Cited pages 22 and 23

[35] R. Weinstein, “RFID: a Technical Overview and its Application to The Enterprise,” IT Professional, vol. 7, no. 3, pp. 27–33, 2005. Cited page 22

[36] H. D. Chon, S. Jun, H. Jung and S. W. An, “Using RFID for Accurate Positioning,” International Symposium on GNSS, December 2004. Cited page 22

[37] J. Hightower, R. Want and G. Borriello, “SpotON: An Indoor 3D Location Sensing Technology Based on RF Signal Strength,” University of Washington, February 2000. Cited page 23

[38] M. G. Di Benedetto and B. R. Vojcic, “Ultra Wide Band Wireless Communications: a Tutorial,” Journal of Communications and Networks, vol. 5, no. 4, pp. 290–302, 2003. Cited page 23

[39] I. Y. Immoreev, “Practical Applications of UWB Technology,” IEEE Aerospace and Electronic Systems Magazine, vol. 25, February 2010. Cited page 23

[40] S. J. Ingram, D. Harmer and M. Quinlan, “UltraWideBand Indoor Positioning Systems and Their Use in Emergencies,” IEEE Conference on Position Location and Navigation Symposium, pp.706-715, April 2004. Cited page 23

[41] Y. Zhang, W. Liu, Y. Fang and D. Wu, “Secure Localization and Authentication in Ultra-Wideband Sensor Networks,” IEEE Journal on Selected Areas in Communications, vol. 24, no. 4, pp. 829-835, 2006. Cited page 24

[42] `https://bluflux.com/what-happened-to-ultra-wideband-uwb-technology`. Cited page 24

[43] `https://www.eliko.ee/uwb-technology-indoor-positioning`. Cited page 24

[44] `http://www.ubisense.net`. Cited page 24

[45] S. Gezici, “A Survey on Wireless Position Estimation,” Wireless Personal Communications, vol. 44, no. 3, pp. 263–282, 2008. Cited page 25

[46] R. Faragher and R. Harle, “Location Fingerprinting with Bluetooth Low Energy Beacons,” IEEE Journal on Selected Areas in Communications, vol. 33, no. 11, pp. 2418–2428, 2015. Cited page 27

[47] A. R. Jimenez, J. C. Prieto, J. L. Ealo, J. Guevara and F. Seco, “A Computerized System to Determine the Provenance of Finds in Archaeological Sites using Acoustic Signals,” Journal of Archaeological Science, vol. 36, no. 10, pp. 2415–2426, October 2009. Cited page 27

[48] A. Rice and R. Harle, “Evaluating Lateration-based Positioning Algorithms for Fine-grained Tracking,” Joint Workshop on Foundations of Mobile Computing, pp. 54-61, 2005. Cited page 27

[49] S. Tsuzuki, “High-speed Power-line Communication and its Application to a Localization System,” IEICE Transactions on Fundamentals of Electronics, Communications and Computer Sciences, no. 11, pp. 3006-3012, 2006. Cited page 27

[50] R.J. Fontana, “Recent System Applications of Short-Pulse Ultra- Wideband (UWB) Technology,” IEEE Microwave Theory and Techniques, vol. 52, no. 9, September 2004. Cited page 28

[51] L. Zwirello, T. Schipper, M. Harter and T. Zwick, “UWB Localization System for Indoor Applications: Concept, Realization and Analysis,” Journal of Electrical and Computer Engineering, 2012. Cited page 30

[52] R. Merz, F. Chastellain, C. Botteron, A. Blatter and A. Farine, “An Experimental Platform for an Indoor Location and Tracking System,” European Navigation Conference, April 2008. Cited page 30

[53] L. Zwirello, T. Schipper, M. Jalilvand and T. Zwick, “Realization Limits of Impulse-based Localization System for Large-Scale Indoor Applications,” IEEE Transactions on Instrumentation Measurement, vol. 64, no. 1, pp. 3951, January 2015. Cited page 30

[54] Y. Bai and X. Lu, “Research on UWB Indoor Positioning Based on TDOA Technique,” International Conference on Electronic Measurement and Instruments, pp. 1167–1170, August 2009. Cited page 31

[55] R. J. Fontana, E. Richley and J. Barney, “Commercialization of an Ultra Wideband Precision Asset Location System,” IEEE Conference on Ultra Wideband Systems and Technologies, pp. 369–373, November 2003. Cited page 31

[56] T. Phebey, “The Ubisense Assembly Control Solution for BMW,” RFID Journal Europe Live, 2010. Cited page 31

[57] B. Krulwich, “Ultra-Wideband Poised to Enter Smartphones: A Location Opportunity,” GPS Business News, 2014. Cited page 31

[58] C. Gabriel, “UWB’s Dream is Still Alive in Micro-Location,” Rethink Wireless, 2014. Cited page 32

[59] A. Ramn, J. Ruiz and F. S. Granja, “Comparing Ubisense, BeSpoon, and DecaWave UWB Location Systems: Indoor Performance Analysis,” IEEE Transactions on Instrumentation Measurement, vol. 66, no. 8, August 2017. Cited page 32

[60] Z. Xiao, G. Tan, R. Li and K. Yi, “A Joint Localization Scheme Based on IR-UWB for Sensor Network,” International Conference on Wireless Communications, Networking and Mobile Computing, September 2011. Cited page 33

[61] R. Kumar, "Indoor Localisation For Telemonitoring," Ph.D. dissertation, Telecom Paristech, Electronics and Communications, Paris, France, 2014. Cited page 34

[62] T. Jalloul and W. Ajib, "DME/DME Navigation Using a Single Low-Cost SDR and Sequential Operation," Digital Avionics Systems Conference, October 2014. Cited page 34

Chapter 2

Proposed UWB-based Method for Position Estimation

2.1 Introduction

Several properties associated with UWB signals, such as high accuracy, high multipath immunity, limited interference and immunity to other radio systems, etc., have a direct relationship to the location problem. The features of UWB technology allow to explore a new range of applications, including military applications, medical applications (patient tracking), family communications (child monitoring), search and rescue (communications with firefighters, avalanche or earthquake victims), home control applications, logistics (package tracking) and security applications (tracking authorized persons in high security areas). Therefore, the characteristics of UWB technology make it the promising solution for indoor localization systems.

To exploit the potential centimeter-level positioning accuracy provided by the large bandwidth of UWB systems, a significant number of studies based on the ToA estimation have been conducted, which are application-specific. For example, some proposals focus on achieving maximum resolution regardless of the complexity of the system, while others seek a less complex system that is sufficiently accurate for the desired application.

This chapter outlines the essential elements of UWB technology required for its implementation in the ILS. The definition of UWB signals, UWB regulations and the characterization of UWB indoor propagation are described in Section 2.2. The Cramer-Rao lower bound (CRLB) for ToA estimation in multipath channels is presented in Section 2.3. Several state-of-the-art methods based on ToA estimation with UWB pulses are illustrated in Section 2.4. A brief description of the proposed system and the adopted waveform are provided in Section 2.5. Two methods for estimating distance and small path difference are proposed in Section 2.6 and Section 2.7, respectively. Finally, the chapter ends with a conclusion in Section 2.8.

2.2 UWB Features

Faced with the emergence of communication and localization systems, it is essential and even primordial that these systems can coexist with each other (optimal use of existing frequency resources). For this reason, in 2002, the Federal Communications Commission (FCC) authorized the use of UWB signals with other signals in the same band, under certain conditions and without License. This section will provide the definition of the UWB and some of its specific features as well as the regulations in force.

2.2.1 Definition

UWB signals are very short pulses of the order of a few pico or nano seconds having a bandwidth Bw greater than 500 MHz according to the FCC definition. Another way to distinguish UWB signals from other types of signals is through the fractional bandwidth B_f defined as the ratio of the bandwidth Bw at -10 dB points to the center frequency f_c, as shown in Figure 2.1, i.e.

$$B_f = \frac{Bw}{f_c} = 2 \times \frac{f_H - f_L}{f_H + f_L} \tag{2.1}$$

where f_H and f_L are the upper and lower frequencies of the -10 dB emission points respectively.

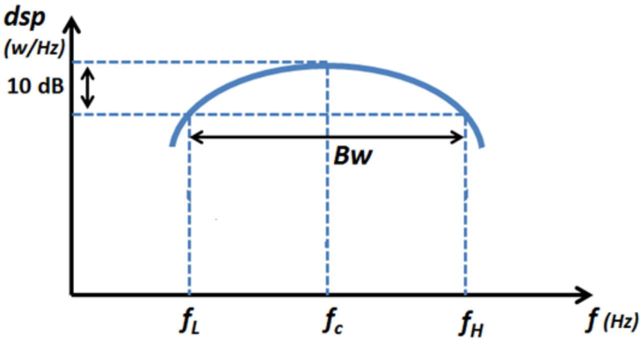

Figure 2.1 – Power spectral density of an UWB signal.

Depending on the value of B_f , FCC has classified the signals as follows

- Narrowband: $B_f < 1\%$
- Wideband: $1\% < B_f < 20\%$
- Ultra-Wideband: $B_f > 20\%$

Therefore, UWB signals must have a fractional bandwidth B_f larger than 20% at all times of transmission [1]. An UWB signal can be any wideband signal [2–4], such as Gaussian, chirp, wavelets or hermit-based short-duration pulses.

2.2.2 UWB Regulations and Standards

The United States (U.S.) regulations for UWB systems were first established in February 2002 by the FCC [5], providing some very conservative rules to ensure that UWB technology would not interfere with other radio systems. For instance, the FCC has allocated in this law the $3.1 - 10.6$ GHz frequency band for UWB systems, in order to protect existing communication systems offering services in the lower frequency bands. In this way, the authorized power is also limited and the power spectral density must be very low to not exceed -41.3 dBm/MHz in average power.

Figure 2.2 and Figure 2.3 represent the UWB emission limit under U.S. regulations for indoor and outdoor systems, respectively. As can be seen, to protect GPS receivers in the $0.96 - 1.61$ GHz band, the degree of attenuation required in the $1.61 - 3.1$ GHz band is higher in an outdoor environment.

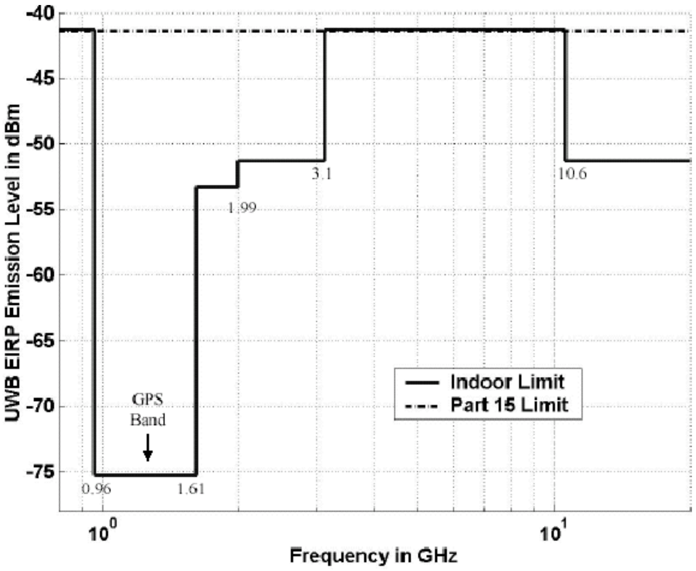

Figure 2.2 – Spectral masks defined by the FCC for Indoor environment [6].

In 2007, the Electronic Communications Committee (ECC) - a committee of the Conference of Postal and Telecommunications Administrations (CEPT) in Europe - also allocated a frequency band in Europe for the unlicensed use of UWB communications and radar systems [8]. This mask provides a maximum mean Effective Isotropic Radiated Power (EIRP) density of -41.3 dBm/MHz from 6 to 8.5 GHz. The signal level below 6 GHz must be attenuated by 28.7 dB to -70 dBm/MHz and above 8.5 GHz by 23.7 dB to -65 dBm/MHz. Figure 2.4 compares the authorized Power Spectral Densities (PSDs) between ECC and

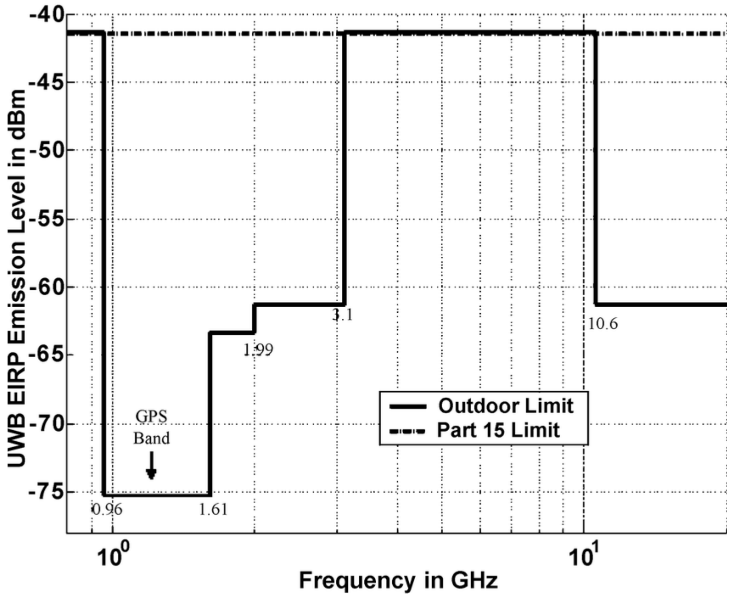

Figure 2.3 – Spectral masks defined by the FCC for outdoor environment [7].

FCC regulations.

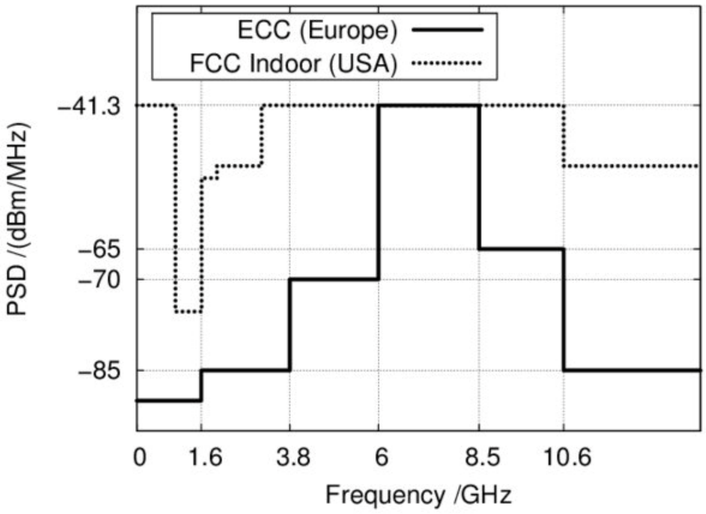

Figure 2.4 – Comparison between the European UWB mask and the FCC indoor mask [9].

Parallel to the international regulatory process, a standardization framework was established in the U.S. and ended up by proposing

- **The IEEE 802.15.3a standard [10]**, which targets high-rate and short-range applications around the 2.4 GHz frequency.
- **The IEEE 802.15.4a standard [11]**, which targets low rate communications (250

Kbps) dedicated to wireless personal networks.

In practice, the adoption of the IEEE 802.15.4a standard involves two Physical (PHY) layers:

- The Impulse Radio - UWB (IR-UWB) PHY layer for communication and/or localization systems. This physical layer uses three sub-bands Sub-GHz (0.25 – 0.75 GHz), Low band (3.244 – 4.742 GHz) and High band (5.944 – 10.234 GHz).
- The Chirp Spread Spectrum (CSS) PHY layer uses the 2.4 – 2.4835 GHz band for communications only.

For this standard, the frequency bands of the IR-UWB PHY layer have been divided into 16 sub-bands of 499.2 MHz width as shown in Table 2.1.

Table 2.1 – UWB channels for IEEE 802.15.4a standard

UWB Band	**Channel number**	**Central Frequency (MHz)**	**Bandwidth (MHz)**
Sub-GHz	0	499.2	499.2
Low band	1	3494.4	499.2
	2	3993.6	499.2
	3	4492.8	499.2
	4	3993.6	1331.2
High band	5	6489.6	499.2
	6	6988.8	499.2
	7	6489.6	1081.6
	8	7488.0	499.2
	9	7987.2	499.2
	10	8486.4	499.2
	11	7987.2	1331.2
	12	8985.6	499.2
	13	9784.8	499.2
	14	9984.0	499.2
	15	9484.8	1354.97

UWB technology is seen as a very interesting and innovative solution for a large number of applications that are generally classified into three categories [12]:

- **Imaging systems:** include Ground Penetration Radar (GPR) and penetration into or through walls, surveillance and medical imaging systems. These systems are allowed to transmit below 960 MHz or between 3.1 and 10.6 GHz.

- **Vehicle radar systems:** These are integrated into the vehicle's navigation system to determine the distance to objects. Systems in this category are mainly used outdoor, which could increase the risk of jamming other services. They are allowed to transmit between 22 and 29 GHz with some restrictions below 24 GHz.

- **Communication systems:** This category includes short-range communication systems, such as wireless personal networks and measurement systems. They are allowed to use the frequency band 3.1 – 10.6 GHz in both indoor and outdoor environments using portable terminals.

2.2.3 UWB Indoor Channel Model

The particularities of the UWB signal make its channel characteristics different from the existing narrow-band communication systems based on the Continuous Wave (CW). On the top of that, the propagation environment of the UWB signal is one of the most important factors that affects the performance of a wireless communication system. For this reason, it is crucial to establish an accurate channel model to design and analyze the positioning system. To this end, the IEEE 802.15.4a standard working group has developed a statistical model for the propagation of UWB signals [13], relevant for the 3 – 10 GHz frequency band.

The channel model of the IEEE 802.15.4a standard is based on the Saleh-Valenzuela model [14]. This model begins with the physical realization that the rays arrive in clusters, i.e. each cluster consists of several rays. The cluster arrival times, or the arrival times of the first cluster rays, are modelled as a Poisson arrival process with a fixed rate Λ. Within each cluster, the subsequent rays also arrive according to a Poisson process with another fixed rate λ. Moreover, the amplitudes of the multiple trajectory follow a Rayleigh distribution, the phase angles are uniform and independent random variables, the power decreases exponentially with a time constant Γ for clusters and a constant γ_l in each cluster l, as shown in Figure 2.5.
Thus, the Channel Impulse Response (CIR) is expressed as

$$h(t) = \sum_{l=0}^{L} \sum_{k=0}^{K} \alpha_{k,l} e^{j\phi_{k,l}} \delta(t - T_l - \tau_{k,l}) \tag{2.2}$$

where $\alpha_{k,l}$ is the channel gain coefficient of the k-th component in the l-th cluster, T_l is the delay of the l-th cluster, and $\tau_{k,l}$ is the delay of the path k relative to the l-th cluster arrival time T_l. The phases $\phi_{k,l}$ are uniformly distributed, i.e. for a bandpass system, the phase is considered as a random variable uniformly distributed in the range $[0, 2\pi]$.

The resulting model for the 3 – 10 GHz range is a generalized Saleh-Valenzuela (SV) model, in which the parameters are defined for indoor residential, indoor office, industrial,

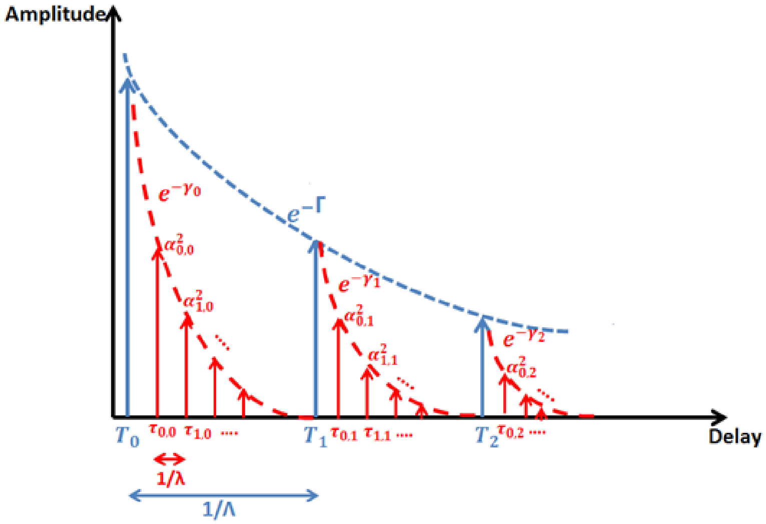

Figure 2.5 – Concept of the SV model.

outdoor and farm environments. For each one of these environments, LoS and NLoS are identified, except in farm environments, where only NLoS situations are considered as shown in Table 2.2. The models are based on measurement campaigns, excluding again the farm environment, which is based solely on simulations.

Table 2.2 – Environments of the IEEE propagation model for UWB signals

Channel	Description
CM1	Residential LoS
CM2	Residential NLoS
CM3	Office LoS
CM4	Office NLoS
CM5	Outdoor LoS
CM6	Outdoor NLoS
CM7	Industrial LoS
CM8	Industrial NLoS
CM9	Farm, Snow-Covered Open Area

2.3 Cramer-Rao Lower Bound for ToA estimation

The time of flight of a signal traveling from one node to another, also known as ToA, provides information about the distance between these two nodes, as explained in Chapter 1. Therefore, estimating this parameter is crucial for localization. To do so, it is possible to use probabilistic models to perform a statistical estimation that attempts to determine the value of the parameter of interest through observations over a set of samples associated with the model under consideration. In the following, we will introduce some general notations and definitions about the estimation theory, then proceed to its application in the ToA estimation.

In general, if the true value of the parameter to be measured is θ, its statistical estimate $\hat{\theta}$ is derived as a function of a sequence of the process samples/realizations associated with θ, i.e.

$$\hat{\theta}(X_1, X_2, \cdots, X_n) \tag{2.3}$$

where $\{X_1, X_2, \cdots, X_n\}$ are independent real random variables.

Ideally, the average value of the estimator, aka its expectation, should be equal to the true value

$$\mathbb{E}_\theta\Big[\hat{\theta}(X_1, X_2, \cdots, X_n)\Big] = \theta \tag{2.4}$$

Otherwise, the estimator has a bias, $b(\theta)$, and is considered to be biased

$$b(\theta) = \mathbb{E}_\theta\Big[\hat{\theta}(X_1, X_2, \cdots, X_n)\Big] - \theta \tag{2.5}$$

The performance of an estimator can be measured according to different criteria; among the most commonly used, the mean square error $MSE(\theta)$

$$MSE(\theta) = \mathbb{E}_\theta\bigg[\Big(\hat{\theta}(X_1, X_2, \cdots, X_n) - \theta\Big)^2\bigg] \tag{2.6}$$

Therefore, the estimator is better when the error is low. Note that the $MSE(\theta)$ of an unbiased estimator is equal to its variance

$$\begin{aligned} MSE(\theta) &= \mathbb{E}_\theta\bigg[\Big(\hat{\theta}(X_1, X_2, \cdots, X_n) - \mathbb{E}_\theta\big[\hat{\theta}(X_1, X_2, \cdots, X_n)\big]\Big)^2\bigg] \\ &= Var\Big(\hat{\theta}(X_1, X_2, \cdots, X_n)\Big) \end{aligned} \tag{2.7}$$

An unbiased estimator with minimal variance is defined as one that has the minimal variance for any value of θ. This minimum value or maximum possible accuracy can be calculated using CRLB [15]

$$MSE(\theta) = Var\Big(\hat{\theta}(X_1, X_2, \cdots, X_n)\Big) \geq CRLB \tag{2.8}$$

The minimum variance estimator does not always exist. The Cramer-Rao bound can be used to evaluate the quality of an estimator by indicating whether or not it has a minimum variance.

Back to the localization problem, and more precisely to the case of estimating the distance from the ToA. A first model considers only the received signal $r(t)$ via the direct path (without multiple paths)

$$r(t) = \alpha.s(t - \tau) + n(t) \tag{2.9}$$

where τ is the ToA, α is the gain of the channel, $s(t)$ is a unit energy pulse and $n(t)$ is a centered Gaussian noise with a spectral density equal to $N_0/2$.

The Cramer-Rao bound for the parameter τ is given by [16]

$$Var[\hat{\tau}] \geq \frac{1}{8 \times \pi^2 \times \beta^2 \times SNR} \tag{2.10}$$

where $\hat{\tau}$ is an unbiased estimator, $SNR = \alpha^2 E_p/N_0$ is the signal to noise ratio, E_p is the mean received energy from $s(t)$ and β is its effective bandwidth expressed as a function of the Fourier transform $S(f)$ of the transmitted signal $s(t)$

$$\beta = \sqrt{\frac{\int_{-\infty}^{+\infty} f^2 |S(f)|^2 df}{\int_{-\infty}^{+\infty} |S(f)|^2 df}} \tag{2.11}$$

This result shows that the accuracy of the ToA measurement can be improved by increasing the SNR and the effective bandwidth of the received signal. Therefore, UWB signals are particularly suitable for ToA measurement.

For multipath propagation, the above formula can be generalized if the received signals from the different paths do not overlap, i.e. the signals are separated by a larger width than the transmitted pulse τ_p

$$|\tau_{li} - \tau_{lj}| \geq \tau_p \qquad \forall i \neq j \tag{2.12}$$

In this case, the signal model can be expressed as

$$r(t) = \sum_{l=1}^{L} \alpha_l.s(t - \tau_l) + n(t) \tag{2.13}$$

where $s(t - \tau_l)$ is a unit energy pulse, L is the number of paths, α_l and τ_l are the gains and the delays of these paths respectively, and $n(t)$ is a centered Gaussian noise with a spectral density equal to $N_0/2$.

Then, the Cramer-Rao bound can be expressed for each path l characterized by its signal to noise ratio $SNR_l = \alpha_l^2 E_p/N_0$ as [17]

$$CRLB[\hat{\tau}_l] = \frac{1}{8 \times \pi^2 \times \beta^2 \times SNR_l} \tag{2.14}$$

Figure 2.6 shows the CRLB variation in the ToA estimation as a function of the SNR for different bandwidths. For instance, the 1 GHz bandwidth signal has a standard deviation of 0.02 ns (0.3) cm for an SNR of 15 dB and 0.01 ns (0.19) cm at 20 dB. This variation becomes very small when the SNR exceeds 15 dB for any given bandwidth. For this reason, we decided in this work to fix the SNR between 15 and 20 dB.

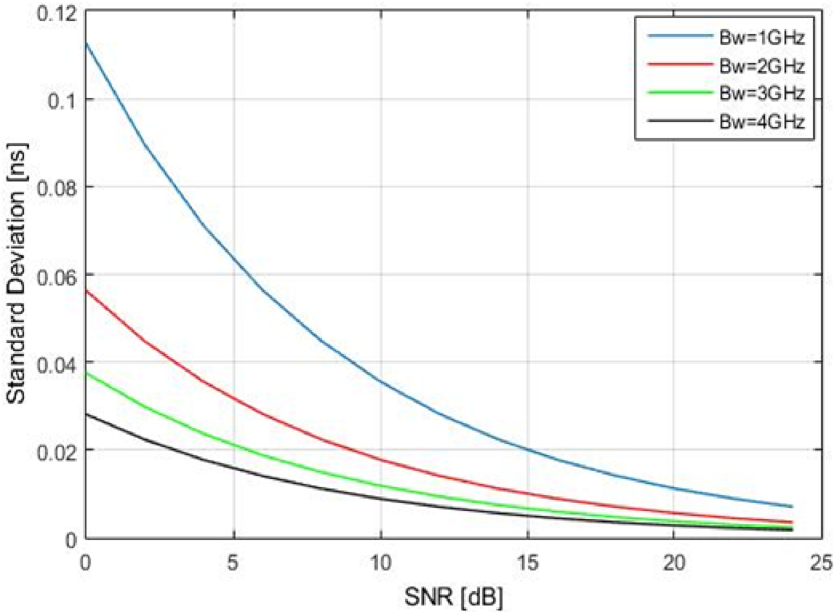

Figure 2.6 – Standard deviation for ToA estimation.

However, the CRLB yields a precision reference that is difficult to approach in practice. In the case of UWB signals, it is mandatory to sample at frequencies higher than the Nyquist frequency, thus involving several GHz. Furthermore, the bound is less accurate when the signal to noise ratio is low.

2.4 ToA Estimation Methods

The high temporal resolution of UWB signals allows a very accurate ToA estimation, as reflected in the Cramer-Rao lower bound. Hence, different approaches for UWB's estimated ToA are addressed in the literature.This section summarizes some of these approaches and provides the corresponding details in Appendix A if necessary.

Optimization Techniques

In [18], the performance of two different position estimation methods based on ToA estimation of the UWB signal for a set of receivers/sensors is investigated. The first one is based on the direct calculation method which gives the exact solutions of a set of simultaneous equations, expressed as the range (distance) between the tag and sensor i

$$\sqrt{(x-x_i)^2+(y-y_i)^2+(z-z_i)^2} = c.(t_i-t_0)^2 \qquad i=1,2,3,4 \tag{2.15}$$

where c is the speed of light, t_i is the ToA at sensor i, t_0 is the transmit time at the tag and (x,y,z) and (x_i,y_i,z_i) are the coordinates of the tag and sensor i, respectively.

On the other hand, the second method examines classical non-linear optimization techniques, and more precisely the Davidon Fletcher-Powell (DFP) quasi-Newton algorithm. The optimal position is estimated by minimizing the objective function $f(p)$ defined as the summation of the quadratic errors for all the sensors N

$$f(p) = \sum_{i=1}^{N}\left[\sqrt{(x-x_i)^2+(y-y_i)^2+(z-z_i)^2} - c.(t_i-t_0)\right]^2 \tag{2.16}$$

where $p = [x,y,z,t_0]^T$ is the unknown vector of the position coordinates (x,y,z) and the transmission time t_0 to be estimated.

Multiple Hypothesis Testing System Model

In [19], the problem of distance estimation in a dense multipath environment is studied by applying a technique that relies on the analysis of the Power Delay Profile (PDP) of the received UWB signal and the theory of segmentation of non-stationary processes. Assuming that the ToA estimate for LoS is equivalent to locating the Break-Point (BP) in a stationary piecewise process characterized by different powers before and after BP, the BP detection is equivalent to the segmentation of non-stationary processes with abrupt changes as shown in Figure 2.7.

The objective is to estimate the BP from the measurements $y = [y_0, \cdots, y_{L-1}]$ according to the optimal classification rule derived from the Neyman-Pearson criterion and extended to several assumptions [20]. The null hypothesis H_0 indicates that there is no change while H_n is the hypothesis of having the BP in the n-th sample.

Matched Filter

In [21], an algorithm for accurately determining the ToA is presented using a combination of match filtering and peak search techniques. This technique aims to detect the direct path signal by searching the measurement results in the time domain for the first peak

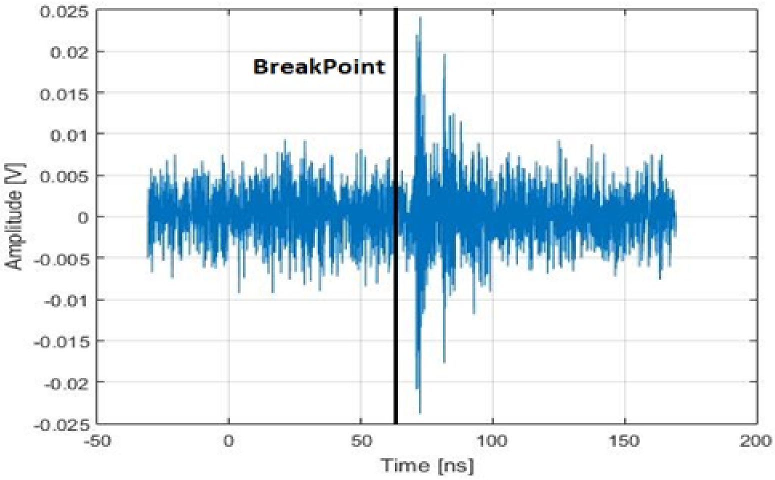

Figure 2.7 – Segmentation Process.

above a dynamic threshold. To do this, the received signal is multiplied by a template signal and then the first peak above the threshold is searched.

Direct Sampling Receiver

In [22], the performance of Stored-Reference (SR), Transmitted-Reference (TR) and Energy Detection (ED) schemes based on ToA estimation techniques are analysed for IR-UWB systems using sub-Nyquist sampling rates. The collected signal at the receiver antenna passes through a Low Noise Amplifier (LNA) and a Band-Pass Filter (BPF). At this stage, any of the previous approaches (SR, TR or ED) can be used to collect energy. Then, the received signal can be sampled after correlation with a SR signal, after correlation with a TR signal, or after a square-law device as shown in Figure 2.8, Figure 2.9 and Figure 2.10, respectively. With the first method (SR signaling), optimal detection is envisaged, i.e. matched filtering. However, in order to have accurate timing and efficient energy capture, high sampling rates in the order of the Nyquist rate are required for SR scheme. On the other hand, both ED and TR schemes can efficiently capture the received energy without requiring the knowledge of the sampling time or the pulse shape (assuming specific delay lines for TR signal), even at sub-Nyquist sampling rates.

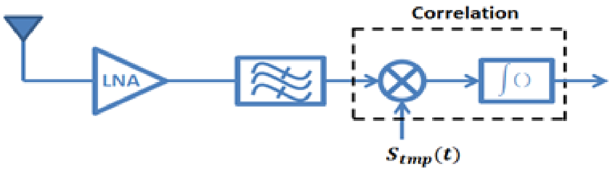

Figure 2.8 – Correlation with a Stored−Reference signal.

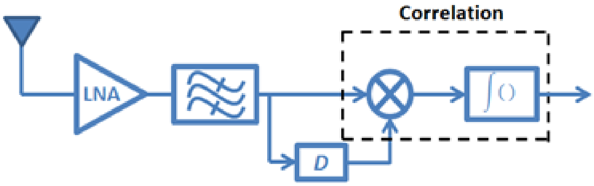

Figure 2.9 – Correlation with a Transmitted–Reference signal.

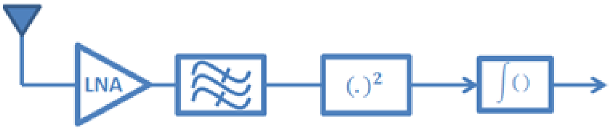

Figure 2.10 – Energy Detection.

The coarsest way to obtain a ToA estimate is the Maximum Energy Selection (MES) from the individual energy samples E_n, while neglecting the information from the neighboring samples, which yields the following

$$\hat{n}_{ToA} = \arg\max_{n}[E(n)] \qquad n = 1, \cdots, N \tag{2.17}$$

where N is the number of samples. However, the energy of neighboring multipath components can be exploited by dividing N into I windows of N_w samples, then combining the energy samples E_n within a window.

$$E_i^{N_w} = \sum_{n=1+iN_w}^{(i+1)N_w} E_n \qquad i = 0, \cdots, I \tag{2.18}$$

Therefore, the main block estimate $\hat{n}_{ToA}$ using the Maximum Energy Sum Selection (MESS) scheme is given by

$$\hat{n}_{ToA} = \arg\max_{i}[E_i^{N_w}] \tag{2.19}$$

Two-step TOA estimators

In [23], a two-step ToA estimation based on the Time Delayed Sampling and Correlation (TDSC) method for Transmitted Reference UWB (TR-UWB) signals is presented. A TR-UWB symbol $d(t)$ consists of a pair of pulses $g_1(t)$ and $g_2(t)$, referred to as a doublet, where $g_1(t)$ is a reference pulse and $g_2(t)$ is an information pulse delayed by a few seconds T_D with respect to the first one. The TDSC method uses a general structure similar to the one used in the delay and correlation receiver to detect TR-UWB signals.

In the coarse step, this method estimate $\hat{\tau}_{ToAc}$ by relying on the sliding correlation over a symbol length to find a signal block where the direct path is enclosed.

In the fine step, the sliding correlation is finely evaluated over the signal block obtained by the coarse step to accurately estimate the starting point of the pulse $\hat{\tau}_{ToAf}$.

Finally, the absolute ToA estimate is the sum of the coarse and fine estimates

$$\hat{\tau}_{ToA} = \hat{\tau}_{ToAc} + \hat{\tau}_{ToAf} \tag{2.20}$$

In [24], strategies based on SR and ED are applied to estimate the ToA, using a signal that corresponds to the IEEE.802.15.4a standard. This signal is transmitted as a frame where each frame, of duration T_f, is divided into N_b blocks, each of duration T_b. These N_b blocks contain a total of N_c chips, each of a duration T_c ns.

The estimation is performed in two steps. In the first one, the frame is analyzed to find the higher energy block $\hat{k}_b$, using an energy detector. To ensure reliable decision variables in this step, the energy for each block is combined from N_1 different frames of the received signal $r(t)$.

In the second step, the estimated block $\hat{k}_b$ is analyzed to find the chip $\hat{k}_c$ where the first signal path is located, by correlating the received signal with a shifted version of the template signal. In this process, the arrival time of the first signal path is estimated through a hypothesis test approach.

Finally, the ToA is obtained by

$$\hat{\tau}_{ToA} = \hat{k}_b T_b + \hat{k}_c T_c \tag{2.21}$$

Dirty Templates

In [25], a blind timing acquisition algorithm for frame-level synchronization is developed. This algorithm is based on simple integrate-and-dump operations over one symbol duration to collect the available multipath diversity. Every symbol information of duration T_s consists of N_f frames, each of duration T_f, making $T_s = N_f.T_f$. Each frame is then used to transmit an ultra-short pulse $p(t)$ of duration $T_p \ll T_f$, , as shown in Figure 2.11. To acquire timing with frame-level resolution, the product of two received waveforms for two adjacent symbols is computed for M symbols. Then, the estimated frame $\hat{n}_f$ is obtained by searching for the maximum average value across the $M/2$ pairs.

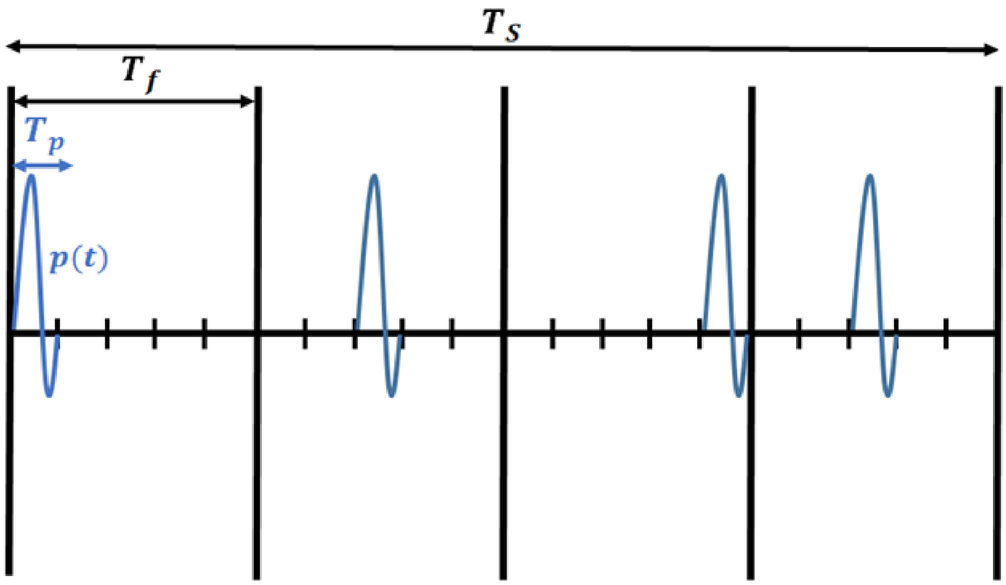

Figure 2.11 – Symbol Format.

Energy Detection

In [26], various ToA estimation algorithms for UWB systems that use a low sampling rate and the energy detection method are analyzed. A symbol of the considered signal is composed of N_s frames. Each frame, of duration T_f, is used to transmit a pulse. In this scheme, the different users are separated through pseudo-random Time Hopping (TH) codes (C_j). In order to estimate the ToA, each frame is divided into N_b blocks of duration $T_b = \frac{3T_f}{2N_b}$ each. Next, the energy E_n in each block $n \in \{1, \cdots, N_b\}$ is calculated from the received signal $r(t)$. Finally, the energies E_n of the block n, calculated in the different N_s frames, are combined as follows

$$Z_n = \sum_{j=1}^{N_s} \int_{(j-1)T_f+(C_j+n-1)T_b}^{(j-1)T_f+(C_j+n)T_b} |r(t)|^2 dt \tag{2.22}$$

For leading edge detection, basic ToA estimation algorithms such as MES algorithm, Threshold Comparison (TC) approach and Maximum Energy Selection with Search-Back (MES-SB) work with Z_n values.

Using MES, the ToA estimate corresponds to the center of the block n that contains the maximum energy Z_n.

$$\hat{\tau}_{MES} = \left(\arg\max_n \{Z_n\} - 0.5\right) T_b = (n_{max} - 0.5) T_b \tag{2.23}$$

In TC approach, the obtained values Z_n are compared to an appropriate threshold ξ, and the center of the first block n that exceeds the threshold corresponds to the ToA estimate

$$\hat{\tau}_{TC} = \left(\min_{n} \left\{ \arg\{Z_n \geq \xi\} \right\} - 0.5 \right) T_b \tag{2.24}$$

where ξ is defined according to the received signal statistics. In addition, a normalized threshold ξ_{norm} can be used based on the minimum and maximum energy values.

$$\xi_{norm} = \frac{\xi - \min\{Z_n\}}{\max\{Z_n\} - \min\{Z_n\}} \tag{2.25}$$

The MES-SB is used to improve the performance of the TC approach when the SNR is low. In this method, once the maximum energy block is identified, w_{SB} blocks preceding it are searched. Note that w_{SB}, known as the search back window, is defined according to the channel statistics. The ToA estimate based on thresholding and backward search is then given by

$$\hat{\tau}_{MES-SB} = \left(\min_{n} \left\{ \arg\{\tilde{Z}_n \geq \xi\} \right\} - 0.5 + (n_{max} - w_{SB} - 1) \right) T_b \tag{2.26}$$

where $\tilde{Z}_n = \left[Z_{n_{max}-w_{SB}}, Z_{n_{max}-w_B-1}, \cdots, Z_{n_{max}} \right]$ is a vector of the w_{SB} blocks.

Most of the algorithms mentioned above are based on the ToA estimate of the strongest path. For instance, the simplest technique is the one using Matching Filtering (MF) of the received signal, where the ToA estimate corresponds to the maximum of the MF output. However, since the strongest path is not necessarily the first arrival path in dense multipath channels, their ToA accuracy is limited.

To solve this problem, channel information techniques can be used, particularly Maximum Likelihood (ML) approaches that jointly estimate channel amplitude and arrival time. However, apart from the great complexity of this approach, the partial overlap of signal paths makes the channel estimation insoluble and therefore degrades the ToA estimation.

Similarly, in some algorithms, prior knowledge of the received pulse shape also adds limitations to the ToA estimate. Therefore, with the change in shape of the different multipath components, it is more difficult to adapt exactly to the received pulse shape.

Due to the above limitations, algorithms based on energy detection are proposed, where energy is collected after certain analog front-end processing. These algorithms do not require precise synchronization or pulse shapes, but rather need a strong signal at the detector input. This requirement is crucial since the ToA estimation is seen as a problem of detecting the leading edge of the signal, which can be erroneous when the noise power is higher than the signal power.

Therefore, even if it is theoretically possible to obtain very accurate ranging, the practical limitations of the above algorithms prevent the localization system from achieving the desired high resolution. At the same time, a trade-off between the required accuracy, resolution and complexity must be taken into account when developing a ToA estimation algorithm. To this end, our objective is to design a new algorithm of low complexity capable of outperforming current algorithms and thereby creating an ILS of higher resolution and accuracy.

2.5 Overview of the Proposed System

Our proposed ILS delivers the 2D position of an AT by estimating a distance d and an Azimuth angle α, as shown in Figure 2.12. The system architecture will be described in detail in Chapter 3.

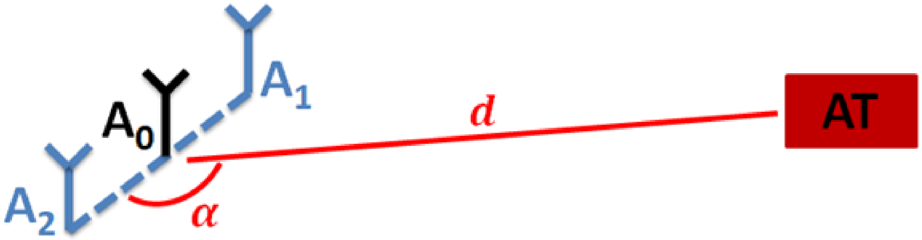

Figure 2.12 – AT Position Estimation.

The radial distance d is obtained by estimating the absolute ToA of the received signals on A_1 and A_2. The azimuth angle α is estimated by computing the TDoA between the two received signals on A_1 and A_2.

To examine the performance of these two methods, we resort to a previous work on UWB radar system [27]. This system uses an impulse signal that generally covers the 3 – 5 GHz bandwidth, which is the lower part of the UWB spectrum. Using ultra-short pulses (nanoseconds) that generate a very large bandwidth confers it many advantages over other systems. They showed that this system could achieve a spatial resolution of about ten cm thanks to its large frequency bandwidth according to

$$R = \frac{c}{2Bw} \tag{2.27}$$

where R is the spatial resolution of the radar, c the speed of light, and Bw the frequency bandwidth.

For instance, for a frequency bandwidth of 2 GHz, the smallest distance that the UWB Radar system can detect is equal to 7.5 cm and the corresponding time of arrival is equal to 0.25 ns.

Based on this result, we can conclude that both the above-mentioned ToA and TDoA estimation algorithms are unable to achieve a high resolution. Therefore, to improve distance and angular resolution, we propose a new algorithm that combines the Duplex UWB method to estimate d and the Phase Correlation (PC) method to determine α through the estimation of the path difference.

2.5.1 Waveform

According to the UWB's low rate standardization, the $3-4$ GHz band is of interest to us. In the time domain, the used unit waveform typically corresponds to a cosine carrier modulated by a Gaussian pulse [28].

$$S(t) = A\cos\left(2\pi f_0 t\right)e^{-\left(\frac{t}{T_p}\right)^2} \tag{2.28}$$

where A is the amplitude of the signal, f_0 the center frequency and $T_p = \frac{1}{\zeta Bw\sqrt{2\pi}}$ with $\zeta = 0.43$ defining the cutoff frequency at -3 dB from the maximum of the power spectral density.

Figure 2.13 shows the used waveforms for a bandwidth frequency Bw of 1 GHz and 500 MHz and Figure 2.14 shows their corresponding spectrum.

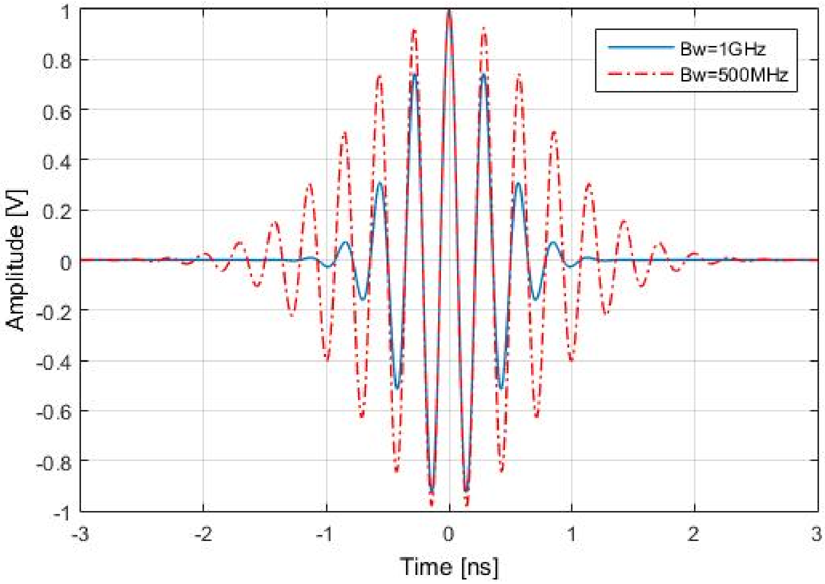

Figure 2.13 – Waveform shapes.

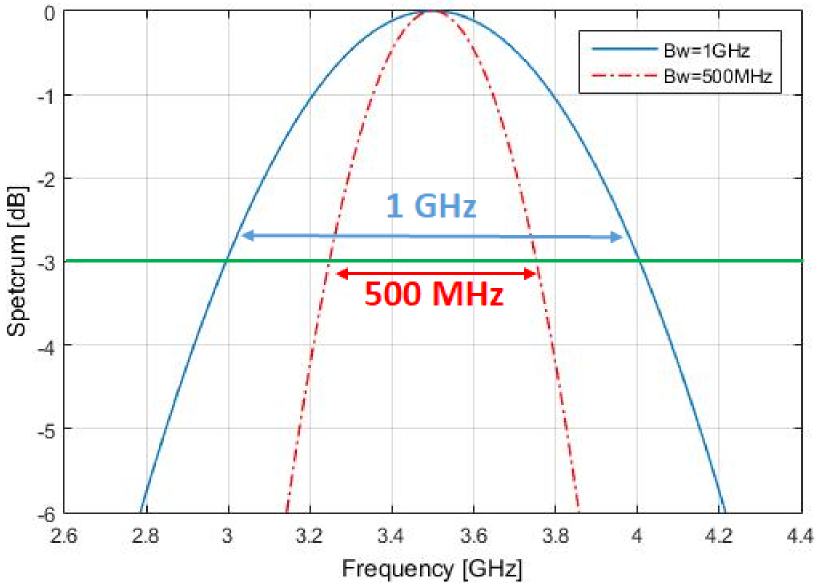

Figure 2.14 – Normalized spectrum.

2.6 Proposed Method for Distance Estimation

In the literature, one way to estimate the distance is through the duplex method [29,30]. This approach consists in transmitting two CW signals at different frequencies, such that the frequency difference Δf is small compared to the used frequency values. Consequently, the information about the distance at which the target is located can be obtained from the difference between the phase shifts of the two signals. Such systems were proposed to measure the range and radial velocity of moving targets, particularly in automotive applications. It is important to mention that the maximum distance in this system is affected by the frequency difference Δf. The major drawback of these solutions is that the accuracy is affected by the multipath channel environment even in LoS situation.

This method can be adjusted to give our system the ability to measure distances using UWB signal. Thus, instead of relying on two CW signals, we propose a new algorithm that uses two different cosine carriers modulated by a Gaussian pulse as a waveform to determine the distance at which a target is located.

2.6.1 Duplex UWB Method

The distance is estimated through the corresponding ToF of a signal, obtained by correlating the emitted signal with the received signals on both receiving chains. The correlation function being used is based on a Duplex UWB method.

This method estimates the distance by using the phase difference while sending two pulses of equal width and two different center frequencies f_1 and f_2, respectively.

Let U and V be defined according to Eq. (2.28) as the two emitted signals by the transmitting chain. Each signal is sent at different time and using distinct center frequency (f_1 and f_2) as shown in Figure 2.15.

$$U(t) = A\cos\left(2\pi f_1 t\right)e^{-\left(\frac{t}{T_p}\right)^2} \tag{2.29}$$

$$V(t) = A\cos\left(2\pi f_2(t-t_s)\right)e^{-\left(\frac{t-t_s}{T_p}\right)^2} \tag{2.30}$$

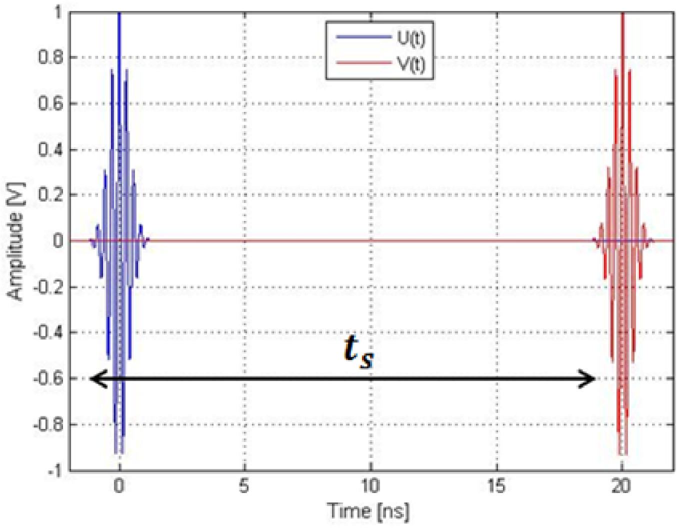

Figure 2.15 – Emitted signals at f_1 and f_2.

where t_s is the starting time of the second emitted pulse.

Let U_i and V_i be the two received signals on the receiving chain i ($i = 1, 2$), as shown in Figure 2.16. We assume that the channel is flat i.e. the channel remains constant during the transmission of the two pulses and that the deformation and distortion of these signals by the circuit components and the environment are exactly the same on both receiving chains. These assumptions are justified since f_1 and f_2 are very close and the distance between the two receiving antennas is much smaller than the distance d, to guarantee that the Plane Wave Condition (PWC) holds.

Therefore, these two pairs of received signals can be expressed as follows

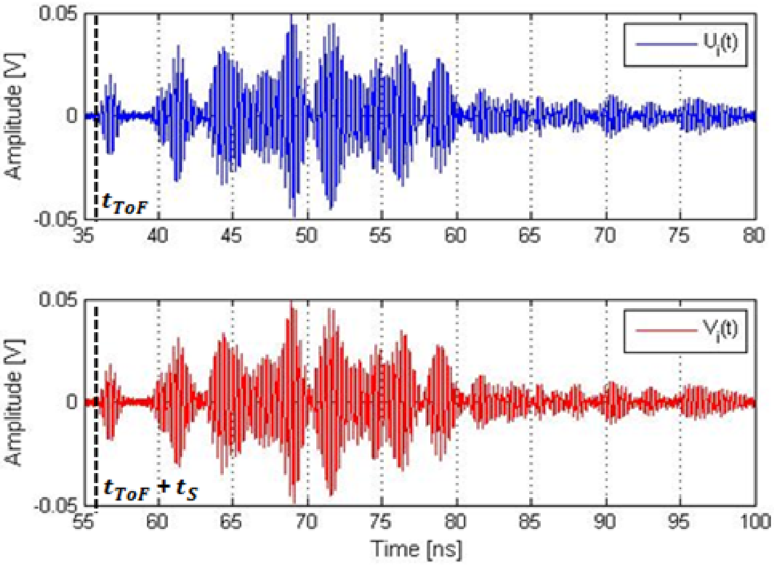

Figure 2.16 – Received signals at f_1 and f_2 on the receiving chain i.

$$\begin{cases} U_1(t) = A' \cos\left(2\pi f_1(t - t_{ToF})\right) e^{-\left(\frac{t-t_{ToF}}{T'}\right)^2} \\ V_1(t) = A' \cos\left(2\pi f_2(t - t_s - t_{ToF})\right) e^{-\left(\frac{t-t_s-t_{ToF}}{T'}\right)^2} \end{cases} \tag{2.31}$$

$$\begin{cases} U_2(t) = A' \cos\left(2\pi f_1(t - t_{ToF} - \Delta t)\right) e^{-\left(\frac{t-t_{ToF}-\Delta t}{T'}\right)^2} \\ V_2(t) = A' \cos\left(2\pi f_2(t - t_s - t_{ToF} - \Delta t)\right) e^{-\left(\frac{t-t_s-t_{ToF}-\Delta t}{T'}\right)^2} \end{cases} \tag{2.32}$$

where A' is the amplitude of the received signal, t_{ToF} the time of flight of the signal (round trip time), Δt the time difference between the two received signals on the two receiving chains and T' the duration of the distorted and broadened pulse.

The duplex UWB method follows the following step to estimate the distance

1. The first step consists in synchronizing all the signals by eliminating the known start time t_s from the pulses of frequency f_2 (the synchronization of the emitted pulses is given in Figure 2.17 as an example and the same operation is performed on V_1 and V_2). Then, the signals of frequency f_1 will be multiplied by the synchronized signals of frequency f_2 on each transmitting/receiving chain as follows

$$U(t).V(t) = \frac{A^2}{2} e^{-2(\frac{t}{T_p})^2} . \left[\cos\left(2\pi(f_2 + f_1)t\right) + \cos\left(2\pi(f_2 - f_1)t\right)\right] \tag{2.33}$$

$$U_1(t).V_1(t) = \frac{A'^2}{2} e^{-2(\frac{t-t_{ToF}}{T'})^2} . \left[\cos\left(2\pi(f_2+f_1)(t-t_{ToF})\right) + \cos\left(2\pi(f_2-f_1)(t-t_{ToF})\right)\right] \tag{2.34}$$

$$U_2(t).V_2(t) = \frac{A'^2}{2} e^{-2(\frac{t-t_{ToF}-\Delta t}{T'})^2} . \Big[\cos\big(2\pi(f_2+f_1)(t-t_{ToF}-\Delta t)\big) + \cos\big(2\pi(f_2-f_1)(t-t_{ToF}-\Delta t)\big)\Big] \tag{2.35}$$

Note that this multiplication can only be done if each pair of signals (U_i, V_i) takes the same time to reach the receiver i.

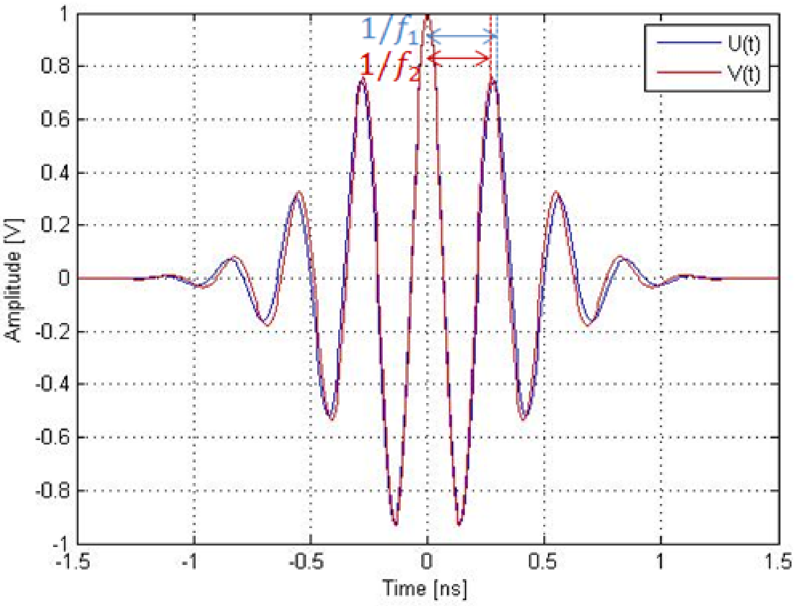

Figure 2.17 – Synchronized emitted signals.

As we can see in Eq. (2.33), (2.34) and (2.35), the resulting signals, shown in Figure 2.18 and Figure 2.19, have two center frequencies $f_2 + f_1$ and $f_2 - f_1$. The second center frequency $f_2 - f_1$ is of interest, since the maximum range of the system is higher when the center frequency is smaller.

2. Then, a low-pass filter is applied to all the pulses obtained above in order to extract the frequency $f_2 - f_1$. The resulting signals after filtering are expressed as follows

$$S(t) = \frac{A^2}{2} e^{-2(\frac{t}{T_p})^2} . \cos\big(2\pi(f_2 - f_1)t\big) \tag{2.36}$$

$$S_1(t) = \frac{A'^2}{2} e^{-2(\frac{t-t_{ToF}}{T'})^2} . \cos\big(2\pi(f_2 - f_1)(t - t_{ToF})\big) \tag{2.37}$$

$$S_2(t) = \frac{A'^2}{2} e^{-2(\frac{t-t_{ToF}-\Delta t}{T'})^2} . \cos\big(2\pi(f_2 - f_1)(t - t_{ToF} - \Delta t)\big) \tag{2.38}$$

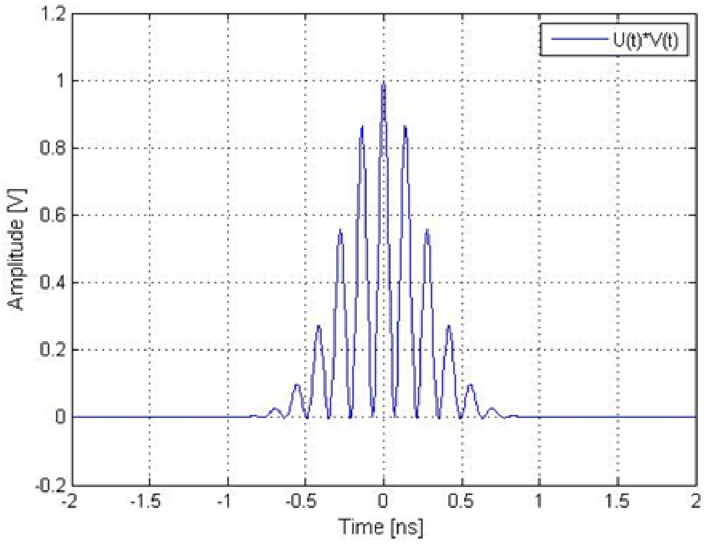

Figure 2.18 – Obtained emitted signal after multiplication of U and V.

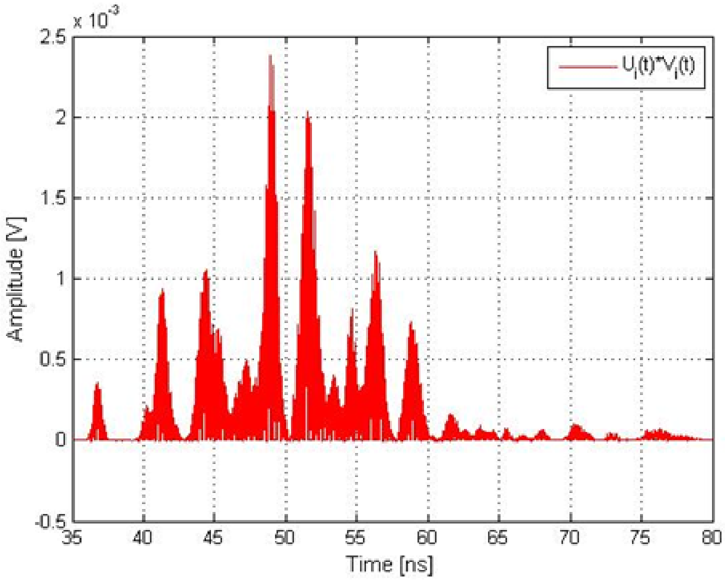

Figure 2.19 – Obtained received signal on the receiving chain i after multiplication of U_i and V_i.

where $S(t)$ and $S_i(t)$ $(i = 1, 2)$ are the pulses obtained at center frequency $f_2 - f_1$ on the transmitting chain and the receiving chains i, as shown in Figure 2.20 and Figure 2.19, respectively.

3. Finally, the distance is estimated by detecting the direct path of each transmission represented by the first peak of $S_1(t)$ and $S_2(t)$, respectively. The difference between the time corresponding to the peak of $S(t)$ and the time corresponding to each above-

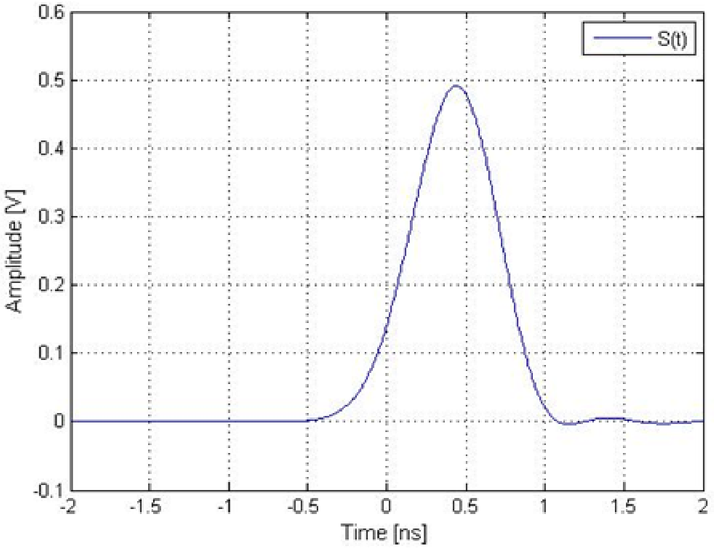

Figure 2.20 – Obtained emitted signal after filtering.

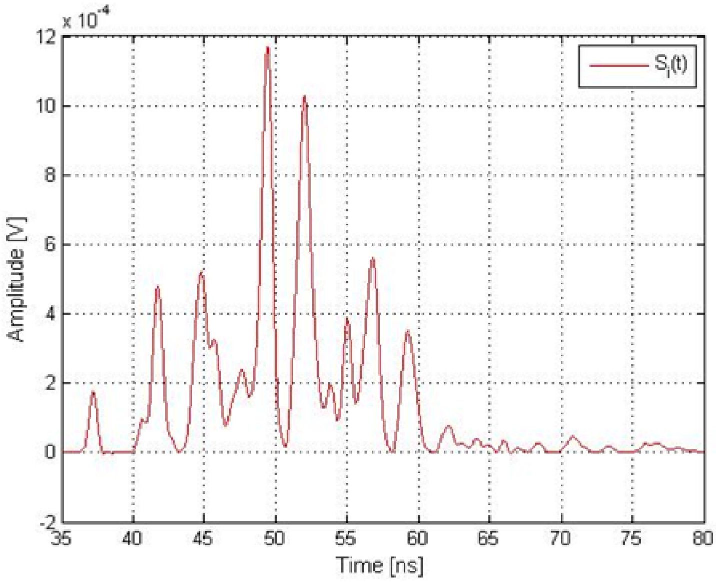

Figure 2.21 – Obtained received signal on the receiving chain i after filtering.

mentioned peak gives us t_{ToF} which is then used to find the distance according to

$$d = c.\frac{t_{ToF}}{2} \tag{2.39}$$

Figure 2.22 shows the block diagram of the Duplex UWB method.

The duplex UWB method is based on the difference $\Delta\varphi$ between the phase shifts of the two signals U and V. Therefore, to avoid the phase ambiguity, $\Delta\varphi$ should respect the

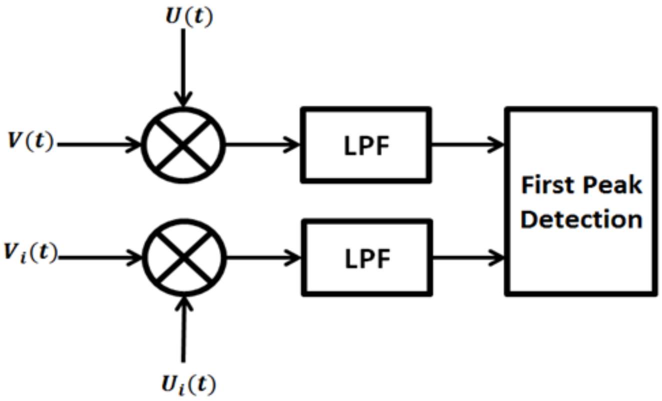

Figure 2.22 – Block diagram of the Duplex UWB method.

following constraint

$$\Delta\varphi = 2\pi(f_2 - f_1)t_{ToF} \leq 2\pi \tag{2.40}$$

Consequently, the maximum time of flight $t_{ToF-max}$ that can be detected is given by

$$t_{ToF-max} = \frac{1}{\Delta f} \tag{2.41}$$

where $\Delta f = f_2 - f_1$ is the difference between the two center frequencies f_1 and f_2.

Finally, the maximum time of flight $t_{ToF-max}$ is used to determine the maximum estimated distance d_{max} as follows

$$d_{max} = c.\frac{t_{ToF-max}}{2} = \frac{c}{2\Delta f} \tag{2.42}$$

In our case where we selected f_1 and f_2 so that $\Delta f = 50$ MHz, this method made it possible to estimate distances up to 3 m.

2.7 Proposed Method for Path Difference Estimation

Our goal now is to determine the azimuth angle α through the estimation of the path difference. According to previous proposals, the smallest path difference that an UWB radar system can detect is 30 cm for a bandwidth 1 GHz. However, this resolution is considered small for future indoor applications.

Therefore, many approaches are proposed to improve the resolution without increasing the frequency bandwidth. Among them, we can mention the work of [31] in which the phase difference of a CW signal is exploited. As previously stated, this solution is constrained by the multipath channel environment that reduces its accuracy, even in LoS situations.

To tackle this challenge, this method can be adapted to make our system capable of detecting smaller path difference using UWB signal instead of CW signals. The proposed algorithm is based on a phase correlation between the two received signals.

2.7.1 Phase Correlation Method

The path difference between two received signals is estimated through the corresponding time difference, obtained by correlating these two signals on the two receiving chains. The correlation function being used is based on a PC method.

Compared to the previous method, this one requires only one signal to estimate the path difference. Therefore, we have decided to select the lowest center frequency f_1, i.e. U_1 and U_2 defined in Eq. (2.31) and Eq. (2.32). This choice will be justified at the end of this section.

Recall that the deformation and distortion of these signals by the circuit components and the environment are exactly the same on both receiving chains. In the same equations (2.31) and (2.32), T' is greater than the duration of the emitted pulse ($T' \gg T_p$) due to the distortion. In addition, the duration of the received pulse is much longer than the time difference ($T' \gg \Delta t$) when the path difference is very small.

Figure 2.23 shows the parameters definition of the PC method applied to U_1 and U_2.

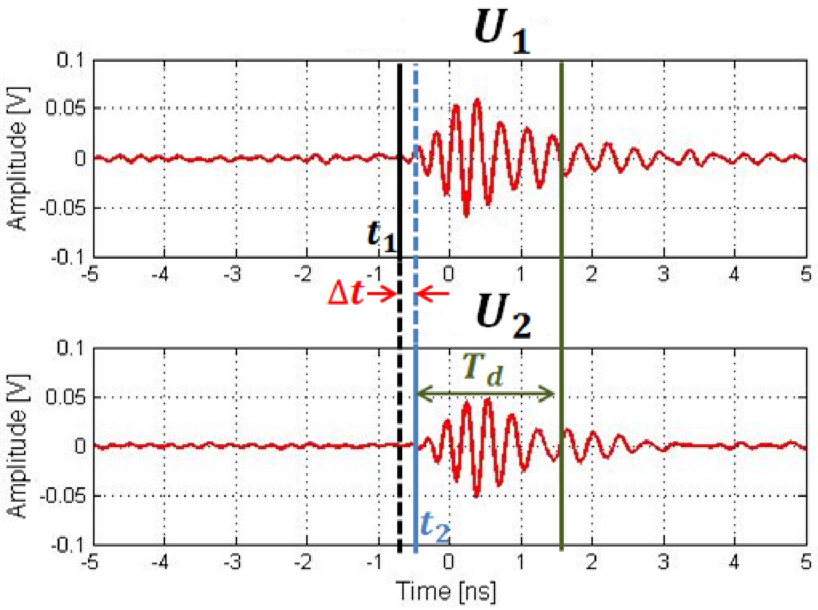

Figure 2.23 – Parameters definition.

The PC method proceeds as follows to estimate the path difference

1. The first step consists in determining the beginning of the received pulse; t_1 and t_2 which correspond respectively to the beginning of the impulse of U_1 and U_2. To determine t_1 and t_2, the signals are divided into N_b blocks of duration T_b each. Each block is shifted from the previous one by the duration Δ_b, as shown in Figure 2.24. Therefore, the total interval time T of the recovered signal is expressed as follows

$$T = N_b T_b - (N_b - 1)(T_b - \Delta_b) \tag{2.43}$$

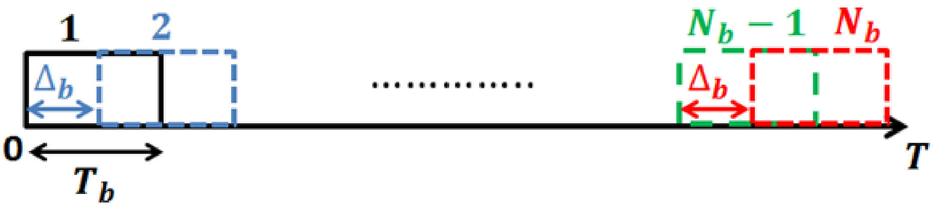

Figure 2.24 – ED signal decomposition.

In each block, the energy E_n^j of the received signal U_j is calculated

$$E_n^j = \sum_{i=(n-1).i_{\Delta_b}+1}^{(n-1).i_{\Delta_b}+i_{T_b}} {U_j}^2(i) \tag{2.44}$$

where $j = 1, 2$ and $1 \leq n \leq N_b$

$$\begin{cases} T_b = i_{T_b}.T_e \\ \Delta_b = i_{\Delta_b}.T_e \end{cases} \tag{2.45}$$

where T_e is the sampling time, i_{T_b} and i_{Δ_b} represents the number of samples corresponding to the duration T_b and Δ_b respectively.

Hence, t_j ($j = 1, 2$) corresponds to the block that contains the maximum energy.

$$t_j = \max_n(E_n^j).\Delta_b \tag{2.46}$$

2. Then, a window of width T_d is defined as shown in Figure 2.23. The choice of T_d depends on certain parameters which will be discussed at the end of this section.

3. Finally, a correlation between the two signals is applied in the interval $[t_1; t_2 + T_d]$. The discrete cross-correlation function is given by the following expression.

$$C_p = \sum_{q=i_1}^{i_2+i_{T_d}} U_1(q).U_2(q-p) \tag{2.47}$$

with $0 \leq p \leq 2(i_2 + i_{T_d} - i_1) + 1$

$$\begin{cases} t_j = t_0 + (i_j - 1)T_e \\ T_d = i_{T_d}.T_e \end{cases} \tag{2.48}$$

where $j = 1, 2$, T_e is the sampling time, t_0 the sampling starting time, i_j corresponds to the pulse starting index of discrete signal U_j and i_{T_d} represents the number of samples corresponding to the window T_d.

Therefore, the analysis window T_w is given by

$$T_w = t_2 + T_d - t_1 \tag{2.49}$$

In the following, the cross-correlation function is detailed in the time domain for a small path difference. In this case, the analysis window T_w will be approximately equal to the window T_d defined in step 2 ($T_w \approx T_d$).

By applying the cross-correlation function to the two received signals $U_1(t)$ and $U_2(t)$, we obtain

$$C_{U_1U_2}(\Delta t) = \frac{A'^2}{T_w} \int_0^{T_w} \underbrace{\cos(2\pi f_1 t').\cos[2\pi f_1(t' - \Delta t)]}_{\text{f(t')}} . \underbrace{e^{-\left(\frac{t'}{T'}\right)^2} . e^{-\left(\frac{t'-\Delta t}{T'}\right)^2}}_{\text{g(t')}} dt' \tag{2.50}$$

where $t' = t - t_{ToF}$.

By detailing the expression $g(t')$ in Eq. (2.50), we obtain

$$g(t') = e^{-2\frac{t'^2}{T'^2} - \frac{\Delta t^2}{T'^2} + \frac{2t'\Delta t}{T'^2}} \tag{2.51}$$

For a small path difference case, we have $\Delta t \ll T' \Rightarrow e^{-\frac{\Delta t^2}{T'^2} + \frac{2t'\Delta t}{T'^2}} \approx 1$.

In addition, the analysis window T_w which is equal to T_d is chosen to be smaller than the duration of the broadened received signal T' as shown in Figure 2.25, $T_w \ll T' \Rightarrow e^{-2\frac{t'^2}{T'^2}} \approx 1$.

So, we can write $g(t') \approx 1$.

The expression $f(t')$ in Eq. (2.50) can be detailed as follows

$$\begin{aligned} f(t') &= \cos(2\pi f_1 t')[\cos(2\pi f_1 t').\cos(2\pi f_1 \Delta t) + \sin(2\pi f_1 t').\sin(2\pi f_1 \Delta t)] \\ &= \cos(2\pi f_1 \Delta t).\cos^2(2\pi f_1 t') + \sin(2\pi f_1 \Delta t).\cos(2\pi f_1 t').\sin(2\pi f_1 t') \\ &= \cos(2\pi f_1 \Delta t).\frac{1 + \cos(4\pi f_1 t')}{2} + \sin(2\pi f_1 \Delta t).\frac{\sin(4\pi f_1 t')}{2} \end{aligned} \tag{2.52}$$

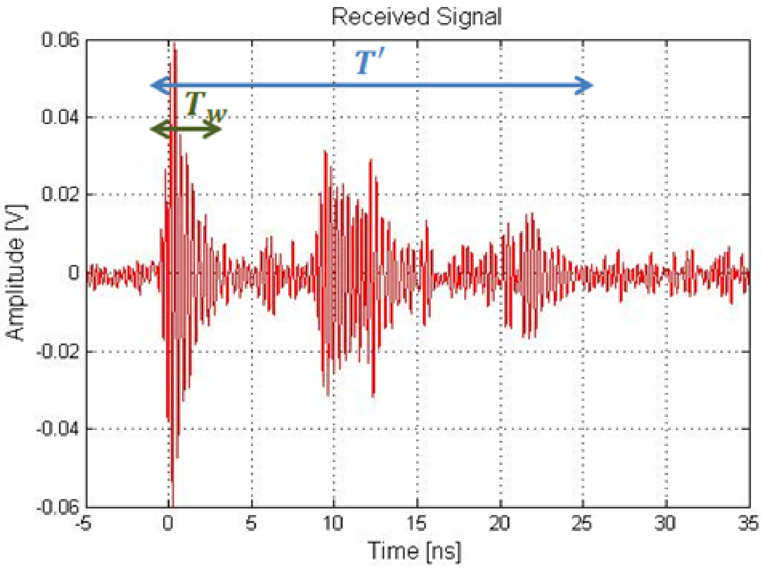

Figure 2.25 – Broadened received signal for each channel.

Integrating $f(t')$ from Eq. (2.52) yields the following

$$\begin{aligned}\int_0^{T_w} f(t')dt' &= \cos(2\pi f_1 \Delta t).\Big[\frac{T_w}{2} + \frac{1}{8\pi f_1}\sin(4\pi f_1 T_w)\Big] \\ &+ \sin(2\pi f_1 \Delta t).\frac{1}{8\pi f_1}[1 - \cos(4\pi f_1 T_w]\end{aligned} \tag{2.53}$$

Assuming that $T_w = \frac{a}{f_1}$ with a is an integer, Eq. (2.53) becomes

$$\int_0^{T_w} f(t')dt' = \frac{T_w}{2}\cos(2\pi f_1 \Delta t) \tag{2.54}$$

Therefore, the cross-correlation function in Eq. (2.50) will be expressed as follows

$$C_{U_1U_2}(\Delta t) = \frac{A'^2}{2}\cos(2\pi f_1 \Delta t) \tag{2.55}$$

Eq. (2.55) is considered as the core of the PC method by linking it directly to the path difference through the time difference Δt.

Based on the above detailed calculation, the choice of the analysis window T_d in step 2 of the PC method has to satisfy several conditions:

1. T_d should be smaller than the duration of the broadened received signal T', i.e. $T_d \ll T'$.
2. T_d should be a multiple of the center frequency f_1, i.e. $T_d = \frac{a}{f_1}$.
3. T_d should be larger or equal to the emitted pulse width T_p, i.e. $T_d \geq T_p$.

This method is based on a phase difference measurement given by $2\pi f_1 \Delta t$. The phase difference is also bounded here by 2π ($0 \leq \varphi_{f_1} \leq 2\pi$) to avoid again the phase ambiguity problem. This fact will impose limits on the maximum path difference $Path - dif_{max}$ detected by the PC method

$$\varphi_{f_1} = 2\pi f_1 \Delta t \leq 2\pi \Rightarrow \Delta t \leq \frac{1}{f_1} \tag{2.56}$$

$$Path - dif_{max} = \frac{c}{f_1} \tag{2.57}$$

where c is the celerity of light.

From Eq. (2.57), we can see that increasing the frequency results in a lower $Path - dif_{max}$. For this reason, we selected the signals at f_1 to apply the PC method. For instance, $f_1 = 3.5$ GHz will make this method able of achieving a $Path - dif_{max}$ of 8.6 cm.

2.8 Conclusion

In this chapter, UWB signals were defined and classified according to the FCC. Then, the UWB regulations and standards were presented, in particular the IEEE 802.15.4a standard and its channels used for localization systems. Moreover, the UWB indoor channel model based on the SV model was described where 9 environments of the IEEE propagation model (CM1,. . . , CM9) were identified.

In a second part, it was revealed that the performance of any estimator can be bounded using CRLB. Based on this inequality, the ToA estimation can provide the best accuracy of the position estimation for an UWB signal.

Thus, various ToA estimation algorithms were presented, such as direct calculation, PDP analysis, segmentation theory of non-stationary processes, matching filtering, time-delayed sampling and correlation, threshold comparison and energy detection. Despite their numerous advantages, these algorithms cannot achieve the desired resolution of the future ILS.

To overcome this problem and improve the resolution of the system, two methods were proposed to estimate the position of an AT given by its distance and Azimuth angle. The distance is estimated through the Duplex UWB method and the Azimuth angle is determined through the estimation of the path difference using the PC method.
Therefore, the Duplex UWB and PC methods have the potential to meet the UWB indoor localization system specifications in terms of accuracy and resolution. For this reason, we define in the next chapter the architecture of the desired UWB indoor localization

system capable of achieving high resolution in distance and angle measurements using the Duplex UWB and PC methods.

Bibliography

[1] F. Sabath, E.L. Mokole and S.N. Samaddar, “Definition and Classification of Ultra-Wideband Signals and Devices,” The Radio Science Bulletin, no. 313, June 2005. Cited page 45

[2] X. Chen and S. Kiaei, “Monocycle Shapes for Ultra Wideband System,” IEEE International Symposium on Circuits and Systems (ISCAS), vol. 1, pp. 597–600, 2002. Cited page 45

[3] H. Sheng, P. Orlik, A.M. Haimovich, L.J. Cimini and J. Zhang, “On the Spectral and Power Requirements for Ultra-wideband Transmission,” IEEE International Conference on Communications (ICC), vol. 1, pp. 738–742, May 2003. Cited page 45

[4] S. Gezici, Z. Sahinoglu, H. Kobayashi and H.V. Poor, “Ultra-wideband Impulse Radio Systems with Multiple Pulse Types,” IEEE Journal on Selected Areas in Communications, vol. 24, no. 4, pp. 892–898, April 2006. Cited page 45

[5] M. Welborn and K. Siwiak, “First Report and Order on Ultra-Wideband Technology,” IEEE P802.15 Working Group for Wireless Personal Area Networks (WPANs), 2002. Cited page 45

[6] G.R. Aiello, “Challenges for Ultra-wideband (UWB) CMOS Integration,” IEEE Radio Frequency Integrated Circuits (RFIC) Symposium, 2003. Cited page 45

[7] A. Batra, J. Balakrishnan, G.R. Aiello, J.R. Foerster and A. Dabak, “Design of a Multiband OFDM System for Realistic UWB Channel Environments,” IEEE Transactions on Microwave Theory and Techniques, vol. 52, issue 9, September 2004. Cited page 46

[8] Electronic Communications Committee (ECC) within the European Conference of Postal and Telecommunications Administrations (CEPT), “Commission Decision of 21 February 2007 on Allowing the Use of the Radio Spectrum for Equipment Using Ultra-wideband Technology in a Harmonised Manner in the Community,” Official Journal of the European Union, document number C(2007) 522, February 2007. Cited page 45

[9] B. Schleicher and H. Schumacher, “Impulse Generator Targeting the European UWB Mask,” Topical Meeting on Silicon Monolithic Integrated Circuits in RF Systems (SiRF), 2010. Cited page 46

[10] ECMA-368, “High Rate Ultra Wideband PHY and MAC Standard,” December 2008. Cited page 46

[11] IEEE P802.15-03, “Part 15.4: Wireless Medium Access Control (MAC) and PHYsical Layer (PHY) Specifications for Low-Rate Wireless Personal Area Networks (LR-WPANs),” July 2006. Cited page 46

[12] Federal Communications Commission, “Revision of part 15 of the commission’s rules regarding UltraWideband transmission systems,” TMemorandum Opinion and Order, 2010. Cited page 47

[13] A. F. Molisch, K. Balakrishnan, C. C. Chong, S. Emami, A. Fort, J. Karedal, J. Kunisch, H. Schantz, U. Schuster and K. Siwiak, “IEEE 802.15.4a channel model - final report”, IEEE 802.15.4a channel modeling subgroup, 2004. Cited page 48

[14] A. A. M. Saleh and R. A. Valenzuela, “A Statistical Model for Indoor Multipath Propagation,” IEEE Journal on Selected Areas in Communication, vol. 5, pp. 128–137, February 1987. Cited page 48

[15] D. Dardari, A. Conti, U. Ferner, A. Giorgetti and M.Z. Win, “Ranging with Ultrawide Bandwidth Signals in Multipath Environments,” Proceedings of the IEEE, vol. 97, Issue 2, pp. 404–426, February 2009. Cited page 50

[16] S. Gezici, “A Survey on Wireless Position Estimation, Wireless Personal Communications,” vol. 44, Issue 3, pp. 263–282, February 2008. Cited page 51

[17] S. Gezici, Z. Tian, G. B. Giannakis, H. Kobayashi, A. F. Molisch, H. V. Poor, and Z. Sahinoglu, “Localization via Ultra-Wideband Radios: a Look at Positioning Aspects for Future Sensor Networks,” IEEE Signal Processing Magazine, vol. 22, no. 4, pp. 70-84, July 2005. Cited page 51

[18] K. Yu and I. Oppermann, “Performance of UWB Position Estimation Based on Time-of-Arrival Measurements,” IEEE Ultra Wideband Systems and Technologies, pp. 400–404, May 2004. Cited page 53

[19] C. Mazzucco, U. Spagnolini and G. Mulas, “A Ranging Technique for UWB Indoor Channel Based on Power Delay Profile Analysis,” IEEE Vehicular Technology (VTC), pp. 2595–2599, September 2004. Cited page 53

[20] J.V. Di Franco, and W.L. Rubin, “Radar Detection,” Prentice-Hall - Engle- woad Cliffs, 1968. Cited page 53

[21] Z.N. Low, J.H. Cheong, C.L. Law, W.T. Ng and Y.J. Lee, "Pulse Detection Algorithm for Line-of-Sight (LoS) UWB Ranging Applications," IEEE Antennas and Wireless Propagation Letters, vol. 4, pp. 63–67, 2005. Cited page 53

[22] I. Guvenc, Z. Sahinoglu and P.V. Orlik, "ToA Estimation for IR-UWB Systems with Different Transceiver Types," IEEE Transactions on Microwave Theory and Techniques, vol. 54, no. 4, 2006. Cited page 54

[23] J.A. Pardinas-Mir, R. Lamberti, M. Muller and C. Gimenes, "An Experimental Approach to a Low-Complexity Two-Step TOA Measurement for TR-UWB Signals," IEEE International Conference on Communications (ICC), 2012. Cited page 55

[24] S. Gezici, Z. Sahinoglu, A. F. Molisch, H. Kobayashi and H. V. Poor, "A Two-Step Time of Arrival Estimation Algorithm for Impulse Radio Ultra Wideband Systems," European Signal Processing Conference, pp. 4–8, 2005. Cited page 56

[25] L. Yang and G. B. Giannakis, "Blind UWB Timing with a Dirty Template," IEEE International Conference on Acoustics, Speech, and Signal Processing, 2004. Cited page 56

[26] I. Guvenc and Z. Sahinoglu, "Threshold-based TOA Estimation for Impulse Radio UWB Systems," IEEE International Conference on Ultra-Wideband, September 2005. Cited page 57

[27] R. J. Fontana, "Recent System Applications of Short-Pulse Ultra-Wideband (UWB) Technology," IEEE Transactions on Microwave Theory and Techniques, vol. 52, no. 9, September 2004. Cited page 59

[28] S. de Rivaz, B. Denis, J. Keignart, M. Pezzin, N. Daniele, D. Morche, "Performances Analysis of an UWB Receiver using Complex Processing," IEEE Conference on Ultra WideBand Systems and Technologies, pp. 229-233, November 2003. Cited page 60

[29] J. Mondal, K. Wong, D. Richardson, K. Vu, K. Peterson, G. Dietz, R. Haubenstricker, N. Calanca, L. Gluck and S. Moghe, "77 GHz MMIC WR Module for Duplex Radar Application in Collision Avoidance Radar (CAR)," IEEE Gallium Arsenide Integrated Circuit Symposium, pp. 181-184, 1998. Cited page 61

[30] B. A. Garcia, "Conception d'un radar d'aide à la conduite automobile utilisant un système discriminateur de fréquence type six-port," ph.D. Dissertation, Telecom Paristech, Electronique et communications, Paris, France, 2002. Cited page 61

[31] A. Benlarbi-Delai, J.C. Cousin, R. Ringot, A. Mamouni and Y. Leroy, "Microwave Short Baseline Interferometers for Localization Systems," IEEE Transactions on Instrumentation and Measurements, vol. 50, no. 1, pp. 32-39, 2001. Cited page 67

Chapter 3

Proposed UWB System for accurate Indoor Localization

3.1 Introduction

Most of today's UWB systems used for indoor localization rely on devices only capable of measuring the relative distance between two nodes [1]. Like GPS, these systems use multilateration techniques to find the position of a target [2] in which 2D positioning requires at least three anchors. To do this, the distances between each anchor and the target are first calculated. These distances which together form a cluster will then be shared between all the anchors. Finally, trilateration techniques can be applied to locate the target using the aforementioned cluster in conjunction with the various anchors. However, apart from the prior knowledge of at least three anchors, the position estimation also requires a good synchronization between the different anchors. Therefore, anchor clock drifts, RF and ADC front-end delays and their long-term variations are the main factors limiting the performance of these systems. In addition, these systems do not perform well in the NLoS environment due to the complete difference between the time taken by the NLoS and LoS signals. For example, when an anchor point is not in the LoS, a signal penetration into an obstacle of about 1 ns can introduce 30 cm of error in the estimation of the radial distance. In addition, reliability is relatively low because the estimation of a single position requires at least three anchors, and if a measurement fails, no position can be estimated. The use of more nodes improves reliability but increases the complexity and cost of the system.

To overcome these limitations, another approach is adopted in this work by combining distance and angle measurements. This combination allows a single anchor to determine the 2D position of the tag from a single measurement. The main contribution of this work is to demonstrate that an UWB Indoor localization system using a single anchor is capable of achieving accurate and reliable performance.

This work is a continuation of the one developed by R. Kumar [3] in which a FMCW signal is replaced by an UWB signal with the objective of implementing a tracking system that can provide real-time 2D location of active transponders or tags. Compared to current systems, the developed ILS uses a hybrid technique combining both Duplex UWB and PC methods, which makes it less complex while achieving high resolution with good accuracy (in the order of a few centimeters). The localization is done in polar coordinates (distance and azimuth angle), where the radial distance between the tag and the LBS is estimated through the Duplex UWB method and the angle of arrival of the signals coming from the tag is calculated through the PC method.

This chapter is dedicated to describe the developed UWB ILS. In Section 3.2, the topology of the developed UWB ILS along with the localization method are introduced. In Section 3.3, UWB hardware along with a detailed description of the various components, the antennas design and their characteristics are presented. The initial validation of the developed method is presented in Section 3.4 through experimental results, followed by a discussion of the main constraints related to the developed system in Section 3.5. The link budget of the realized UWB ILS is presented in Section 3.6. Finally, the chapter ends with a conclusion in Section 3.7.

3.2 Localization System Architecture

3.2.1 2D Localization System Conception

The presented 2D ILS shown in Figure 3.1 has two main components, a LBS and an AT.

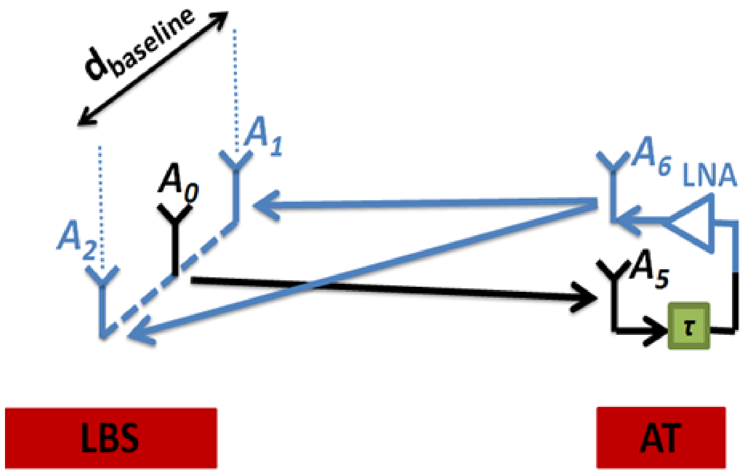

Figure 3.1 – Architecture of the localization system.

The LBS acts as a fixed base station to locate the AT. The purpose of selecting an AT over a passive one is its capability to provide a wide range and the best solution for applications requiring continuous real-time monitoring. The 2D LBS architecture has one RF transmitter chain and two RF receiver chains, each connected to its own antenna, A_0 for the transmitter chain, A_1 and A_2 for the two receiver chains respectively. The antennas are placed on the same axis. A_0 is kept at the origin of the dashed axis, in the center of the baseline ($d_{baseline}$) formed by the antennas A_1 and A_2.

The AT architecture is composed of two antennas, A_5 as receiver antenna and A_6 as transmitter antenna. Both antennas are connected via a LNA and a delay line τ. The AT is used as an active transponder. The main reason for using a known delay τ is to exclude the effects of:

- **Environmental backscattering:** In general, scattered signals from the surrounding indoor environment (clutter, object, $\cdots$) are inevitably present and superimposed on the intended signal, as shown in Figure 3.2. This fact makes the detection of the intended signal at the LBS a major issue in an indoor environment.
- **Antenna coupling:** Signals from other nearby antennas, referred to as antenna coupling also affects the intended signal. In our case, it is the coupling between the receiving antennas (A_1 and A_2) and the transmitting antenna (A_0).

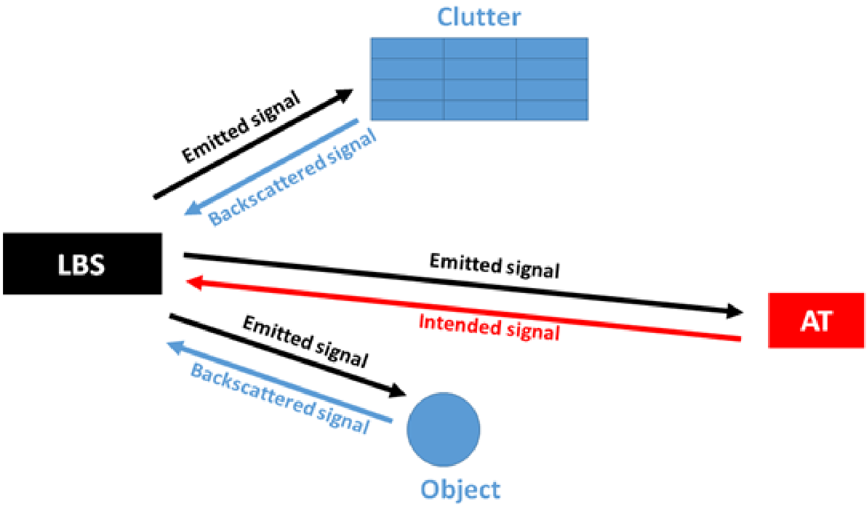

Figure 3.2 – Backscattered signals of an indoor environment.

In order to overcome these two effects, the observation window is shifted by adding a delay τ at the AT side. In this way, the useful signals will be deliberately delayed and therefore will have different time of arrival with respect to the spurious signals caused by backscattering and coupling effects, as shown in Figure 3.3. The effect of this delay is compensated during the processing phase by also applying it to the transmitted signal.

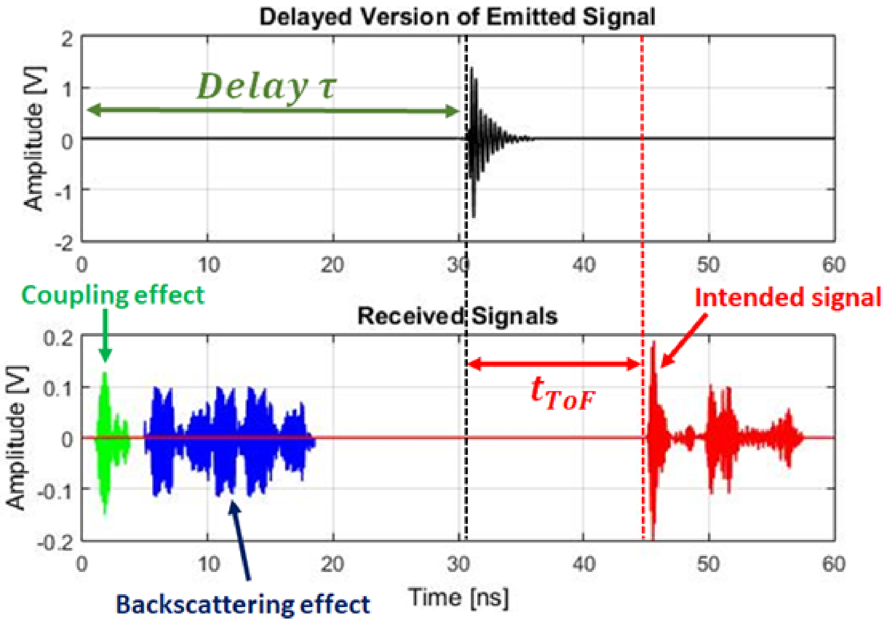

Figure 3.3 – Received signals at LBS.

To sum up, the known delay τ is used to segregate the intended signal at the LBS from the backscattered signals of an indoor environment and the parasitic signals of the antenna coupling. The same approach is used in the ground stations of DME systems dedicated for the aerial navigation [5,6], where the ground transponder replies with the same type pulse pair transmitted by the interrogator after adding a time delay of 50 μs.

The choice of τ depends on the desired maximal range. In this work, τ is chosen to be longer than the time needed for a round trip flight of the wave corresponding to the chosen maximum range. The choice of the maximum range will be discussed in the Section 3.5.3.

3.2.2 Proposed Localization Method

The proposed localization method is based on a jointly range -or radial distance - and angular measurement. The setup of the 2D architecture for the localization technique is shown in Figure 3.4.

Assuming that the total delay τ' (delay τ + cumulative delay of the different components) in the tag, between A_5 and A_6, is known, the radial distance d is obtained by estimating the absolute time of arrival of the received signals on A_1 and A_2. The azimuth angle α can be estimated by computing the time difference of arrival between the two received signals (U_1 and U_2) at the LBS side.

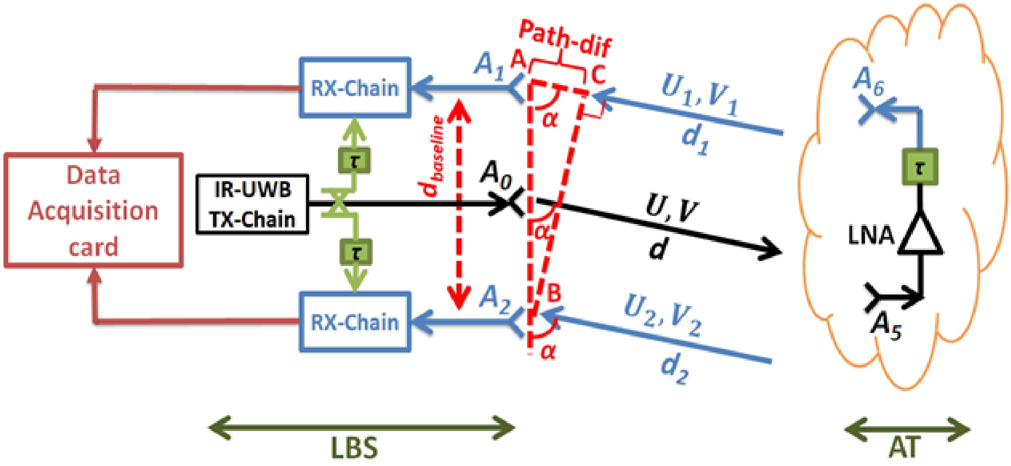

Figure 3.4 – Localization technique.

Two UWB pulses U and V of equal width and at center frequencies f_1 and f_2 ($f_1 < f_2$), respectively, are transmitted through the front end antenna A_0 at different times. We assume that the channel is flat i.e. the channel remains constant during the transmission of the two pulses (f_1 and f_2 are very close and $d_{baseline} \ll d$). At the tag side, these signals are received by the antenna A_5 and a delay τ is applied to each one of them. Next, these signals are transmitted by the antenna A_6 back to the LBS. Let, the received signals U_i and V_i reach A_i with time-of-flight equal to T_i, for $i \in \{1, 2\}$.

The time-of-flight T_i corresponds to the propagation time after removing τ'. As shown in Section 2.6.1, the time of flight T_i can be obtained obtained by applying the Duplex UWB method between the received pair of signals (U_i, V_i) and a delayed version (with the same delay τ) of the transmitted signals (U,V) for $i \in \{1, 2\}$. In this way, the delay imposed in the tag is compensated and at the same time, the effects of natural backscattering of the environment are overcomed. Therefore, T_i can be derived directly from the phase difference $\Delta\varphi_i$ and can be expressed as follows

$$T_i = \frac{\Delta\varphi_i}{2\pi(f_2 - f_1)} \tag{3.1}$$

Where f_1 and f_2 are the center frequencies of the signals (U, U_1, U_2) and (V, V_1, V_2), respectively.

Consequently, the radial-distances d_i are obtained as

$$d_i = \frac{cT_i}{2} \qquad i \in \{1, 2\} \tag{3.2}$$

where c is the speed of light.

The radial distance d, between A_0 and the AT, is the average value of d_1 and d_2

$$d = \frac{d_1 + d_2}{2} \tag{3.3}$$

Nevertheless, the angle estimation does not require two signals with two different center frequencies, so we have chosen the received signals with the lowest center frequency f_1, i.e. U_1 and U_2.

The separation of the two receiving antennas A_1 and A_2 by $d_{baseline}$ creates a time difference $\Delta t = T_2 - T_1$ between two independent incoming signals (U_1 and U_2) which, in turn, gives the path difference (Path-dif). This assumption is valid for a plane waves if the radial-distance d remains relatively larger than the $d_{baseline}$ [3].

Δt can be obtained from the phase φ_{f_1} which is the result of applying the PC method, detailed in Section 2.7.1, between the two received signals U_1 and U_2 on the two receiving chains. It can be expressed as follows

$$\Delta t = \frac{\varphi_{f_1}}{2\pi f_1} \tag{3.4}$$

Consequently, the path-dif can be expressed as

$$Path - dif = c.\Delta t \tag{3.5}$$

On the other hand, for U_1 and U_2 being two plane waves, the Path-dif between these two parallel independent incoming signals at an angle α with the baseline, is given by the base-length (AC) of the right-angle triangle ABC in Figure 3.4 and can thus be expressed as

$$Path - dif = d_{baseline}. \cos(\alpha) \tag{3.6}$$

Finally, the Azimuth angle α is obtained from Eq. (3.5) and Eq. (3.6) as follows

$$\alpha = \cos^{-1}\left(\frac{c.\Delta t}{d_{baseline}}\right) \qquad 0^\circ < \alpha < 180^\circ \tag{3.7}$$

In the sequel, the UWB hardware used to build and test the proposed system is described.

3.3 UWB Hardware

In this section, a detailed specification of each component is provided for the transmitter chain, the AT and the receiver chains.

3.3.1 Transmitter Chain

The block diagram of the transmitter chain is shown in Figure 3.5. A squared signal generator is connected to an impulse generator. This generator consists of a Step Recovery Diode (SRD) and a short-circuited stub line, as shown in Figure 3.6.

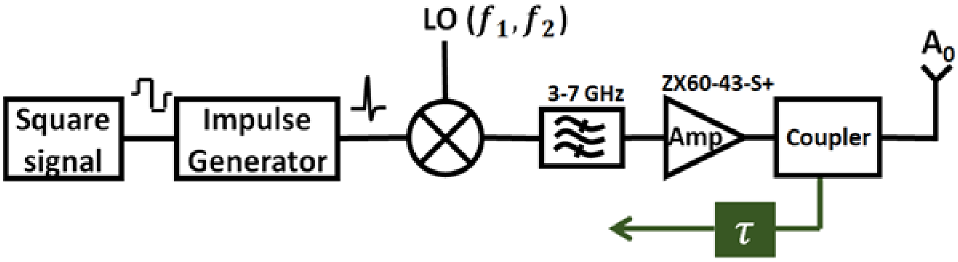

Figure 3.5 – Transmitter chain.

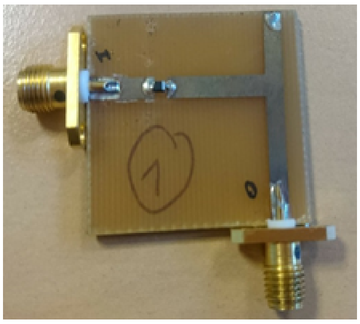

Figure 3.6 – Impulse generator.

The obtained pulse at the impulse generator output, shown in Figure 3.7, is fed to a Local Oscillator (LO) used with a mixer (Mini-circuits ZX05-C42+) [7] in order to create two pulses at two different center frequencies f_1 and f_2. Next, the UWB pulses are filtered by a BPF ($3 - 7$ GHz) (Mini-Circuits 15542) and then amplified by an LNA (Mini-Circuits ZX60-43-S+). Finally, the signals, shown in Figure 3.8 pass through a coupler before being transmitted by the circular polarized antenna A_0. A delay τ is applied on the second output of the coupler to obtain a delayed version of the transmitted signal. This step is mainly undertaken to compensate for the same delay τ imposed in the AT and is only used during processing.

Now, the characterization of different components of the transmitter chain is presented.

Band-Pass Filter $3 - 7$ GHz

The available BPF $3 - 7$ GHz Mini-Circuits is shown in Figure 3.9.

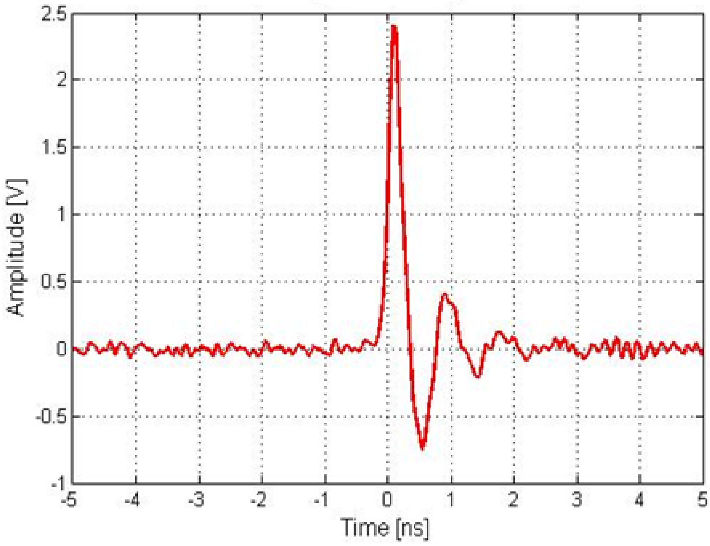

Figure 3.7 – UWB pulse at the impulse generator output.

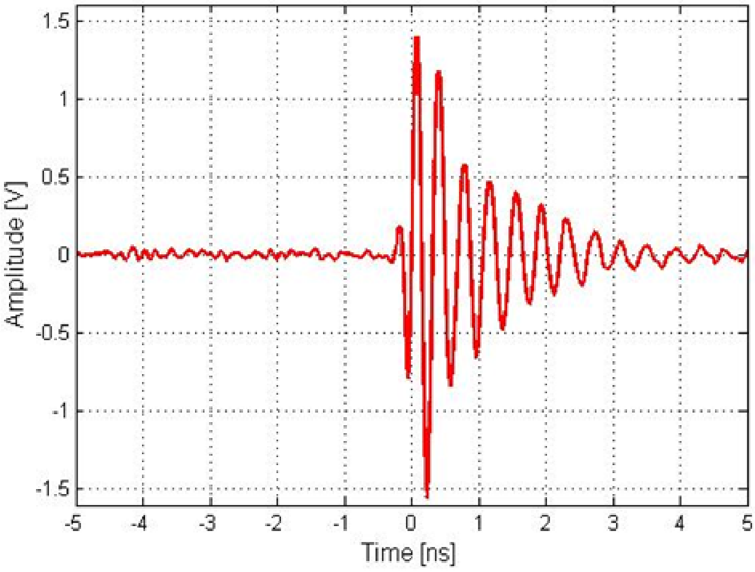

Figure 3.8 – The pulse at the input of antenna A_0.

Figure 3.9 – BPF 3 – 7 GHz.

As shown in Figure 3.10, the measured Insertion Loss (IL) (absolute value of S_{21}) is 0.7 dB and the measured Return Loss (RL) (absolute value of S_{11}) is greater than 8 dB. The BPF $3-7$ GHz has an almost flat response in the considered bandwidth. The performance of this filter is summarized in Table 3.1.

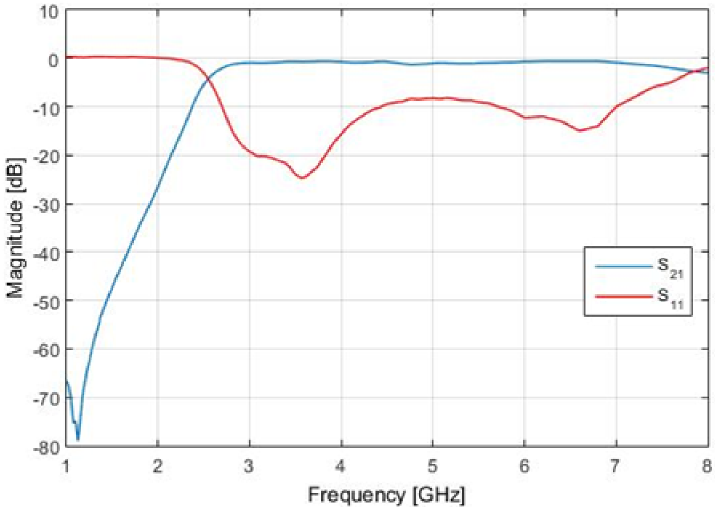

Figure 3.10 – BPF $3-7$ GHz characterization.

Table 3.1 – Filter specifications

Specification	BPF mini-Circuits
Pass Band	3-7 GHz
IL	0.7 dB
RL	>8 dB

Amplifier ZX60-43-S+

The amplifier ZX60-43-S+ from mini-circuits and its measured gain are shown in Figure 3.11 and Figure 3.12, respectively. The maximum observed gain at 3.5 GHz is 15 dB. The input saturation level is -5 dBm with a noise factor of 5.6 dB. The performance of this amplifier is summarized in Table 3.2.

Table 3.2 – Amplifier specifications at 3.5 GHz

Specification	ZX60-43-S+
Gain	15 dB
Input Saturation IP1	-5 dBm

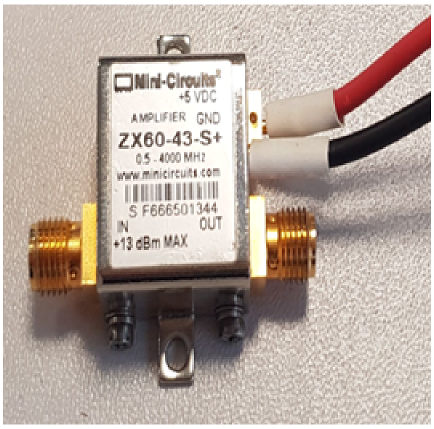

Figure 3.11 – Amplifier ZX60-43-S+.

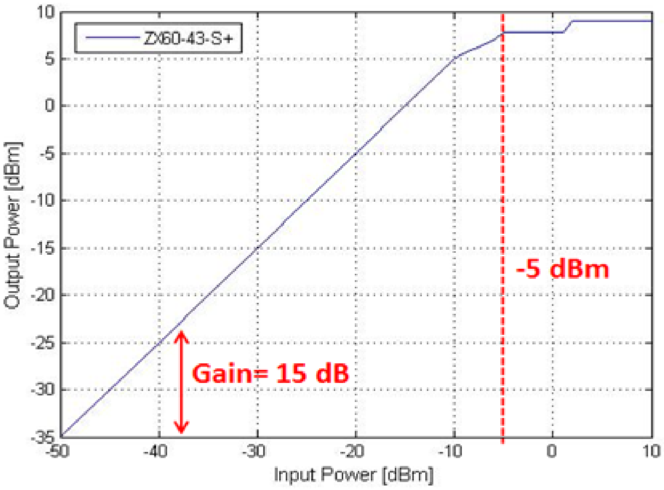

Figure 3.12 – ZX60-43-S+ Gain.

Coupler

The available Narda coupler shown in Figure 3.13 is used in the transmitter chain to extract the reference signal for processing.

As shown in Figure 3.14 and Figure 3.15, the IL is 0.2 dB between the input and output ports, while it is 16 dB between the input port and -16 dB coupled port. The RL is greater than 20 dB in $3-4$ GHz band. The performance of this coupler is listed in Table 3.3.

Table 3.3 – Coupler Specifications

Specification	**Input/output ports**	**Input/-16 dB ports**
IL	0.2 dB	16 dB
RL	>20 dB	>20 dB

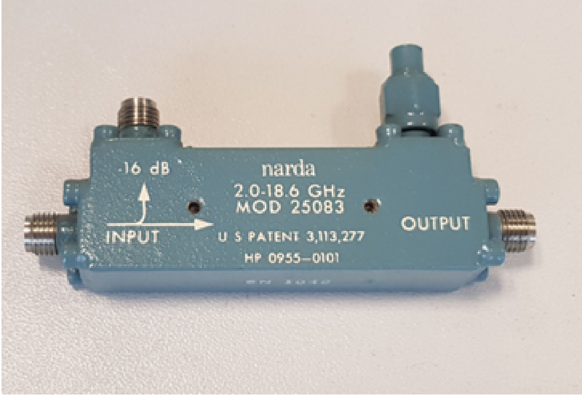

Figure 3.13 – Coupler.

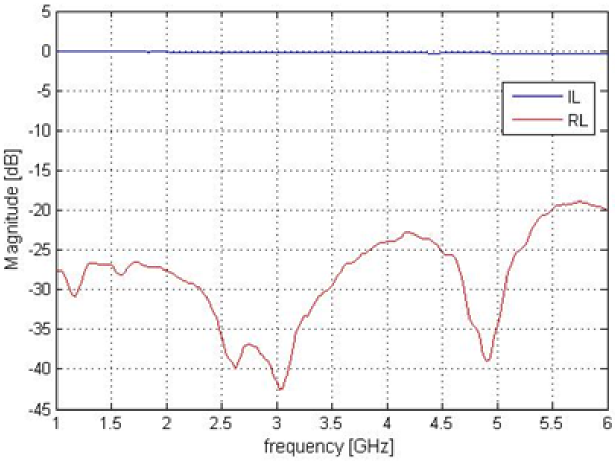

Figure 3.14 – Input/output ports characterization.

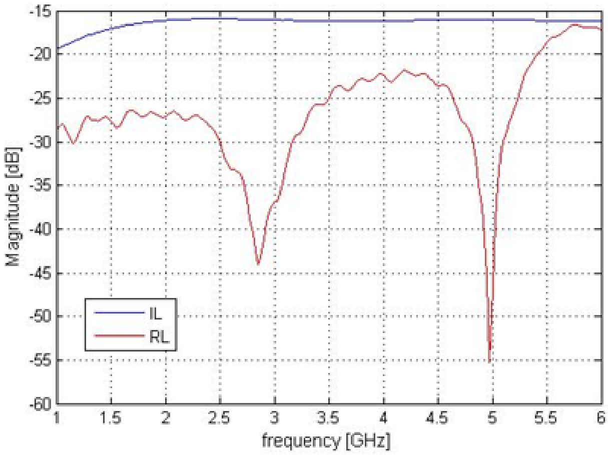

Figure 3.15 – Input/−16 dB ports characterization.

Circular Polarized Antenna

Generally speaking, an antenna can be circularly polarized in 2 different ways: Right Hand Circular Polarization (RHCP) and Left Hand Circular Polarization (LHCP). In both cases, the electric field rotates in a perpendicular plane to the wave direction. For this reason, the circular polarization wave can penetrate an indoor environment more easily and thus offers more opportunities for good reception. Moreover, using a different polarization scheme, i.e. LHCP in transmission and RHCP in reception and vice versa, can help in mitigating the signal's interference effects.

Consequently, the circular polarized antenna is a convenient choice for our ILS. The antenna is designed according to [8] and operates in the upper UWB frequency range between 7 and 10 GHz. An optimization phase using Computer Simulation Technology (CST) was therefore necessary to adapt the antenna to the frequency band of interest $3-4$ GHz. The simulated design is printed on an FR4 substrate with a thickness of 1.58 mm, a relative permittivity (ϵ_r) of 4.2 and a tangent loss ($tan\delta$) of 0.01. The overall size of the antenna is $80 \times 50 \times 1.58$ mm. As shown in Figure 3.16, the two symmetrical quasi-spiral arms are located separately on the upper (RHCP) and lower (LHCP) layers of the substrate. The obtained result has a good RL (more than 10 dB) in the desired frequency band of $3-4$ GHz, as shown in Figure 3.17.

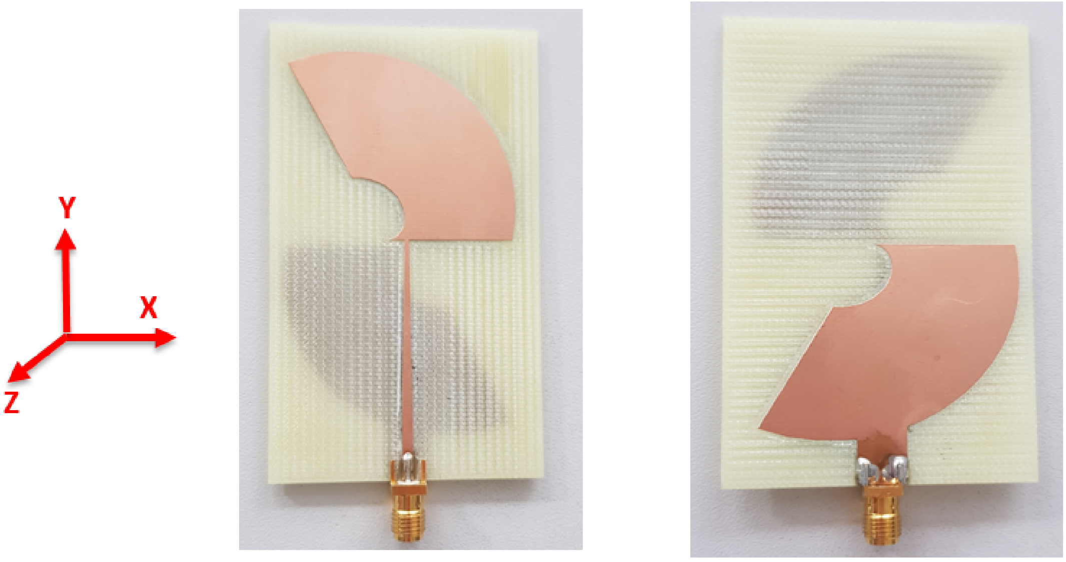

(a) Top side

(b) Bottom side

Figure 3.16 – Circular polarized antenna

The characterization of the optimized antenna was then performed in an anechoic chamber using LINDGREN 3117 Horn as the reference antenna to determine the gain, the radiation pattern and the axial ratio used to quantify the circular polarization. The simulated and measured total gains are illustrated in Figure 3.18. In the $3-4$ GHz band, the

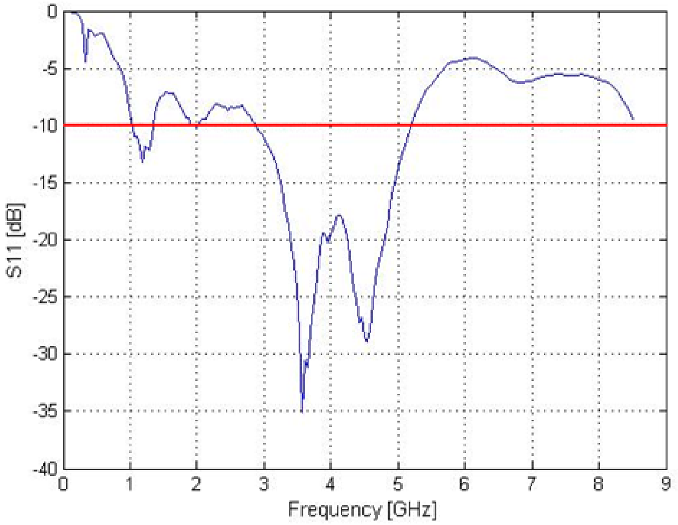

Figure 3.17 – Reflection coefficient of circular polarized antenna.

simulated total gain is between 2 and 2.6 dB while the measured total gain is between 1.4 and 3.3 dB. The maximum observed value is 3.3 dB at 3.6 GHz. The simulated gains for LHCP and RHCP are shown in Figure 3.19. In the 3 – 4 GHz band, the LHCP gain is between 2 and 2.6 dB while the RHCP gain is between 2.5 and 3.5 dB.

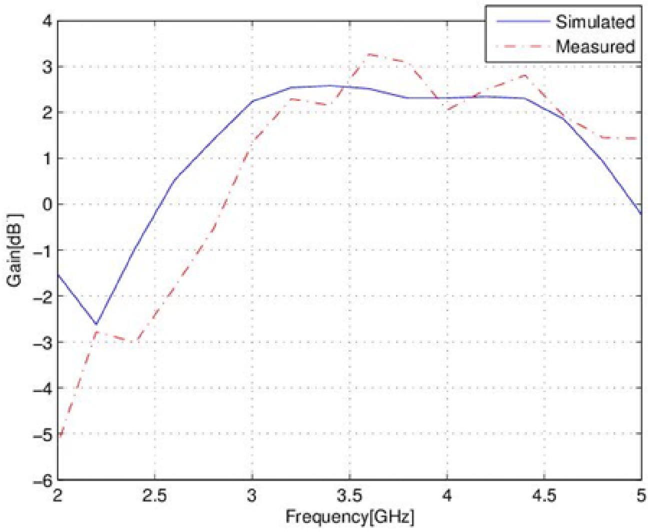

Figure 3.18 – Total gain of circular polarized antenna.

The 3D radiation patterns for LHCP and RHCP are shown in Figure 3.20 at 3.5 GHz. As we can see, the LHCP is in the negative direction of the z-axis (Bottom side) while the RHCP is in the positive direction (Top side).

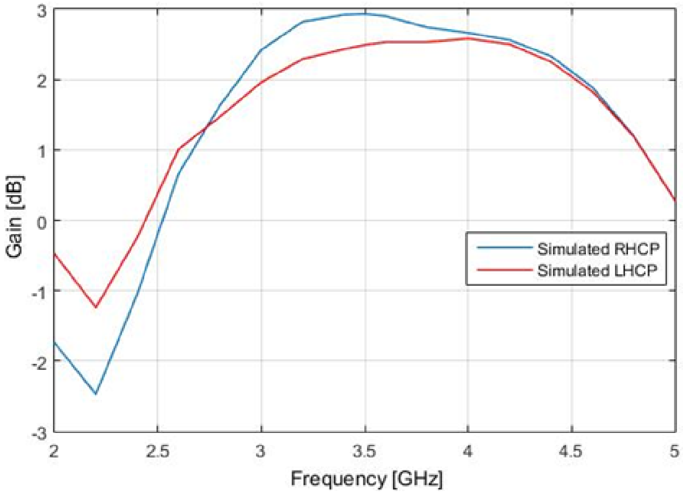

Figure 3.19 – Simulated Gain for LHCP and RHCP.

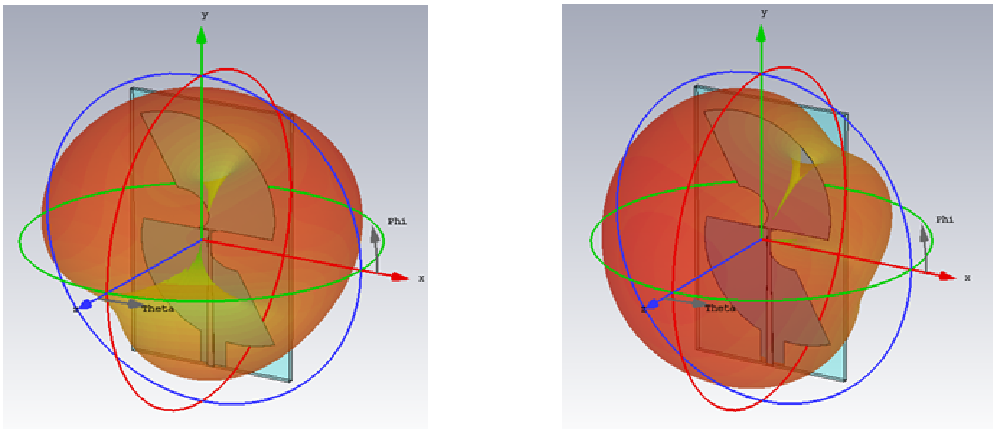

(a) LHCP

(b) RHCP

Figure 3.20 – 3D Radiation pattern

The simulated and measured radiation patterns are presented in Figure 3.21 at 3 GHz and 4 GHz in the XZ plane. The radiation patterns associated with these two frequencies are shown on the left and right side of the figure. As we can see, the measured result is more in line with the 3 GHz simulation than with the 4 GHz.

The Axial Ratio (AR) is mainly used to describe the polarization nature of the antennas. AR is the ratio of orthogonal components of the E-field

$$AR = 20\log\left(\frac{|E_{co}| + |E_{xp}|}{|E_{co}| - |E_{xp}|}\right) \tag{3.8}$$

where E_{co} is the co-polar electric field and E_{xp} the cross-polar electric field. The ideal AR value for circularly polarized fields is 0 dB. In addition, the axial ratio tends to degrade

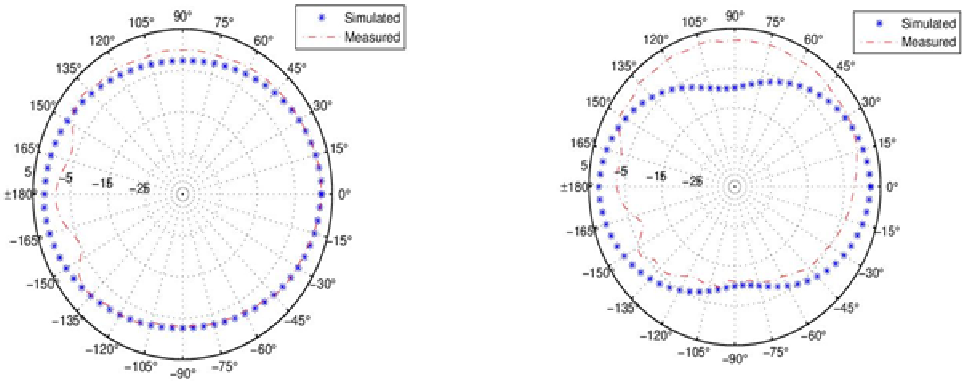

(a) 3 GHz

(b) 4 GHz

Figure 3.21 – Radiation pattern in the XZ plane.

away from the main beam of an antenna. Therefore, the standard maximum value defined for the axial ratio of a radio wave as a circular polarization is limited to 3 dB. As shown in Figure 3.22, the measured AR is below the standard limit of 3 dB over the entire 3 – 4 GHz frequency.

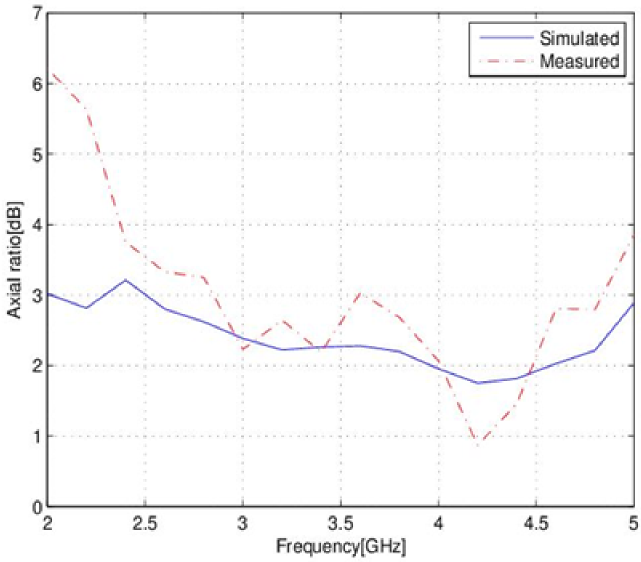

Figure 3.22 – AR of circular polarized antenna.

3.3.2 Active Tag

Figure 3.23 shows the block diagram of the AT. At the tag level, the received signal by the antenna A5 (3-4 GHz) is first amplified by a LNA (Mini-Circuits ZX60-43-S+), and then filtered out with a BPF (3 – 5 GHz) (Micro-Tronics BPC11296). The obtained signal is amplified again using the same LNA before applying the delay τ. Finally, the delayed signal is retransmitted by the antenna A_6 towards the LBS. A_5 and A_6 are both circular polarized antenna (3 – 4 GHz).

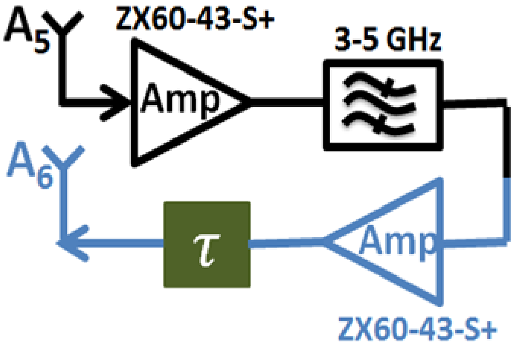

Figure 3.23 – Active Tag.

The characterization of some components is presented in the following.

Band-Pass Filter 3 – 5 **GHz**

The available BPF 3 – 5 GHz Micro-Tronics is shown in Figure 3.24.

Figure 3.24 – BPF 3 – 5 GHz.

As shown in Figure 3.25, the measured IL is 0.5 dB and the measured RL is greater than 16 dB. Similarly, the 3 – 5 GHz filter has an almost flat response in the considered bandwidth. The performance of this filter is summarized in Table 3.4.

Table 3.4 – Filter specifications

Specification	BPF Micro-Tronics
Pass Band	3-5 GHz
IL	0.5 dB
RL	>16 dB

Delay Line

The HUBER+SUHNER delay line of 8 m long, shown in Figure 3.26, is used at the AT level. Using a known delay τ is mainly intended to exclude the effects of environmental

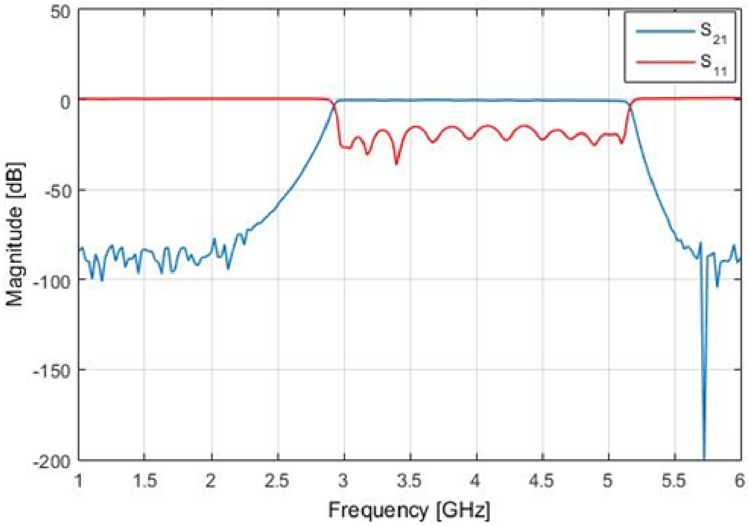

Figure 3.25 – BPF 3 – 5 GHz characterization.

backscattering and antenna coupling as detailed in section 3.3.1. With this 8 m line, a delay of about 32 ns is achieved, as shown in Figure 3.27.

Figure 3.26 – Delay line.

In the 3 – 4 GHz band, this line is characterized by a measured IL of 4.6 dB and a measured RL greater than 25 dB. The performance of the delay line is reported in Table 3.5.

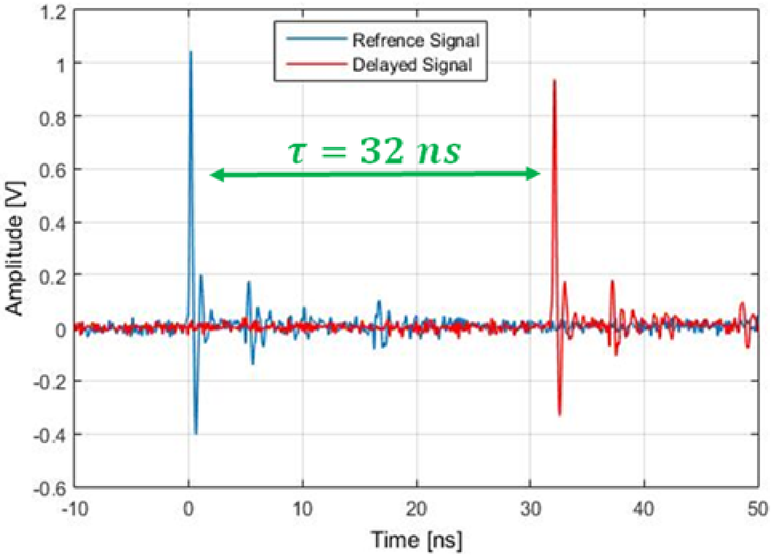

Figure 3.27 – Delayed signal.

Table 3.5 – Delay line Specifications

Specification	**Delay Line**
IL	4.6 dB
RL	> 25 dB

3.3.3 Receiver Chain

The block diagram of the receiver chain is shown in Figure 3.28. The retransmitted signal from the AT is received by the two receiver chains antennas (A_1 and A_2) of the LBS. A_1 and A_2 are identical broadband horn antenna ($1-8$ GHz). The received signals are amplified by a LNA (Mini-Circuits ZX60-6013E-S+) and then filtered by a BPF ($3-7$ GHz) (Mini-Circuits 15542). Next, the signals are acquired to be processed using one of the following systems: Agilent Keysight Infinium MSO 9254A and Tektronix.

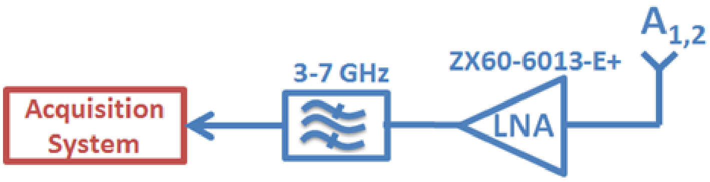

Figure 3.28 – Receiver chain.

In the following some components are characterized.

Horn Antenna

The broadband horn antenna 1 – 8 GHz from A-Info [9] shown in Figure 3.29, is used as a receiving antenna of both receiver chains.

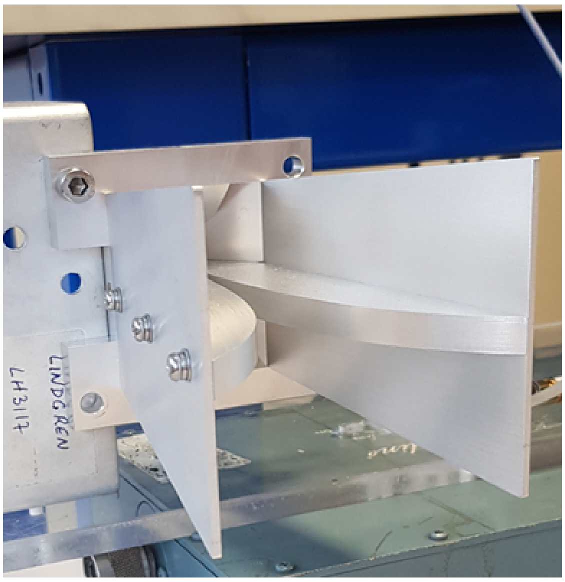

Figure 3.29 – Horn antenna.

While checking the characteristics of this antenna, we are interested in the 3 – 4 GHz band which is the band of the complete system. We can then notice through Figure 3.30 and Figure 3.31 that the measured RL in this band exceeds 10 dB for a gain equal to 7.5 dB.

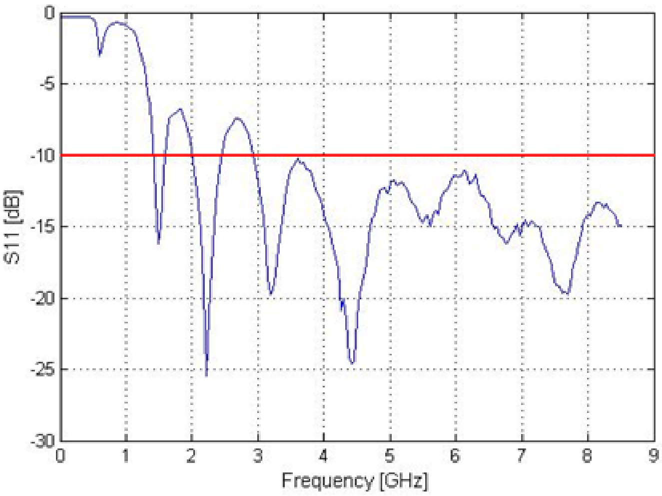

Figure 3.30 – Reflection coefficient of horn antenna.

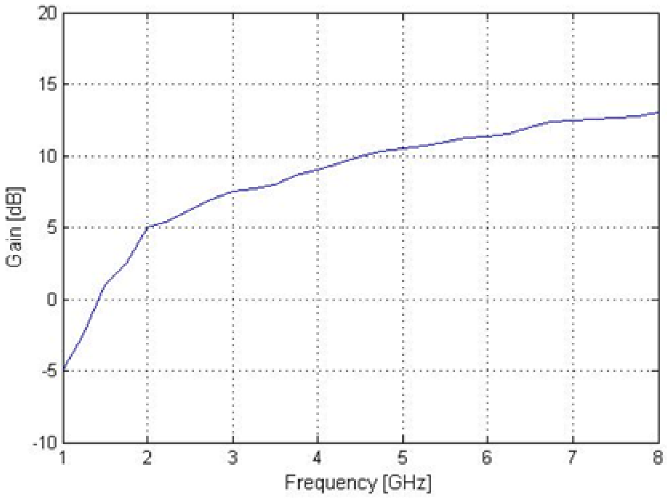

Figure 3.31 – Gain of horn antenna.

Amplifier ZX60-6013E+

The amplifier ZX60-6013-E+ from mini-circuits and its measured gain are shown in Figure 3.32 and Figure 3.33, respectively. The maximum observed gain at 3.5 GHz is 13 dB. The input saturation level is −4 dBm with a noise factor of 3.4 dB. This LNA is used in the receiving chain since it has a lower Figure noise than its counterpart, the ZX60-43-S+. The performance of this amplifier is summarized in Table 3.6.

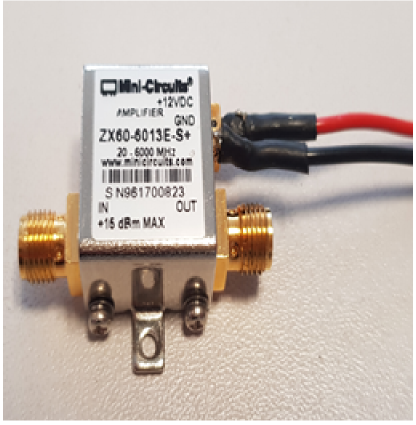

Figure 3.32 – Amplifier ZX60-6013-E+.

Table 3.6 – Amplifier specifications at 3.5 GHz

Specification	**ZX60-6013-E+**
Gain	13 dB
Input Saturation IP1	- 4 dBm

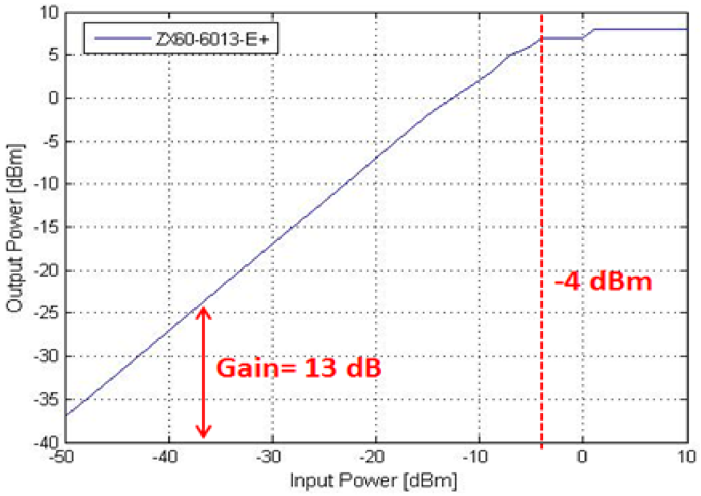

Figure 3.33 – ZX60-6013E+ Gain.

3.4 Concept Validation

This section describes the experimental setup used to validate the proposed PC method and shows the respective results highlighting the improvement of the Azimuth angle α resolution.

3.4.1 Experimental Setup

The defined 2D method of Section 3.2.2 is initially realized using available equipment. The complete experimental setup is shown in Figure 3.34. The output U of the transmitter chain described in Section 3.3.1 is plugged to the port 1 of the acquisition system (MSO 9254A). We propose to validate the method using cables, in order to eliminate the free-space environment and be aware of the performance and limitations. Therefore, the tag is represented by 16 m (65 ns) propagation line consisting of two HUBER+SUHNER delay lines, characterized in Section 3.3.2. This experimental setup is considered sufficient for the validation of the PC method, since our goal is to improve the angular resolution.

The delayed signal at the output of the tag is connected to a splitter to obtain two distinct paths for the signals. The outputs of the splitter are connected to a cable of length 50 cm for the path of U_1 and to a cable of length 50 cm and a short variable delay line for U_2. This variable Delay-line is used to represent the path difference. U_1 is acquired on port 2 of the oscilloscope and Signal U_2 on port 3.

The variable Delay-line consists of different transitions with the value 0.03 ns, 0.04 ns, 0.06 ns, 0.07 ns, 0.09 ns, 0.1 ns, 0.13 ns, 0.16 ns, 0.2 ns and 0.23 ns called "test number" from 1 to 10. These different transitions correspond respectively to a path difference equal to

0.5 cm, 0.6 cm, 0.9 cm, 1.1 cm, 1.4 cm, 1.5 cm, 1.9 cm, 2.4 cm, 3 cm and 3.5 cm.

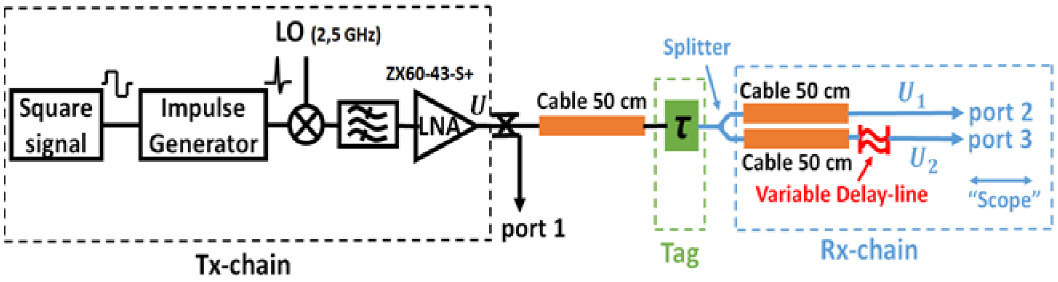

Figure 3.34 – Test bench setup.

The signals (U, U_1 and U_2) are oversampled by 16 using the oscilloscope with a sampling frequency equal to 10 GHz. The data are further processed in MATLAB for computation. The path difference between the two incoming signals (U_1 and U_2) is used to compute the Azimuth angle for $d_{baseline}$ = 29 cm. This value is then compared with the theoretical results obtained by MATLAB.

3.4.2 Experimental Results

The results shown in this sub-section were published in [10].

A calibration step is mandatory to estimate the time unbalance between U_1 and U_2. Figure 3.35 shows the received signals U_1 and U_2 when no delay transition is added. As we can see, these two signals are distorted in the same way and a delay of 0.06 ns is observed between them. This delay must be taken into account when calculating the Azimuth angle.

The azimuth angle α is computed based on the method presented in Section 3.2.2.

An azimuth angle α equal to 90° corresponds to a zero path difference as shown in Figure 3.4.

The path difference is estimated based on the PC method presented in Section 2.7.1 using a window width T_d of 5 ns. T_d is chosen wider than the pulse to insure that all possible signal spreaded by the propagation and the distortions are taken into account. The actual and estimated path difference are presented in Figure 3.36 where the estimated $Path-dif$ is obtained by two methods, namely a simple correlation and the PC method. The test numbers along the x-axis are the 10 transitions used for the short delay. Moreover, the difference between the actual and estimated values along the y-axis represents the error in the $Path-dif$ estimation. The maximal error is 1.7 cm for a simple correlation. However, a maximal error of 0.2 cm is observed with the PC method.

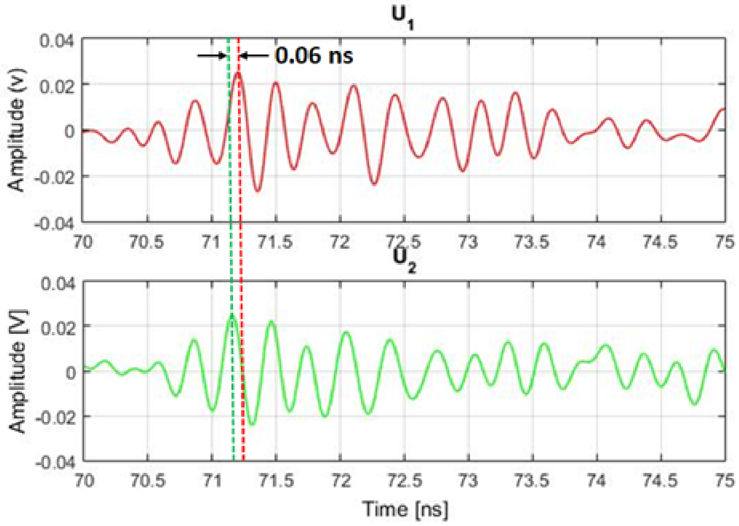

Figure 3.35 – U_1 and U_2 when no delay transition is added.

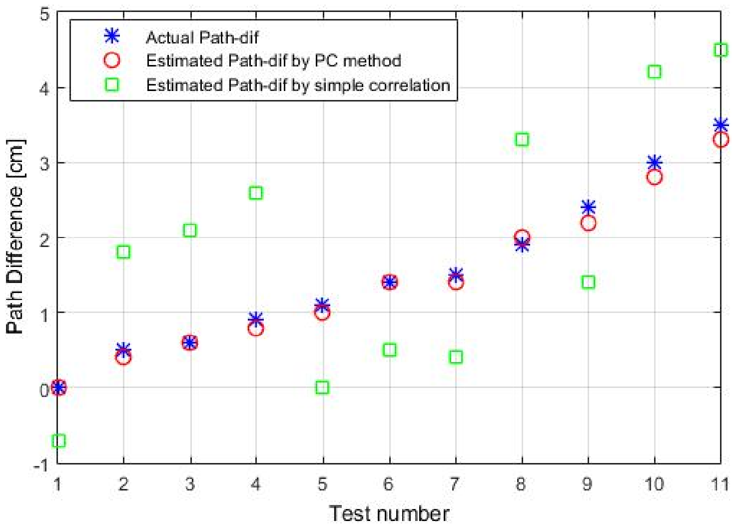

Figure 3.36 – Estimated $Path - dif$.

Table 3.7 shows the actual and estimated Azimuth angles α derived from the $Path - dif$ for $d_{baseline}$ = 29 cm. The maximal error is 3.4° for a simple correlation. However, this error decreases to 0.4° with the PC method. Therefore, the proposed PC method yields a very accurate estimate of the angle with respect to the simple correlation for a nearly negligible path difference (tag in front of the transmitting antenna).

Table 3.7 – Estimated Azimuth angle α

Actual α	**Estimated α**	
	Simple correlation	**PC method**
90°	91.4°	90°
89°	86.4°	89.2°
88.8°	85.8°	88.8°
88.2°	84.8°	88.4°
87.8°	90°	88°
87.2°	89°	87.2°
87°	89.2°	87.2°
86.2°	83.5°	86°
85.2°	87.2°	85.6°
84°	81.7°	84.5°
83°	81°	83.5°

3.5 Performance Limitations of the proposed ILS

Several methods are currently considered for UWB ILS that are mainly intended to locate a person/tag in real time. These systems are expected to provide very high accuracy, but there are in fact several factors that limit their performance in terms of accuracy, resolution, complexity and cost. For this reason, this section is devoted to exploring the different constraints related to the proposed localization technique. Such limitations arise from a variety of sources such as plane wave conditions between received signals at LBS and method parameter selection.

To analyze the behavior of the 2D method and test its limitations in terms of sampling frequency, signal bandwidth, analysis window and $d_{baseline}$, a Matlab simulation bench is designed using the Molisch generated channels (IEEE 802.15.4a).

3.5.1 Plane Wave Condition

The computation of the azimuth angle by the 2D localization method described in Section 3.2.2 requires two parallel received signals to ensure a minimum error in the angle measurement. This condition, known as the PWC, is guaranteed if the distance between the tag and the LBS is very large compared to the complete localization system. Nevertheless, when the AT is at a finite distance from the LBS, the received signals are not totally parallel and a difference between the arrival angles on the two receiving antennas is therefore observed, thus affecting the angle estimation. Consequently, the limitations on the minimum distance d separating the AT and the LBS must be taken into account in order to design a system capable of accurately estimating the Azimuth angle.

The 2D angle measurement is shown in Figure 3.37. Assume that the transmitting antenna A_0 is placed at the origin (0,0) of the axis and the distance between the two receiving antennas A_1 and A_2 is equal to $d_{baseline}$. The AT to be located is at position (x,y). The signal is transmitted from A_0 with an angle α and will be received by A_1 and A_2 with deviations $\delta\alpha''$ and $\delta\alpha'$ respectively. These deviations tend to zero when the two received signals are parallel.

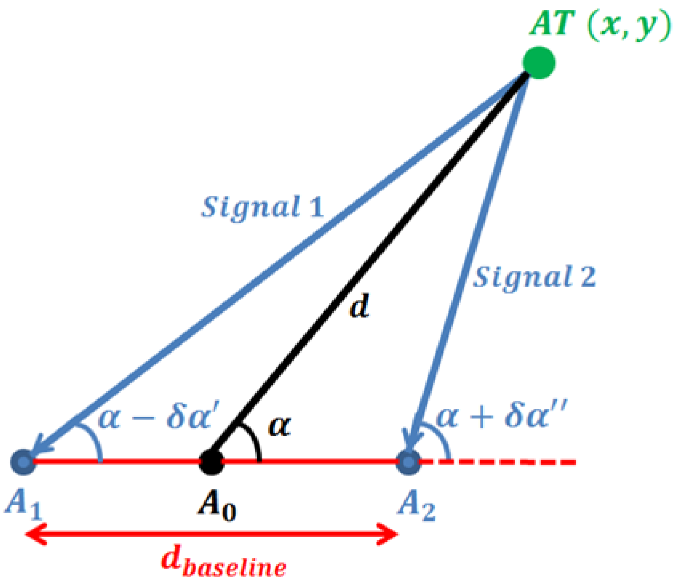

Figure 3.37 – Plane Wave Condition.

The angles of arrival are given by the following expression [3]

$$\begin{aligned} \alpha + \delta\alpha'' &= \tan^{-1}\left(\frac{y}{x - 0.5d_{baseline}}\right) \\ \alpha - \delta\alpha' &= \tan^{-1}\left(\frac{y}{x + 0.5d_{baseline}}\right) \end{aligned} \tag{3.9}$$

The expression (3.9) is rearranged in terms of the baseline factor B_f and the azimuth angle α as follows

$$\begin{aligned} \alpha + \delta\alpha'' &= \tan^{-1}\left(\frac{\tan\alpha}{1 - \frac{1}{B_f \cos\alpha}}\right) \\ \alpha - \delta\alpha' &= \tan^{-1}\left(\frac{\tan\alpha}{1 + \frac{1}{B_f \cos\alpha}}\right) \end{aligned} \tag{3.10}$$

where

$$\begin{cases} \tan\alpha = \frac{y}{x} \\ x = d\cos\alpha \\ B_f = \frac{d}{0.5d_{baseline}} \end{cases}$$

We are interested in the magnitude difference between the angles of arrival

$$|\delta\alpha' + \delta\alpha''| = \left| \tan^{-1}\left(\frac{\tan\alpha}{1 - \frac{1}{B_f\cos\alpha}}\right) - \tan^{-1}\left(\frac{\tan\alpha}{1 + \frac{1}{B_f\cos\alpha}}\right) \right| \tag{3.11}$$

Therefore, decreasing the deviation $\delta\alpha$ leads the signals to be close to PWC, which is expressed as follows

$$\delta\alpha = \frac{\delta\alpha' + \delta\alpha''}{2} = \frac{1}{2}\left[\tan^{-1}\left(\frac{\tan\alpha}{1 - \frac{1}{B_f\cos\alpha}}\right) - \tan^{-1}\left(\frac{\tan\alpha}{1 + \frac{1}{B_f\cos\alpha}}\right) \right] \tag{3.12}$$

The variation of deviation $\delta\alpha$ according to the baseline factor B_f for different angles α is presented in Figure 3.38. For $\alpha = 0°$, the deviation $\delta\alpha$ is zero for any value of B_f. As we can see, $\delta\alpha$ decreases with B_f and becomes constant after a certain value of B_f. For example, for $\alpha = 15°$ it remains under 1° when $B_f > 10$ while for $\alpha = 60°$ it remains under 1° when $B_f > 30$.

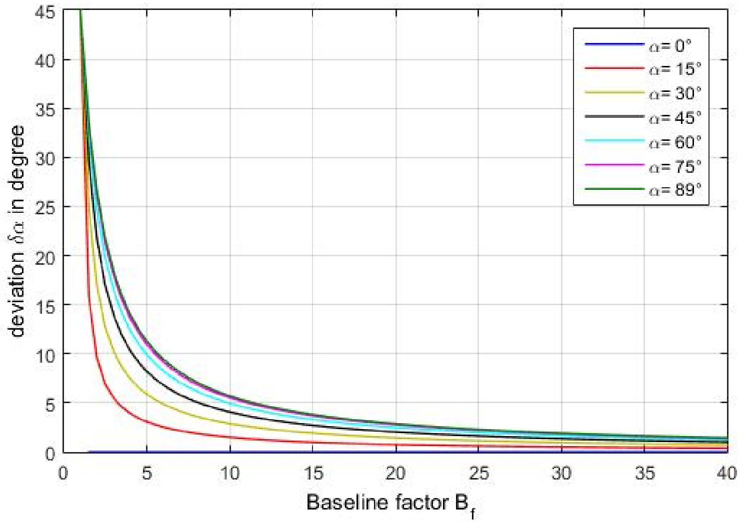

Figure 3.38 – Deviation $\delta\alpha$ according to B_f.

The variation of deviation $\delta\alpha$ according to angle α for different values of $d_{baseline}$ and $d = 1$ m is presented in Figure 3.39. The $\delta\alpha$ reaches the maximum value at the orthogonal position to the baseline. The PWC fails completely for $\alpha = 90°$ and the maximum values of $\delta\alpha$ are 4.2°, 5.7°, 7°, 8.5°, 9.9°, 11.3° for $d_{baseline}$ equals to 15 cm, 20 cm, 25 cm, 30 cm, 35 cm and 40 cm respectively. It also shows that $\delta\alpha$ decreases when B_f increases. This implies that the smaller $d_{baseline}$ will hold the PWC better than the larger one as the B_f increases. It therefore seems viable to use a smaller $d_{baseline}$ length for azimuth angle computation.

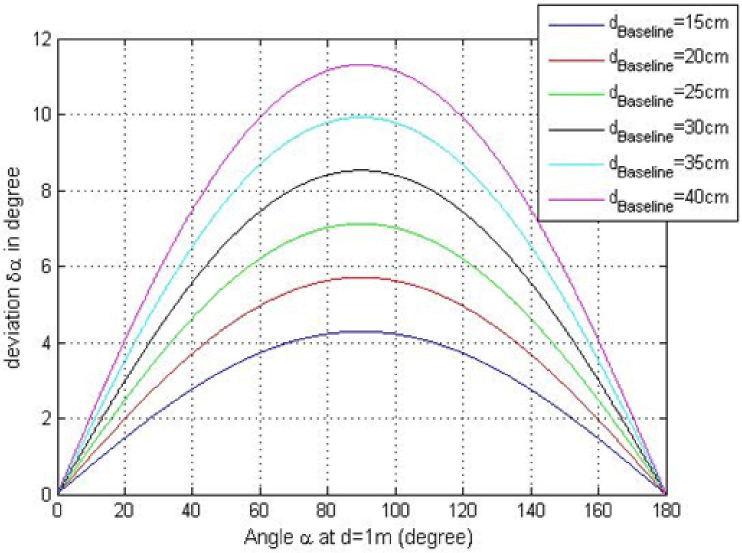

Figure 3.39 – Deviation $\delta\alpha$ according to α at $d = 1$ m.

3.5.2 Path difference condition

The angle computation using the path difference between the two received signals sets limits on the path difference.

$$\cos\alpha = \frac{Path{-}dif}{d_{baseline}}$$
$$|\cos\alpha| \leq 1 \quad \Rightarrow |Path - dif| \quad \leq |d_{baseline}| \tag{3.13}$$

As shown in the relationship (3.13), the path difference always remains less than or equal to $d_{baseline}$, otherwise it will leads to a ridiculous error.

As shown in Figure 3.40, the path difference varies from 0 to $d_{baseline}$ for an angle variation α from 0° to 90°. Table 3.8 shows the relationship between Path-dif and α according to different $d_{baseline}$ values.
As we can see, the α corresponding to 1 cm offset of Path-dif decreases when $d_{baseline}$ increases, which reflects an improvement in angular resolution. In other words, an ILS with a larger $d_{baseline}$ gives a better angular resolution for an angular estimation of an AT in a defined position. However, the Path-dif corresponding to 1° offset of α increases when $d_{baseline}$ increases. Therefore, a trade-off between the desired angular resolution and PWC must be taken into account when choosing $d_{baseline}$.

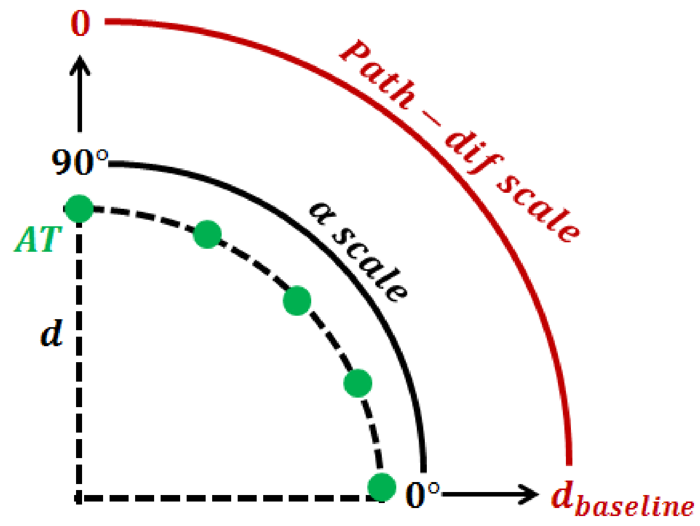

Figure 3.40 – Path-dif and α scales.

Table 3.8 – Path-dif and α correspondence

$d_{baseline}$ [cm]	α **corresponding to** 1 **cm of Path-dif**	**Path-dif [cm] corresponding to** 1° **of** α
15	3.8°	0.26
20	2.9°	0.35
25	2.3°	0.44
30	1.9°	0.52
35	1.6°	0.6
40	1.4°	0.7

3.5.3 Duplex UWB Method limitation

To study the method performance, a Matlab simulation bench is designed using Molisch generated channels (IEEE 802.15.4a) [11]. These tests are performed in the LoS office environment (CM3). As described in Section 2.6, two pulses U and V are used with an amplitude $A = 1$ V and a bandwidth of 1 GHz

$$\begin{aligned} U(t) &= A\cos\left(2\pi f_1 t\right)e^{-\left(\frac{t}{T_p}\right)^2} \\ V(t) &= A\cos\left(2\pi f_2 (t-t_s)\right)e^{-\left(\frac{t-t_s}{T_p}\right)^2} \end{aligned} \tag{3.14}$$

As mentioned in Section 2.6.1, the duplex UWB method is based on the difference $\Delta\varphi$ between the phase shifts of the two signals U and V. Therefore, to avoid the phase ambiguity [12], $\Delta\varphi$ should respect the following constraint

$$\Delta\varphi = 2\pi(f_2 - f_1)t_{ToF} \leq 2\pi \tag{3.15}$$

Therefore, for this method to remain viable, the time of flight of each signal shall not exceed the inverse of the frequency difference, i.e.

$$t_{ToF} \leq \frac{1}{f_2 - f_1} = \frac{1}{\Delta f} \tag{3.16}$$

From this inequality, the maximum range d_{max} that this method can detect is given by

$$d_{max} = \frac{c.t_{ToF-max}}{2} = \frac{c}{2\Delta f} \tag{3.17}$$

Figure 3.41 shows the maximum range d_{max} that the duplex UWB method can estimate as a function of the frequency difference Δf.

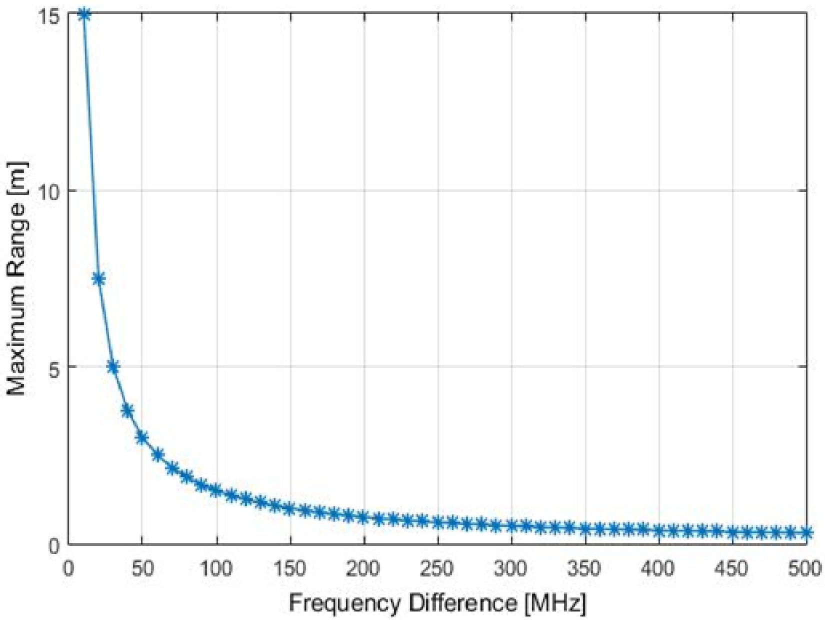

Figure 3.41 – Maximum range d_{max}.

The maximum distance is $d_{max} = 15$ m when $\Delta f = 10$ MHz. This value drops significantly as the frequency difference increases to a point where the method becomes almost useless ($d_{max} = 30$ cm) when Δf gets too large (500 MHz). This leads us to conclude that sending two pulses with a smaller frequency difference yields in a longer detection range.

In our system, the pulse width is equal to 1 GHz in the antenna bandwidth [3 – 4 GHz]. We therefore opted to pick f_1 and f_2 to be equal to 3.5 GHz and 3.55 GHz, respectively, making our system suitable for estimating distances up to $d_{max} = 3$ m for a frequency difference Δf of 50 MHz.

3.5.4 Phase Correlation Method limitations

This section is devoted for presenting the limitations imposed by the PC method.

Sampling Frequency

The minimum path difference that our method can detect is limited by the sampling frequency F_e according to the following relation

$$Path - dif_{min} = \frac{c}{F_e} \tag{3.18}$$

where c is the celerity of light. Figure 3.42 shows the minimum path difference that can be detected with respect to F_e.

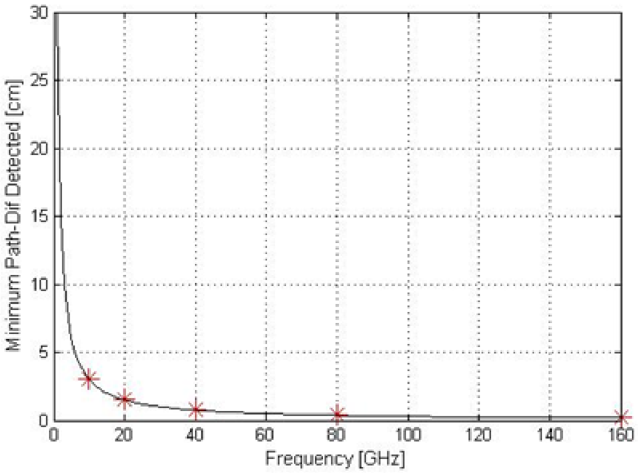

Figure 3.42 – Minimum path difference.

For instance, our system can detect a $Path - dif_{min} = 3$ cm when using $F_e = 10$ GHz. This value becomes even smaller, i.e. it can detect a $Path - dif_{min} = 0.2$ cm if F_e is increased to 160 GHz.

Consequently, the angular resolution α_{res} defined as the minimum angle that can be detected is limited by the minimum path difference

$$\alpha_{res} = 90^\circ - \cos^{-1}\left(\frac{Path - dif_{min}}{d_{baseline}}\right) \tag{3.19}$$

For instance, if $d_{baseline}$ is set to 29 cm, our system can detect an angle more than 6°, i.e. $\alpha_{res} = 6^\circ$ when using $F_e = 10$ GHz. However, increasing F_e to 160 GHz allows the system to detect angles starting from $\alpha_{res} = 0.4^\circ$.

To be confident about the limitations of the PC method, we consider a system with $d_{baseline} = 29$ cm and an AT that can take different positions, each time with a 1 cm offset on a straight line parallel to $d_{baseline}$ at a distance of 1.5 m from it. Recall that the path difference increases when moving away from position 0, which is characterized by a $path - dif = 0$. For instance, an offset of 1 cm on each side of position 0, corresponds to $Path - dif = 0.2$ cm, while an offset of 16 cm from position 0 in both directions, corresponds to $Path - dif = 3$ cm. Figure 3.43 illustrates the different detection zones of the AT for different values of F_e.

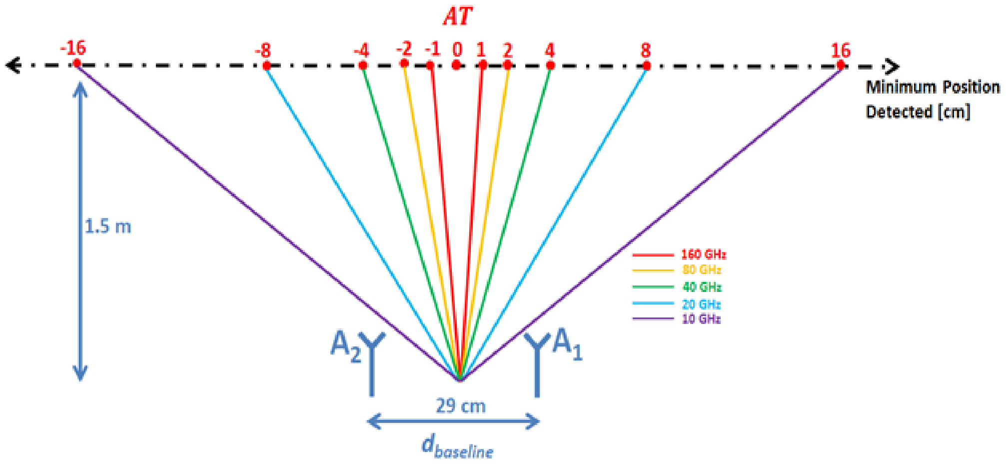

Figure 3.43 – AT detection zones.

As mentioned earlier, the $Path - dif_{min}$ is 3 and 0.2 cm for $F_e = 10$ and 160 GHz, respectively. For our system, this corresponds to a 16 and 1 cm offset of the AT on each side of position 0.

For this reason, when $F_e = 10$ GHz, our method estimates that the AT always occupies the position 0 as long as its actual position lies between 0 and 8 cm and occupies the position 16 when its actual position is between 9 and 16 cm. However, increasing F_e to 160 GHz improves the ability of our system to detect smaller values as of 1 cm from position 0. Therefore, a high sampling frequency yields a better angular resolution, but its implementation in real circuits remains problematic. Hence, we select $F_e = 20$ GHz as a trade-off between cost and angular resolution.

Signal Bandwidth and Analysis window

As shown in Section 2.7, the analysis window T_w is given by $T_w = t_2 + T_d - t_1$, and the window T_d should be larger or equal to the emitted pulse width T_p. According to Gabor theorem, the bandwidth Bw and the window T_d are related as follows

$$T_d = cte.T_p \quad \Rightarrow \quad T_d.Bw = cte \tag{3.20}$$

where Bw is the emitted signal bandwidth.

Phase Ambiguity

As shown in Section 2.7.1, the phase correlation function between two received signals is given by the following relationship

$$C_{U_1U_2}(\Delta t) = \frac{A'^2}{2}\cos(2\pi f_1 \Delta t) \tag{3.21}$$

Based on Eq.(3.21), the phase φ_{f_1} corresponding to the path difference between the two received signals is expressed as

$$\varphi_{f_1} = 2\pi f_1 \Delta t \tag{3.22}$$

The fact that the phase is bounded by 2π ($0 \leq \varphi_{f_1} \leq 2\pi$) will impose limits on the maximum path difference $Path-dif_{max}$ detected by the applied method.

$$\varphi_{f_1} \leq 2\pi \quad \Rightarrow \quad 2\pi f_1 \Delta t \leq 2\pi \quad \Delta t \leq \frac{1}{f_1} \tag{3.23}$$

$$Path-dif_{max} = \frac{c}{f_1} \tag{3.24}$$

Consequently, the maximum computed azimuth angle which is related to $Path-dif_{max}$ will also be affected. In other word, the phase ambiguity reduces the space where the AT can be detected to an angular cone α_c of 90° axis.

$$\alpha_c = 2\left[90^\circ - \cos^{-1}\left(\frac{Path-dif_{max}}{d_{baseline}}\right)\right] \tag{3.25}$$

Moreover, the path difference condition from Eq. (3.13) also imposes constraints on the choice of $d_{baseline}$, i.e. $|d_{baseline}| \geq |Path-dif|$.

Figure 3.44 shows the variation of the angular cone α_c as a function of different $d_{baseline}$ values. From Eq. (3.24), the $Path-dif_{max}$ is equal to 8.6 cm if the center frequency $f_1 = 3.5$ GHz is used. When $d_{baseline} = Path-dif_{max} = 8.6$ cm, the corresponding angular cone is $\alpha_c = 180^\circ$. We can also notice that the angular cone α_c decreases significantly when $d_{baseline}$ increases and reaches 24° for $d_{baseline} = 40$ cm.

Figure 3.45 illustrates the different angular detection zones of the AT as a function of $d_{baseline}$ values. As we can see, for $d_{baseline} = 8.6$ cm, the system can detect any position of the AT, i.e. for any azimuth angle α ranging from 0° to 180°. In contrast, when $d_{baseline} = 40$ cm, the angular cone is reduced to 24°, i.e. the AT can be detected if it is located in the cone [78°,102°].

Therefore, an ILS with a smaller $d_{baseline}$ gives a larger angular zone detection. For this reason, a trade-off between the desired angular cone, the desired angular resolution and

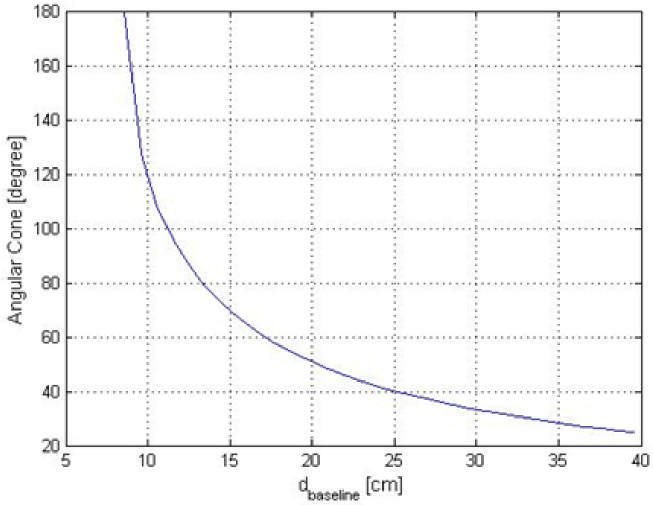

Figure 3.44 – Angular cone α_c.

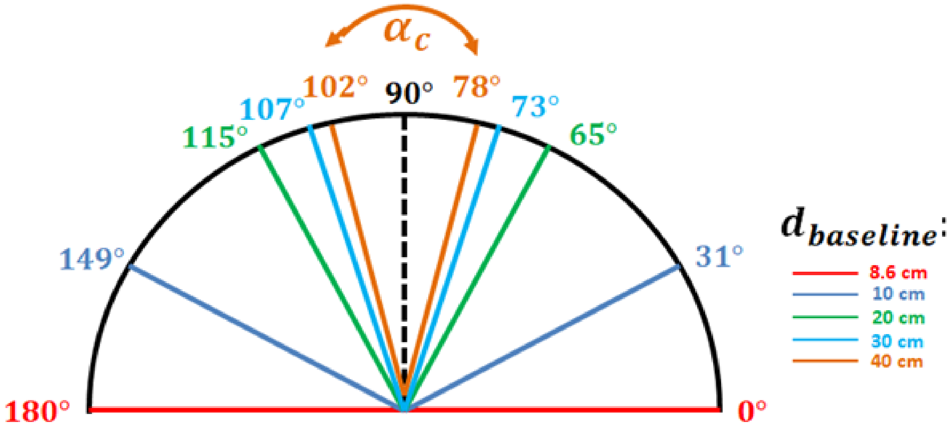

Figure 3.45 – AT angular detection zones.

PWC must be taken into account when choosing $d_{baseline}$.

In this work, and particularly in the experimental measurements, $d_{baseline}$ is also susceptible to limitations imposed by the dimensions of the used antennas. We then decided to choose it equal to 29 cm to comply with all the constraints of the system.

3.6 Realized UWB Indoor Localization System

This section is dedicated for estimating the link budget of the realized system in order to ensure correct measurements. The gains and losses related to the various stages follow the characteristics of each components presented in Section 3.3.

The complete developed LBS and AT are shown in Figure 3.46 and Figure 3.47 respectively.

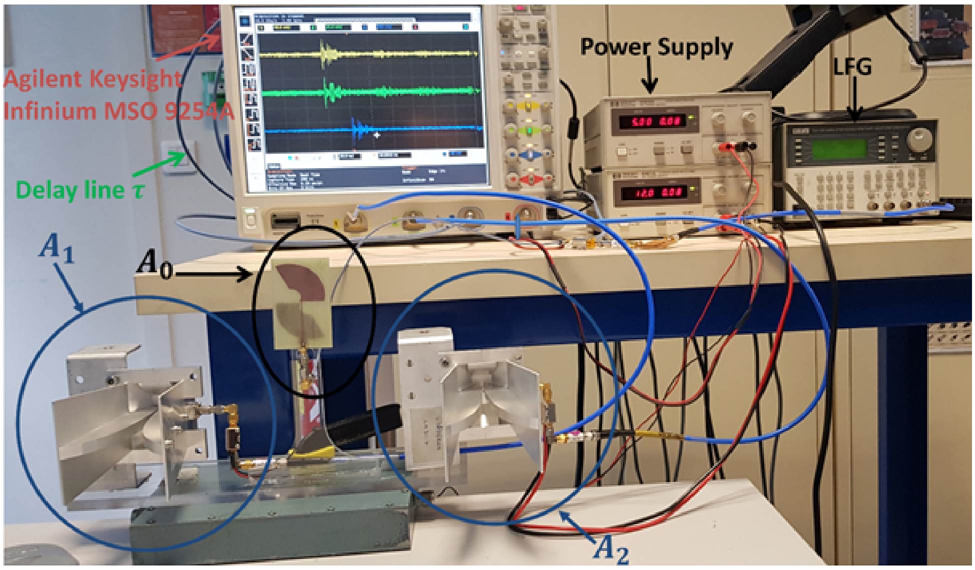

Figure 3.46 – Developed LBS.

The power levels at different stages of the transmitter chain are shown in Figure 3.48. All powers are expressed in dB. Let P be the power generated by the impulse generator. Connection cables and SubMiniature version A (SMA) connectors were identified as a source of 0.5 dB loss. The transmitted signal power by the antenna is then '$P + 16.1$' dB, while the power of the delayed transmitted signal considered as the reference signal for processing is '$P - 7.3$' dB.

Under normal atmospheric conditions, the free space losses are expressed as

$$PL(dB) = 32.44 + 20log(f_0) + 20log(d) \tag{3.26}$$

where d is the range distance in Km, and f_0 is the carrier frequency of the transmitted signal in MHz.

For the sake of simplicity, we consider the direct path case. The signal reaches the active tag located at a distance d from the LBS with a power equal to '$P + 16.1 - PL$' dB. The power levels at the different stages of the active tag are shown in Figure 3.49.
The signal is retransmitted from the active tag with power equal to '$P + 46 - PL$' dB. By travelling the same distance d, this signal reaches the receiver antenna with power equal to '$P + 46 - 2 \times PL$' dB. The power levels of the receiver chain are shown in Figure 3.50.

Table 3.9 shows the power at the output of the receiver chain as a function of distance d for a fixed carrier frequency of 3.5 GHz and $P = -17$ dB.

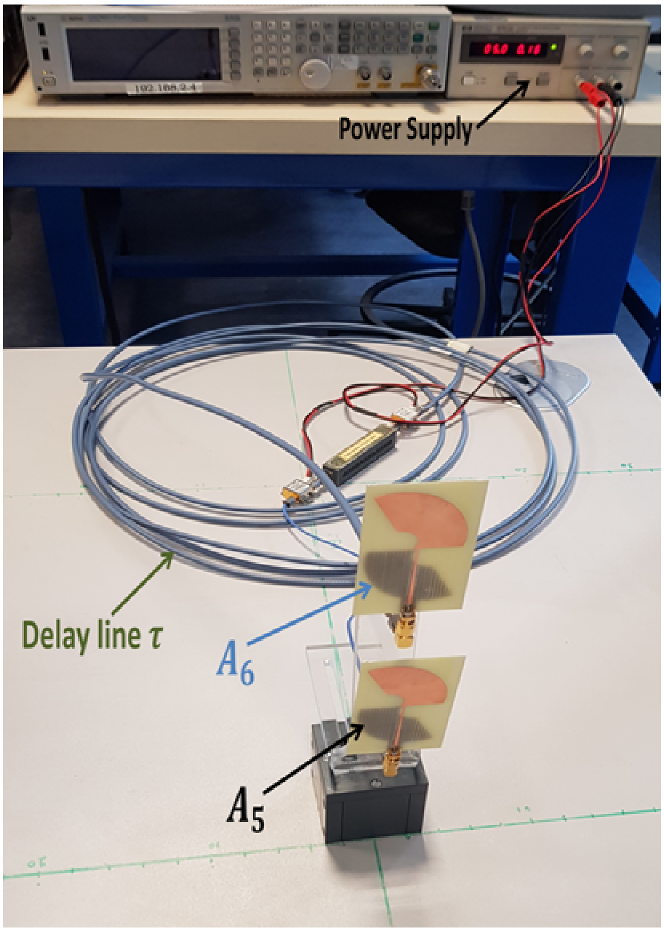

Figure 3.47 – Developed AT.

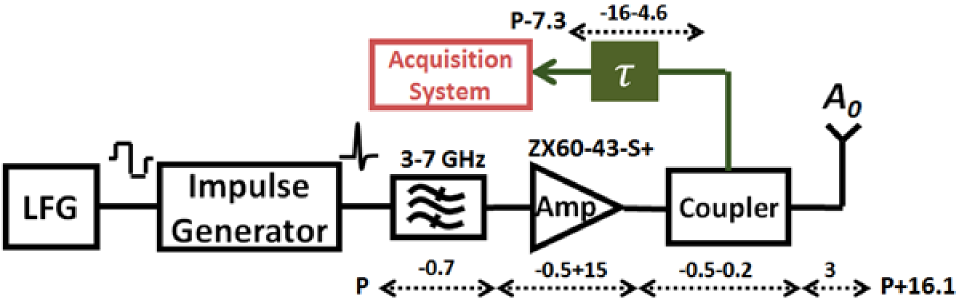

Figure 3.48 – Power levels at transmitter chain.

As shown in Table 3.9, the received power varies between −57.64 dB and −69.68 dB for a free space of 1 to 2 meters. The receiver sensitivity can be enhanced by decreasing the receiver noise figure. To do so, the component with the lowest noise figure is connected to the receiving antenna in order to guarantee better receiving sensitivity. Therefore, the amplifier ZX60-6013E+ with a noise figure lower than ZX60-43-S+ is used in RX-chain.

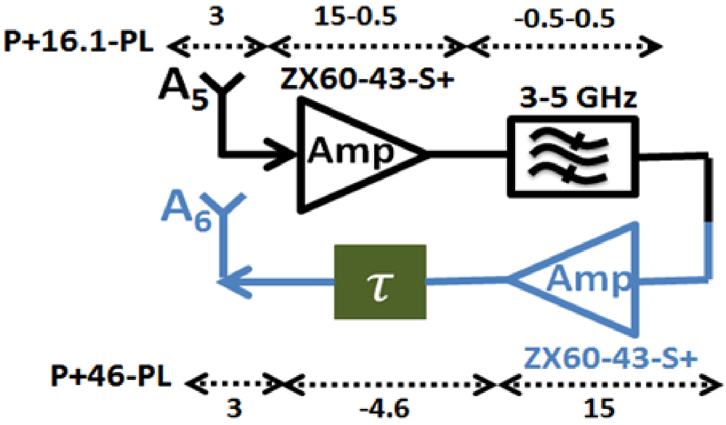

Figure 3.49 – Power levels at AT.

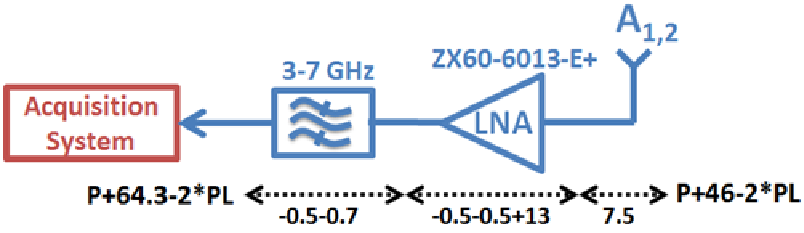

Figure 3.50 – Power levels at receiver chain.

Table 3.9 – Received power

Distance [m]	PL [dB]	Received power [dB]
1	43.32	-57.64
1.5	46.84	-64.68
2	49.34	-69.68

3.7 Conclusion

In this chapter, we have presented an ILS based on the trilateration method, where 3 well-synchronized anchors and whose positions are well known, are used to locate an AT in 2D.

To overcome the limitations imposed by these systems, a 2D localization scheme for a remote AT was presented. The developed architecture is based on the concept of the mono-pulse radar system where a single anchor acting as a localization base station is used without requiring prior knowledge of its position. A 2D UWB indoor localization technique based on the radial distance and azimuth angle measurement is proposed, where the radial distance is obtained by phase difference correlation and the azimuth angle is obtained by phase correlation.

Afterwards, the different components of the proposed ILS are characterized and their specific functions in the system are outlined. Among these components, a circular polarized antenna is designed and optimized for the transmitter and AT chains.

The accuracy of the azimuth measurement is improved by using a phase correlation method. A test bench based on cables set is used as a proof concept. The experimental results show that this proposed method can achieve high accuracy angle measurement (lower than 0.4° Vs. an error of 3.4° for a classical method).

After describing the transmitter, the active tag and the receiver chains, some performance limitations related to the proposed method are presented. This step is mandatory to better select the different system parameters such as sampling frequency, signal bandwidth and $d_{baseline}$ depending on the desired angular resolution, angular cone, accuracy and cost.

Finally, the power level at different stages of the entire system along with the receiving sensitivity are discussed to get some insight into the system's properties.

In the next chapter, system performance will be studied through MATLAB simulations and experimental measurements.

Bibliography

[1] P. Gulden, S. Roehr, and M. Christmann, “An Overview of Wireless Local Positioning System Configurations,” IEEE MTT-S International Microwave Workshop on Wireless Sensing, Local Positioning, and RFID, pp. 1–4, September 2009. Cited page 79

[2] D. Moore, J. Leonard, D. Rus, and S. Teller, “Robust Distributed Network Localization with Noisy Range Measurements,” IEEE International Conference on Embedded Networked Sensor Systems (SenSys), pp. 50, 2004. Cited page 79

[3] R. Kumar, “Indoor Localisation for Telemonitoring,” Ph.D. Dissertation, Telecom Paristech, Electronique et Communications, Paris, France, 2014. Cited pages 80, 84, and 103

[4] M. Mironovova and H. Havlis, “Calculation of GDoP Coefficient,” CTU in Prague: Faculty of Electrical Engineering, 2011. Cited page 15

[5] T. Jalloul and W. Ajib, “DME/DME Navigation using a Single Low-Cost SDR and Sequential Operation,” Digital Avionics Systems Conference , October 2014. Cited page 82

[6] `https://fr.slideshare.net/ahmadsajjadsafi/distance-measurement-equipment-dme`. Cited page 82

[7] `https://ww2.minicircuits.com/pdfs/ZX05-C42.pdf`. Cited page 85

[8] Y. Shen and C.L. Law, “A microstrip-Fed Quasi Spiral Circularly Polarized Ultra-Wideband Antenna,” Antennas and Propagation Society International Symposium (APSURSI), 2011. Cited page 90

[9] `http://www.ainfoinc.com/en/pro_pdf/new_products/antenna/Broadband%20Horn%20Antenna/tr_LB-1080-M.pdf`. Cited page 97

[10] N. Awarkeh, J.C. Cousin, M. Muller and N. Samama, “Improvement of The Angle Measurement Accuracy for Indoor UWB Localization,” European Microwave Week (EUMW), September 2018. Cited page 100

[11] A.F. Molisch, D. Cassioli, C.C. Chong, S. Emami, A. Fort, B. Kannan, J. Karedal, J. Kunish, H.G. Schantz, K. Siwiak and M.Z. Win, “A Comprehensive Standardized Model for Ultrawideband Propagation Channels,” IEEE Transactions on Antennas and Propagation, vol. 54, no. 11, November 2006. Cited page 106

[12] B. A. Garcia, “Conception d’un Radar d’aide à la Conduite Automobile utilisant un Système Discriminateur de Fréquence Type Six-port,” ph.D. Dissertation, Telecom Paristech, Electronique et communications, Paris, France, 2002. Cited page 106

Chapter 4

Performance Analysis of our Proposed ILS

4.1 Introduction

The prototype of the ILS described in Chapter 3 is developed in this chapter to estimate the 2D position of the AT. The performance of the designed ILS is tested in a Matlab simulation bench using Molisch-generated channels (IEEE 802.15.4a) [1] and then validated with field measurements in a real indoor environment.

This chapter presents the main results of the proposed ILS. The simulated and experimental validations of the phase correlation method are performed for a simplified ILS (without AT) in Section 4.2 and for the entire system (with AT) in Section 4.3. In both cases, the results are compared to those obtained with a state-of-the-art method, namely the ED method. In Section 4.4, a simulation bench is designed to validate the duplex UWB method. In Section 4.5 and Section 4.6, the results of our ILS based on radial and angular measurements are compared to a system performing the position estimation using a constellation and trilateration method under LoS and obstructed LoS assumptions, respectively. In Section 4.7, the performance of our ILS is studied in the NLoS situations. Finally, the chapter ends with a conclusion in Section 4.8.

4.2 Phase correlation Method Validation for a Simplified ILS

This section first describes the setup used to validate the PC method of estimating a small path difference and then shows the respective results emphasizing the angular resolution improvement for a simplified ILS, which consists of one transmitter chain TX and two receiver chains RX.

4.2.1 Simulated and Experimental Setup

The complete setup, shown in Figure 4.1, is composed by one RF transmitter chain linked to a circular polarized antenna A_0, and two RF receiver chains, connected to two UWB horn antennas A_1 and A_2. The distance between A_1 and A_2 is denoted by $d_{baseline}$.

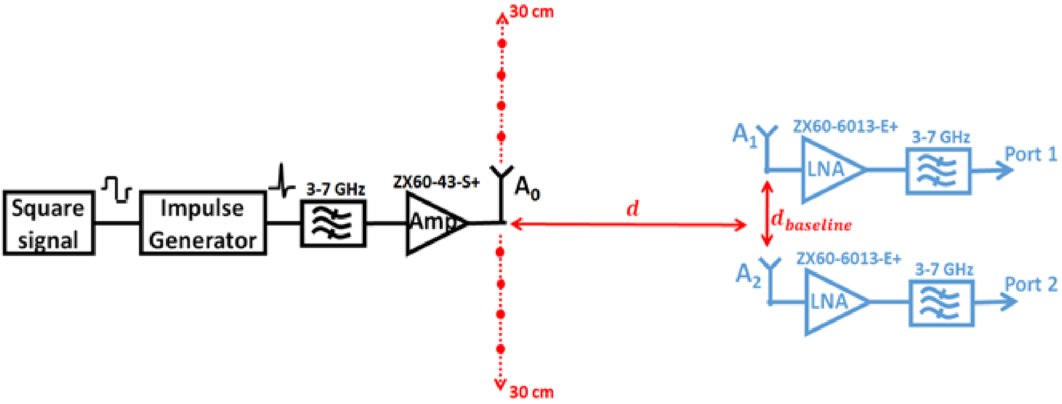

Figure 4.1 – Test bench setup.

The goal of this setup is to validate the PC method. The transmitter chain is identical to the one presented in Section 3.3.1 except that:

- The LO is removed since this method requires only one transmitted signal (in this case, the signal U of center frequency f_1 is selected).
- The coupler is also eliminated, because this method is applied between the two received signals, and therefore no need for a τ-delayed version of the transmitted signal.

The obtained pulses at the output of the Impulse Generator and at the input of the antenna A_0 are shown in Figure 4.2 and Figure 4.3, respectively.

The UWB pulses are transmitted via the front end antenna A_0 and received by two identical receiver chains described in Section 3.3.3. The received pulses U_1 and U_2 are acquired on Ports 1 and 2 of the oscilloscope (Agilent Keysight Infinium MSO 9254A) respectively. The different components of the circuit and their characteristics are described in Section 3.3.

To improve the resolution of the path difference measurement between U_1 and U_2, the antenna A_0 can take 31 different positions p_i with $i \in \{-15, \cdots, 15\}$, as shown in Figure 4.4. At the initial position p_0, the antenna A_0 is placed on an orthogonal axis at a distance d equal to 1.5 m from the center of $d_{baseline}$ in order to satisfy the PWC described in Section 3.5.1. $d_{baseline}$ is chosen here equal to 29 cm due to the limitations imposed by the

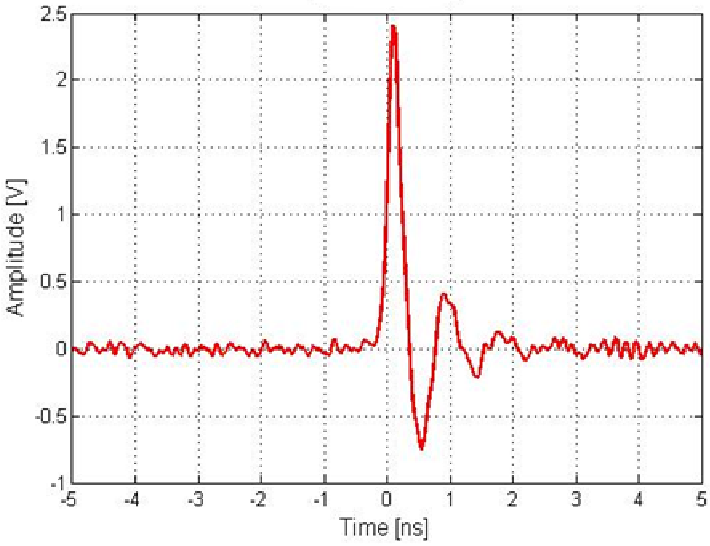

Figure 4.2 – The pulse at the output of the Impulse Generator .

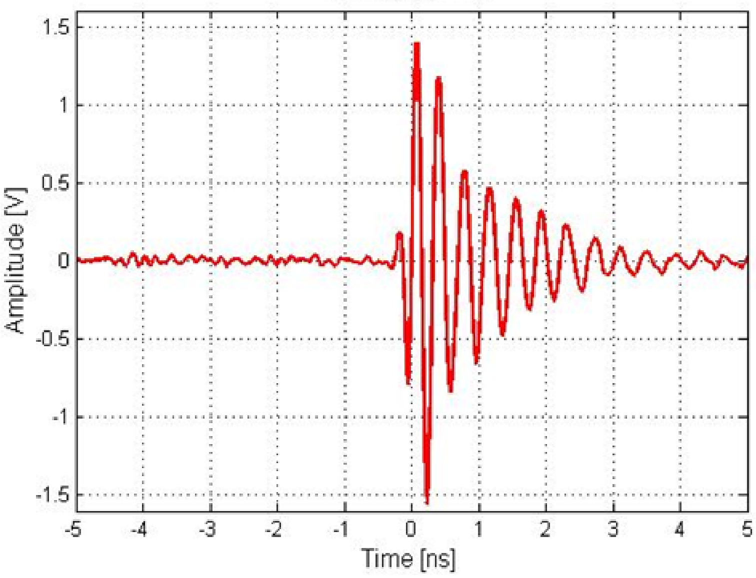

Figure 4.3 – The pulse at the input of the antenna A_0.

dimensions of the used antennas.

To validate the angular resolution improvement obtained with the PC method, A_0 can occupy several positions on a straight line parallel to the baseline, by shifting it 2 cm on each side of its initial position p_0 in the range $[-30\text{ cm}; 30\text{ cm}]$.

The distance between A_0 and A_1 (resp. A_2) is denoted d_1 (resp. d_2). The path difference

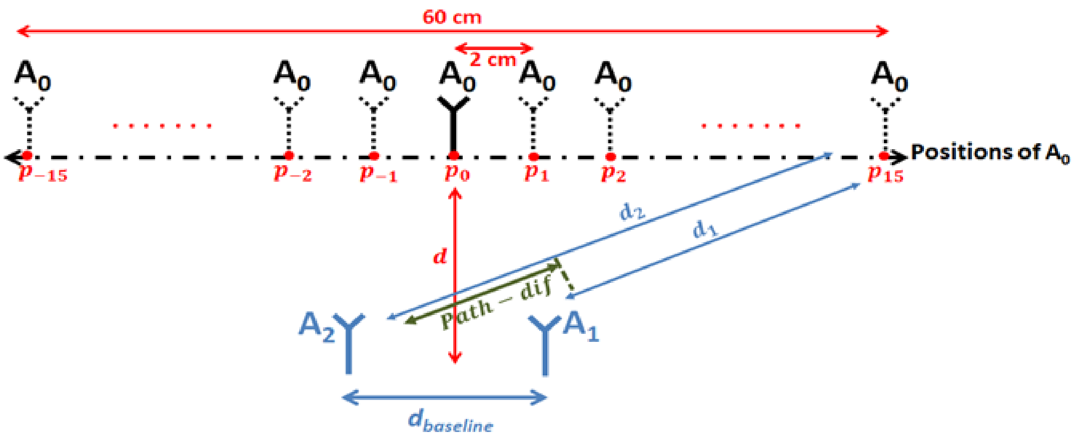

Figure 4.4 – Possible positions of A_0.

between the two received signals U_1 and U_2, denoted $path - dif = d_1 - d_2$, is expressed in terms of the difference between their arrival times T_1 and T_2 at antennas A_1 and A_2, respectively. For this configuration, the maximum actual path difference corresponding to the positions p_{-15} and p_{15} is equal to 5.7 cm.

This configuration is used for the experimental setup and the Matlab simulation bench that uses Molisch-generated channels (IEEE 802.15.4a). The waveform of the emitted signals, shown in Figure 4.3, corresponds to a cosine carrier modulated by a Gaussian pulse. Therefore, the waveform defined in Section 2.5.1 is used as the emitted pulse in all simulations

$$U(t) = A.\cos(2\pi f_1 t)e^{-(\frac{t}{T_p})^2} \tag{4.1}$$

where $A = 1$ V is the amplitude of the signal, $f_1 = 3.5$ GHz the center frequency (center frequency of A_0 pass band $[3 - 4$ GHz$]$), $T_p = \frac{1}{\zeta.Bw.\sqrt{2}.\pi}$ with $\zeta = 0.43$ and $Bw = 1$ GHz the bandwidth of the pulse corresponding to the bandwidth of A_0.

Moreover, the CM3 channel model (office LoS) of IEEE 802.15.4a is adopted and the SNR is set to 15 dB in all simulations.

4.2.2 Simulated and Experimental Results

In Figure 4.5, the broadened recorded signals for the initial position of A_0 are presented. Both signals are distorted in the same way by the circuit components and antennas. These pulses, i.e. $U_1(t)$ and $U_2(t)$, acquired at ports 1 and 2 respectively, can be described by a cosine carrier modulated by a Gaussian pulse as mentioned in Section 2.5.1.

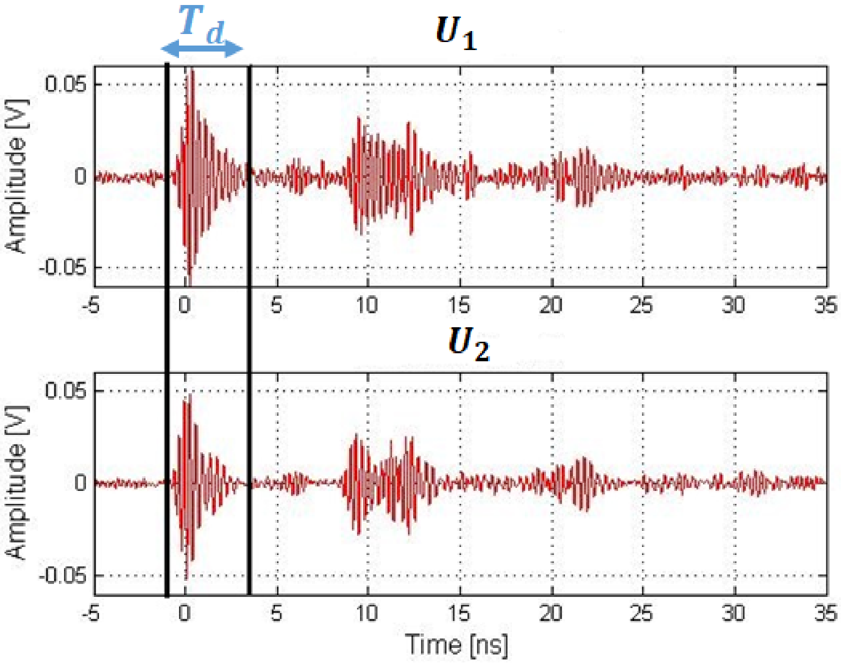

Figure 4.5 – Recorded signals at Ports 1 and 2 for the initial position p_0.

The path difference between U_1 and U_2 is estimated for each position p_i using the configuration shown in Figure 4.1. As a proof of concept, we compare the results of the simulated and measured path difference obtained by the PC method with the ED method [2].

As shown in Figure 4.3 and Figure 4.5, the duration T_p of the emitted pulse by A_0 is equal to 2 ns and the duration of the received broadened signal T' is 23 ns, respectively.

Following the fundamental principle of the ED method in which the energy is calculated by block, each of duration 4 ns (must be greater than T_p) with a displacement step Δ_b equal to 1 ns. Then, the ToA of the received pulse is estimated based on the detection of the block carrying the maximum energy.

For the PC method, the beginning of the received pulses is determined by fixing the duration of each block T_b to $T' = 23$ ns and the displacement step Δ_b to 1 ns, in order to ensure that the energy of the entire broadened received pulse is taken into account. On the other hand, setting T_d equal to $T_p = 2$ ns, guarantees that the various conditions mentioned in Section 2.7.1 are fulfilled. Hence, the pulses of interest in the analysis window T_d shown in Figure 4.6, are those that lie between the two black lines in Figure 4.5.

A calibration step is mandatory to estimate the time unbalance between U_1 and U_2. At position p_0, i.e. when A_0 is not shifted yet, we observe a time difference of 0.14 ns which corresponds to a path difference of 4.2 cm. This difference is mainly caused by the un-

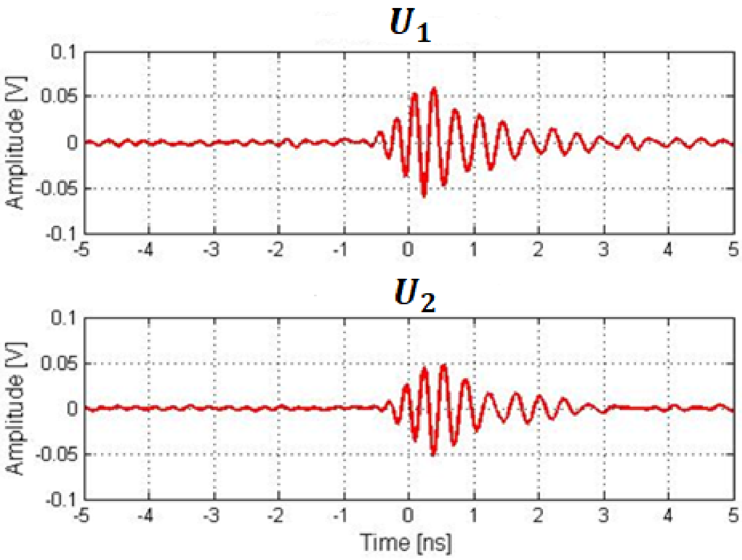

Figure 4.6 – Pulses of interest in the analysis window.

balance between the two RX chains and must be taken into account when calculating the path difference.

Initially, U_1 and U_2 are oversampled by 16 with a sampling frequency equal to 10 GHz using the oscilloscope (F_e = 160 GHz). This configuration is an ideal case study that helps us to get an insight about the best performance by reducing the imposed limits on the minimum path difference that can be detected. Note that the system calibration step is also performed with this sampling frequency.

However, as the implementation of a high sampling frequency in real circuits remains challenging, the PC method is also validated with a smaller sampling frequency F_e = 20 GHz.

For Fe = 160 GHz, we compare in Figure 4.7 the real path difference with that simulated and measured by the ED and PC methods. The x-axis represents the 31 different positions of the antenna A_0. Moreover, the difference between the actual and estimated values along the y-axis represents the error in the Path-dif estimation. Figure 4.8 shows the error in the simulated and measured path difference by the aforementioned methods, for the 31 different positions of the antenna A_0.

The same comparison is carried out for the Azimuth angle in Figure 4.9 and Figure 4.10, since it is derived directly from the Path-dif.

We noticed that the obtained results of both simulations and measurements using the ED method are identical. These results are also quite similar using the PC method.

Since the considered displacement step Δ_b is equal to 1 ns, the minimum path difference that the ED method can detect is 30 cm. Thus, it is not able to detect a path difference in the order of 5.7 cm which corresponds to the maximum Path-dif obtained by this configuration (at p_{15} and p_{-15}). On the other hand, the minimum path difference that the PC method can detect is determined by the sampling frequency; and therefore it is able to detect a path difference of 0.2 cm when Fe = 160 GHz.

As we can see, the maximum error in the estimated path difference by the ED method is equal to 5.7 cm, which corresponds to a maximum angle error equal to 11.3°. This error is reduced to 0.5 cm using the PC method, which is reflected by an error reaching 2.5 cm in the position estimation of A_0. This error corresponds to an error of 1° in the azimuth angle estimation.

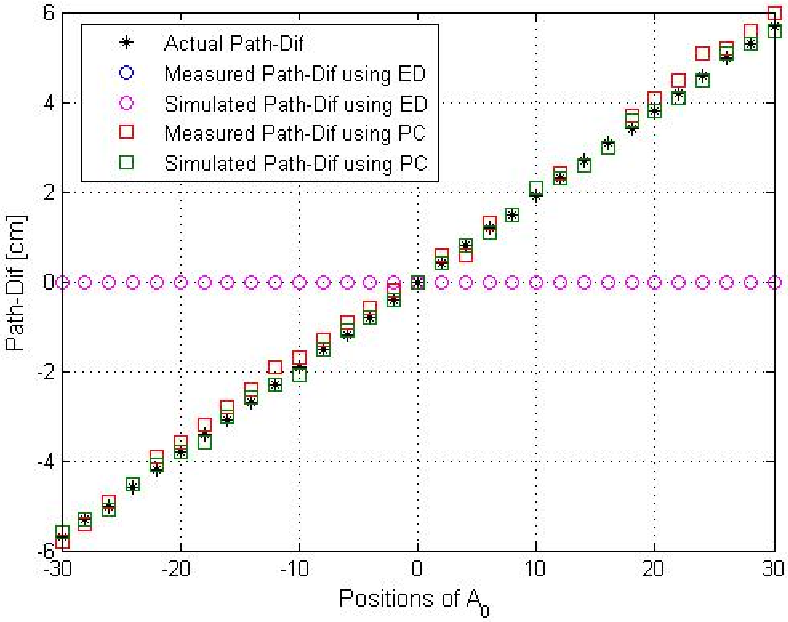

Figure 4.7 – Comparison of the path difference estimation for F_e = 160 GHz.

The same comparison is carried out for Fe = 20 GHz in Figures 4.11-4.14. Here, the minimum path difference that the ED method can detect remains the same (30 cm) since the displacement step is not modified. However, as the sampling frequency has decreased, the PC method can now detect a minimum path difference of 1.5 cm.

As we can see, the maximum error in the estimated path difference by the ED method is equal to 5.7 cm, which corresponds to a maximum angle error equal to 11.3°. This error

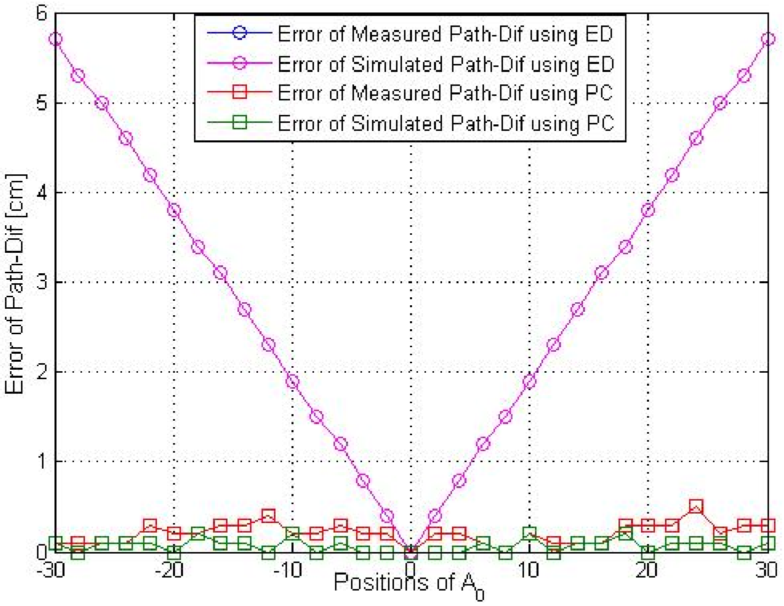

Figure 4.8 – Error in the path difference for F_e = 160 GHz.

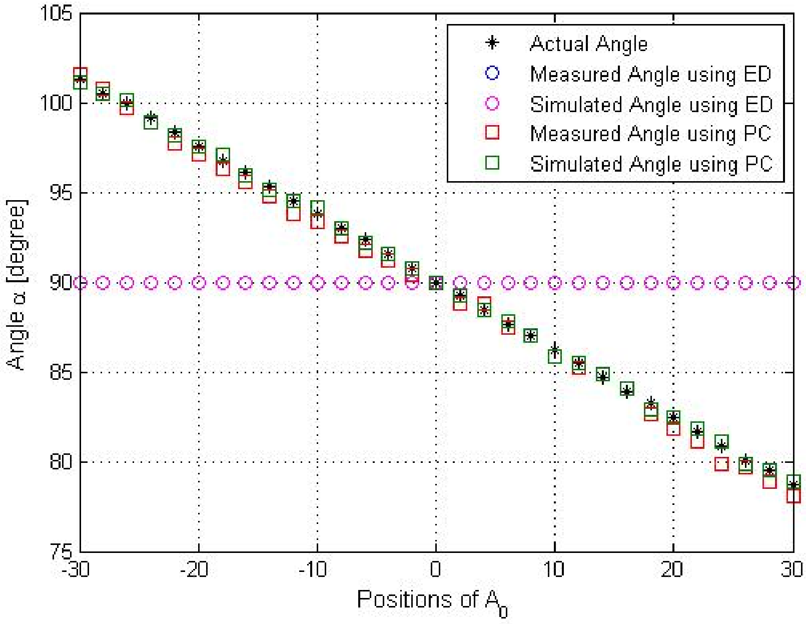

Figure 4.9 – Comparison of the azimuth angle estimation for F_e = 160 GHz.

is reduced to 0.8 cm using the PC method, which is reflected by an error reaching 4 cm in the position estimation of A_0. This error corresponds to an error of 1.6° in the azimuth angle estimation.

To show the effect of the sampling frequency on the limitations of the PC method, we

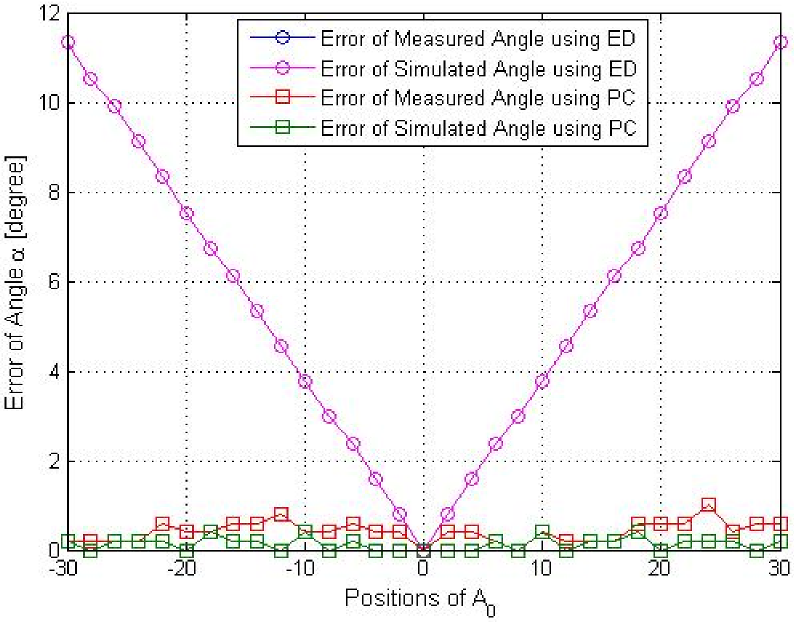

Figure 4.10 – Error in azimuth angle for F_e = 160 GHz.

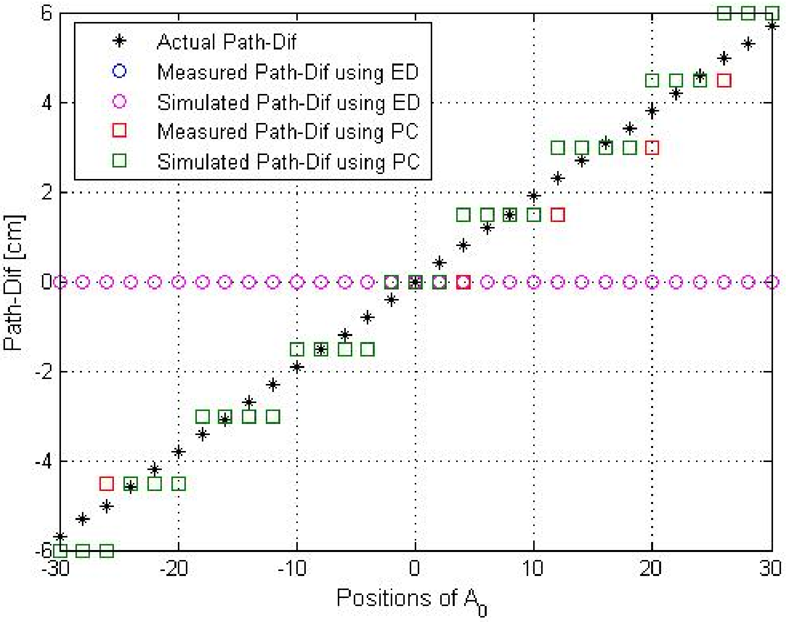

Figure 4.11 – Comparison of the path difference estimation for F_e = 20 GHz.

compare the obtained results in Figure 4.7 and Figure 4.11.

With our configuration, each offset position of A_0 corresponds to an offset of 0.4 cm in the path difference which is represented by the actual path difference (black star).

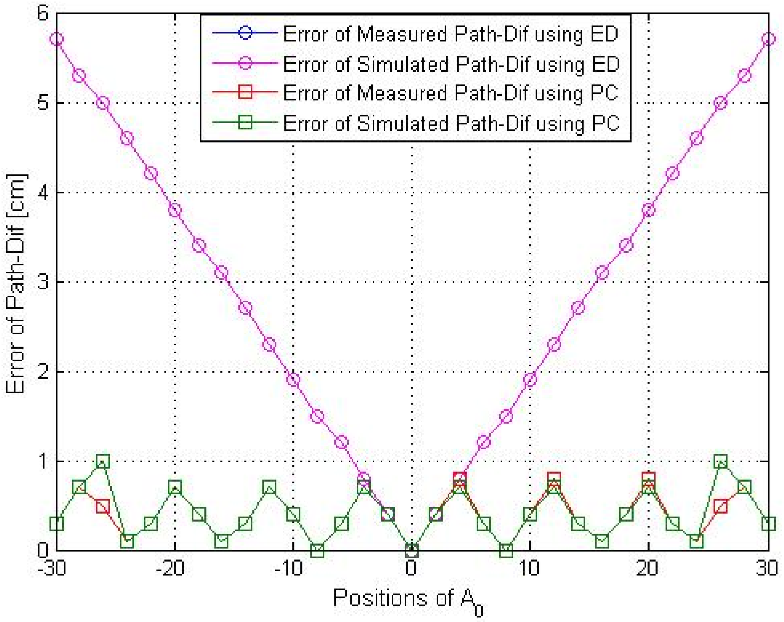

Figure 4.12 – Error in the path difference for F_e = 20 GHz.

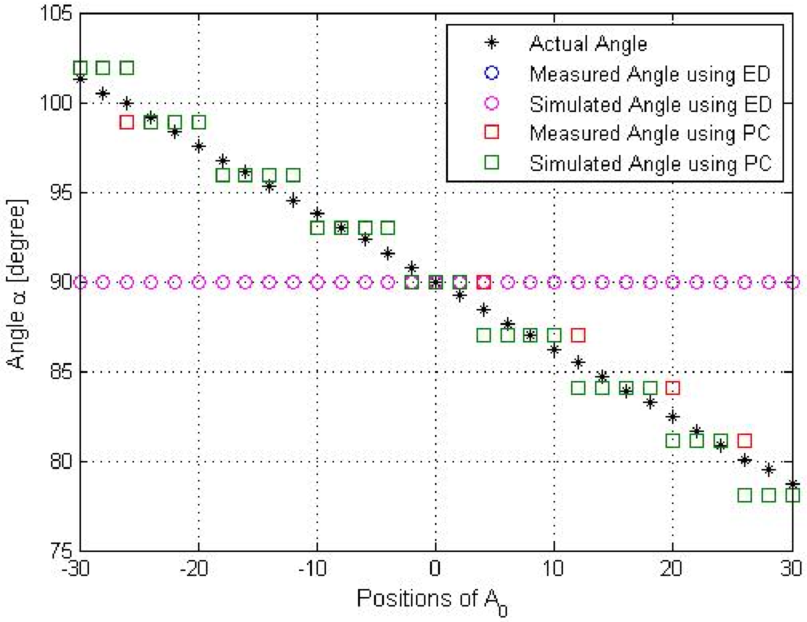

Figure 4.13 – Comparison of the azimuth angle estimation for F_e = 20 GHz.

Since the minimum path difference that the PC method can detect is 0.2 cm when Fe = 160 GHz, the estimated path difference in measurement and simulation (plotted using squares), takes different values very close to the actual ones for each position of A_0,

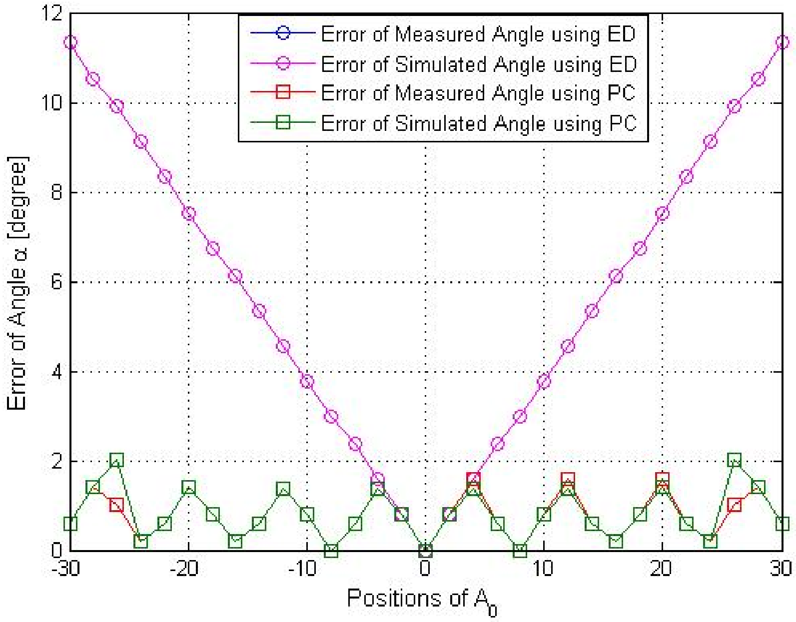

Figure 4.14 – Error in azimuth angle for F_e = 20 GHz.

as shown in Figure 4.7.

However, when Fe = 20 GHz, the PC method cannot distinguish between small path differences, if the latter are less than the minimum path difference it can estimate, in this case 1.5 cm. This is reflected in Figure 4.11, where the estimated measured and simulated path difference (presented by squares) takes the same values for different positions of A_0. For example, the estimated Path-dif is 1.5 cm for 4 different positions of A_0 (p_2 to p_5).

Therefore, a high sampling frequency allows a better angular resolution, but is not always easy to implement in real circuits. Hence, a trade-off between resolution and implementation complexity is required.

Table 4.1 summarizes the results obtained in this section for the two sampling frequency 20 and 160 GHz.

Table 4.1 – Comparison between the maximum error of ED and PC methods

	ED method		**PC method**	
	Path-dif	α	**Path-dif**	α
F_e = 160 **GHz**	5.7 cm	11.3°	0.5 cm	1°
F_e = 20 **GHz**	5.7 cm	11.3°	0.8 cm	1.6°

The PC method is therefore validated for a simplified configuration. We are now seeking to validate it for the proposed ILS presented in Section 3.2 with the integration of the AT.

4.3 Phase correlation Method Validation for the proposed ILS

This section is a generalization of the previous section in which we validate the angular resolution improvement of our proposed ILS described in Section 3.2 using the PC method. Recall that our ILS consists of a fixed LBS and an AT that occupies different arbitrary positions.

4.3.1 Simulated and Experimental Setup

The full setup of our ILS is shown in Figure 4.15. On one hand, the LBS consists of one RF transmission chain connected to a circularly polarized antenna A_0 and two RF receiving chains connected to two UWB horn antennas A_1 and A_2 spaced by a distance denoted $d_{baseline}$. On the other hand, the AT is a transmitting/receiving chain connected to two circularly polarized antennas A_5 and A_6.

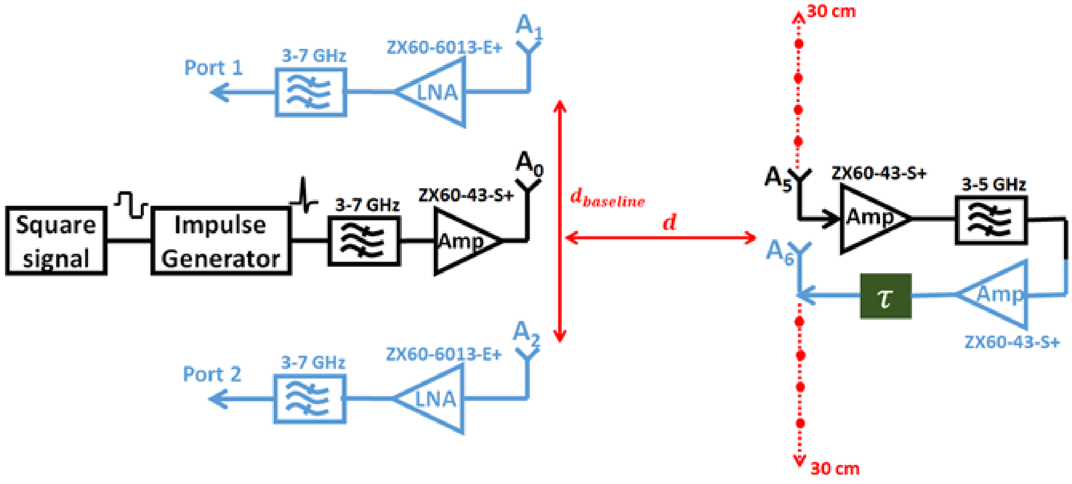

Figure 4.15 – Test bench setup.

The transmitter and receiver chains of the LBS are identical to those described in Section 4.2.1 and the AT is similar to the one presented in Section 3.3.2.

The process starts here in the same way as in the previous case, but instead of receiving the UWB pulses directly by the receiving chain, the AT here receives these pulses via the antenna A_5. At this stage, a delay τ equivalent to a delay line of 8 m in length is applied to the obtained signal before retransmitting it to the LBS with the antenna A_6. The process of receiving this signal by the two RX chains now continues in the same way as before and ends with the acquisition of the BPF outputs U_1 and U_2 on ports 1 and 2 of the oscilloscope (Tektronix), respectively. This oscilloscope has only one sampling frequency (40 GHz), which forces us to consider this value for this configuration, i.e. $F_e = 40$ GHz.

Compared to the previous case where A_0 took 31 different positions p_i for $i \in \{-15, \cdots, 15\}$, here the LBS is supposed to be fixed, so is A_0. Therefore, the AT is the moving entity in this scenario and can take the above-mentioned positions p_i by shifting it 2 cm on each side of its initial position p_0 in the range [−30 cm ; 30 cm] on a straight line parallel to the baseline, as shown in Figure 4.16. In this configuration, we also set $d_{baseline}$ to 29 cm and the PC method is validated for two values of d: 1 m and 1.5 m. These two values are selected to study the effects of d on the PC method's performance. The distance d represents the distance between the center of $d_{baseline}$ and the AT when the latter occupies the position p_0. The maximum actual path difference of our particular system, which corresponds to the positions p_{-15} and p_{15}, is equal to 8.3 cm and 5.7 cm for $d = 1$ and 1.5 m, respectively.

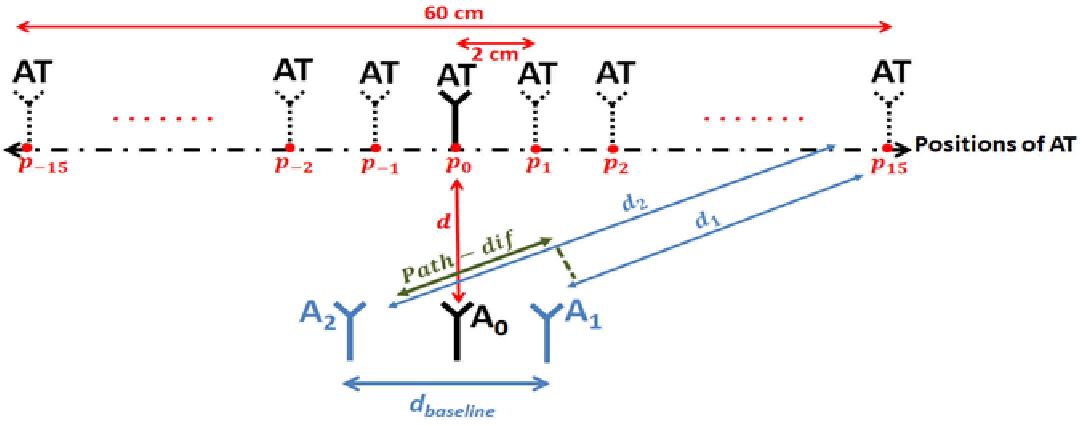

Figure 4.16 – Possible positions of the AT.

Now everything is ready to carry out the experimental setup and the Matlab simulation bench which again uses the CM3 channel model from IEEE 802.15.4a. The 8 m delay line described in Section 3.3.2 used in the experimental setup is translated by a delay of 30 ns in the simulations.

4.3.2 Simulated and Experimental Results

Following the same strategy as before, we can notice from Figure 4.17 that the outputs $U_1(t)$ and $U_2(t)$ of the two receiving chains (connected to the oscilloscope) when the AT is in the position p_0, also depict in this case a cosine carrier modulated by a Gaussian pulse.

The path difference between U_1 and U_2 is estimated for each position p_i using the configuration shown in Figure 4.15 and the obtained results of applying the PC method on the simulated and measured path difference are also compared to the ED method, using the

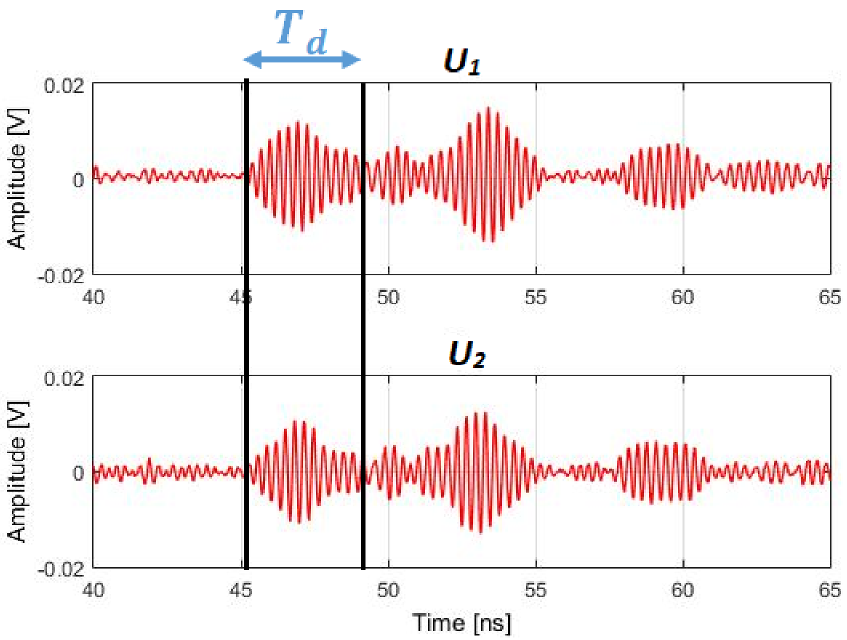

Figure 4.17 – Recorded signals at Ports 1 and 2 for the initial position p_0.

same parameters reported in the simplified case. Compared to the simplified case, the pulses of this system are more spread out, since they are making a round trip to reach the receiver as shown in Figure 4.17. For this reason, the analysis window T_d is now equal to 4 ns.

In Figure 4.17, we highlighted with two black lines the pulse of interest in the analysis window T_d and zoomed it in Figure 4.18.

In this system, the time unbalance between U_1 and U_2 can be overcome by estimating its value through a calibration step in order to take it into account in the computation of the path-difference. Recall that this unbalance occurs because the two receiving chains are not balanced, so that a time difference of 0.1 ns, or alternatively 3 cm of path difference, appears when the AT is not yet displace (position p_0).

For $d = 1$ m, we compare in Figure 4.19 the real path difference with that simulated and measured by the ED and PC methods, and we show in Figure 4.20 the error in the simulated and measured path difference by the aforementioned methods, for the 31 different positions of the AT. The same comparison is carried out for the Azimuth angle in Figure 4.21 and Figure 4.22. As we can see, the ED and PC methods give roughly the same results in simulations and measurements.

Under the same configuration, in particular the displacement step of 1 ns, the ED method allows to detect a minimum path difference of 30 cm. In contrast, the minimum path difference that the PC method can detect is dictated by the sampling frequency; it is

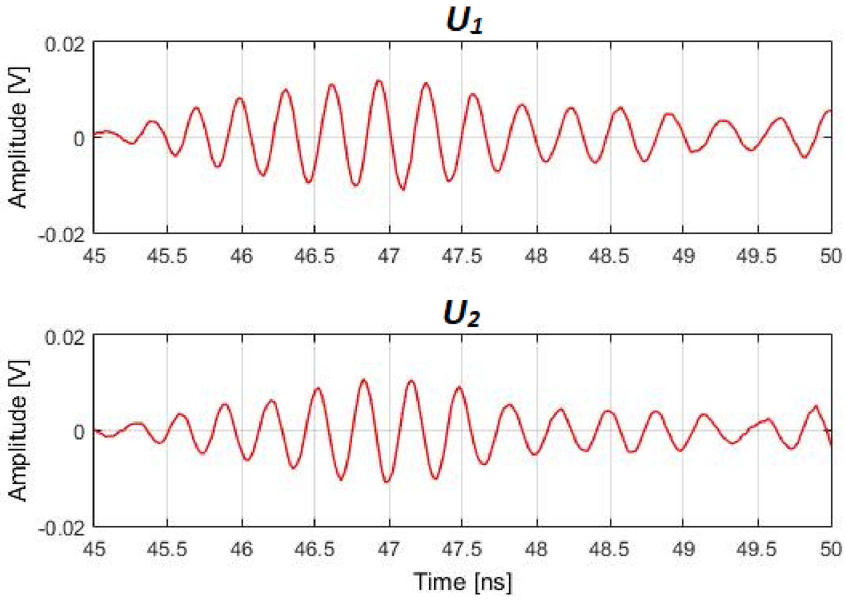

Figure 4.18 – Pulses of interest in the analysis window.

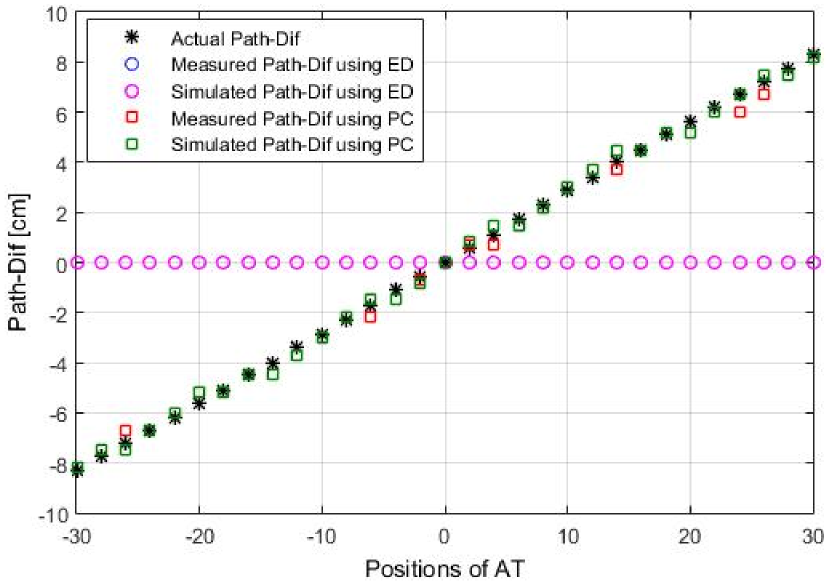

Figure 4.19 – Comparison of the path difference estimation for $d = 1$ m.

therefore capable of detecting a path difference of 0.8 cm for $F_e = 40$ GHz.

As can be seen, the ED method estimates the path difference with a maximum error of 8.3 cm which corresponds to the maximum actual path difference, and is equivalent to a maximum angular error of 16.6°. The PC method significantly improves the position estimation by reducing the error in the path difference estimation to 0.5 cm, or alternatively

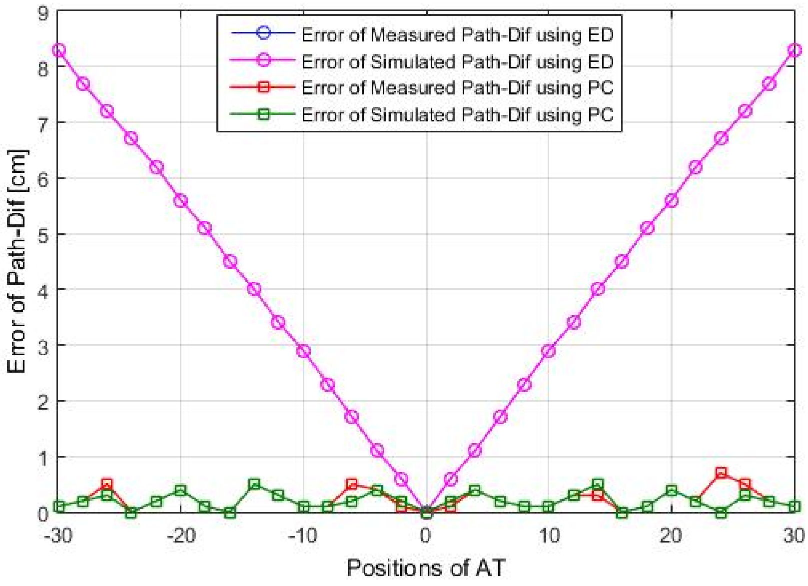

Figure 4.20 – Error in the path difference for d = 1 m.

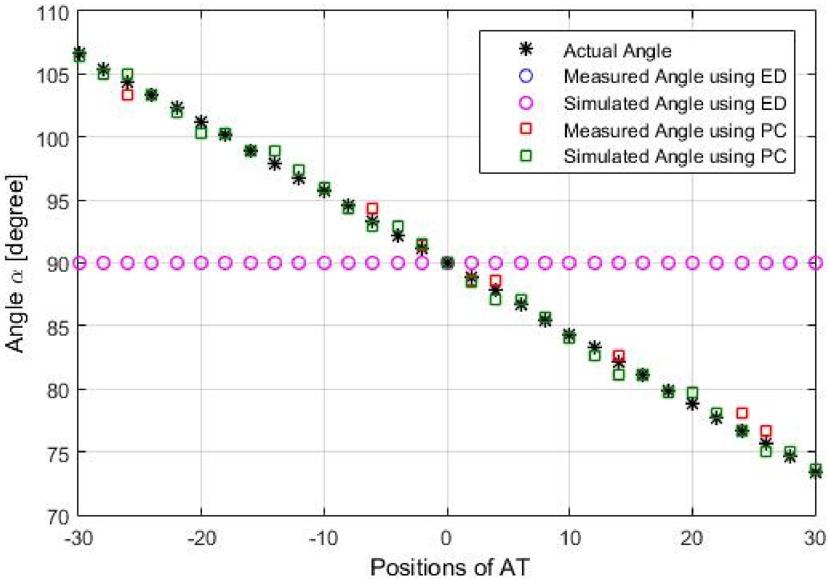

Figure 4.21 – Comparison of the azimuth angle estimation for d = 1 m.

an error reaching 1.6 cm and 1° in the position and azimuth angle estimation of the AT, respectively.

The same comparison is performed for d = 1.5 m in Figures 4.23-4.26. Note that changing the value of the distance d does not affect the minimum path difference that the ED and PC methods can detect.

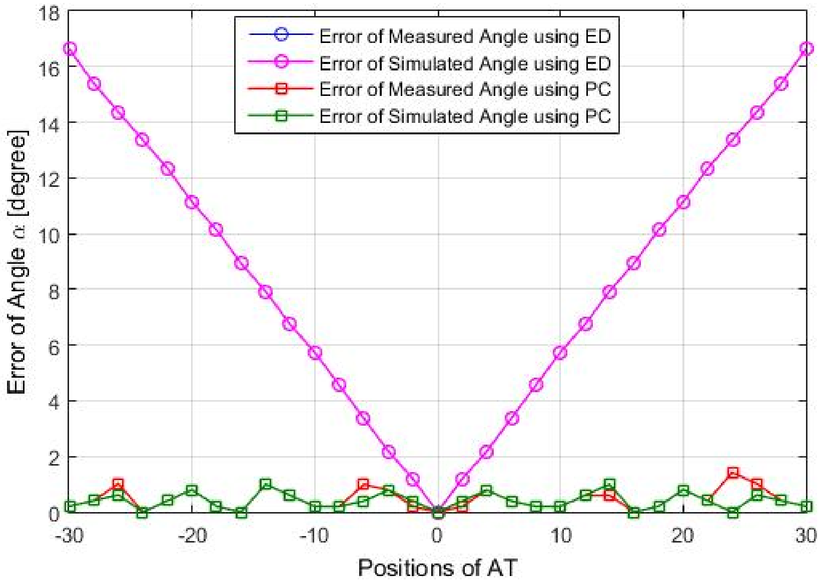

Figure 4.22 – Error in azimuth angle for $d = 1$ m.

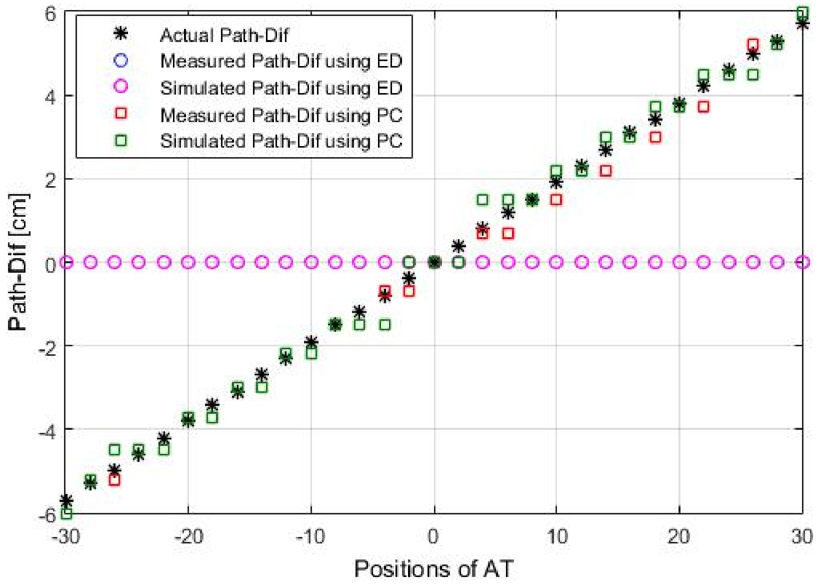

Figure 4.23 – Comparison of the path difference estimation for $d = 1.5$ m.

As we can see, the PC method provides improved position estimation by reducing the maximum error in the estimated path difference and azimuth angle from 5.7 cm and 11.3° to 0.7 cm (3.5 cm in the AT position estimation) and 1.4°, respectively.

To study the effect of the distance on the PC method performance, the obtained results

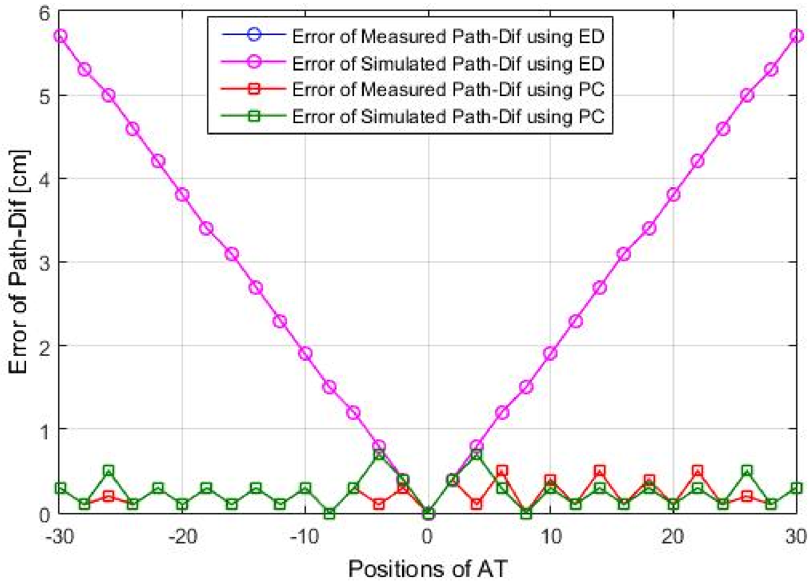

Figure 4.24 – Error in the path difference for d = 1.5 m.

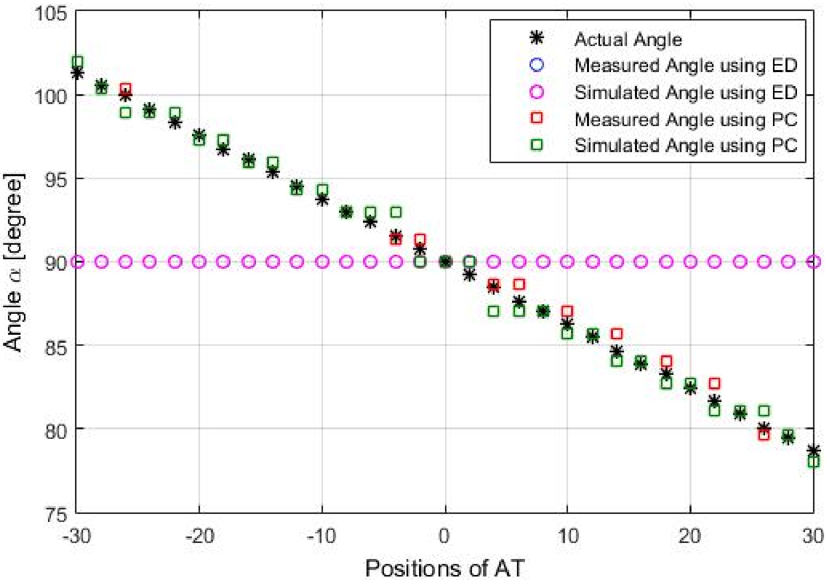

Figure 4.25 – Comparison of the azimuth angle estimation for d = 1.5 m.

for d = 1 and 1.5 m are compared.

As shown in Figure 4.19 and Figure 4.23, each offset position of A_0 corresponds to an offset of 0.6 cm and 0.4 cm in the actual path difference for d = 1 m and d = 1.5 m, respectively. In other words, the minimum path difference that the system shall estimate is equal to 0.6 cm for d = 1 m and 0.4 cm for d = 1.5 cm.

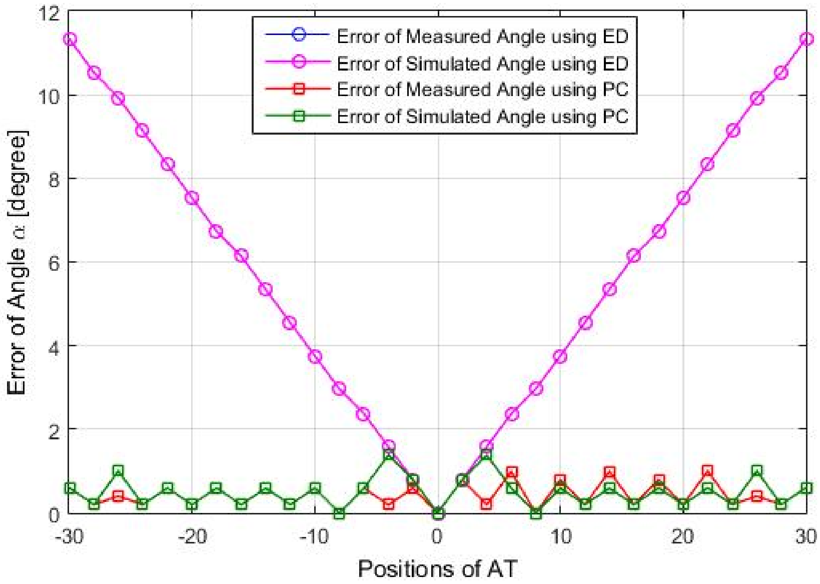

Figure 4.26 – Error in azimuth angle for d = 1.5 m.

Therefore, the performance of the PC method degrades when the distance increases, as the expected resolution also increases although the system cannot provide it.

Table 4.2 summarizes the results obtained in this section for the two distances 1 and 1.5 m.

Table 4.2 – Comparison between the maximum error of ED and PC methods

	ED method		**PC method**	
	Path-dif	α	**Path-dif**	α
d = 1 **m**	8.3 cm	16.6°	0.5 cm	1°
d = 1.5 **m**	5.7 cm	11.3°	0.7cm	1.6°

Finally, the PC method is validated, and we now proceed to the validation of the Duplex UWB method.

4.4 Duplex UWB Method Validation for the proposed ILS

This section describes the setup used to validate the duplex UWB method employed to estimate the distance of an AT. It presents the respective results with a particular focus on showing the improvement of the distance resolution for the proposed ILS compared to the conventional ED and TC methods.

4.4.1 Simulated Setup

The configuration used to validate the duplex UWB method is shown in Figure 4.27. The transmitter chain, the AT and the receiver chains are identical to those detailed in Section 3.3.

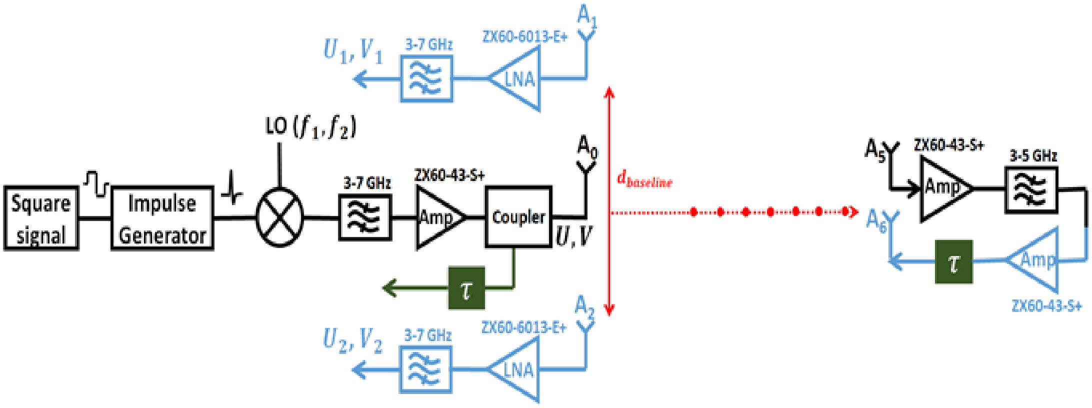

Figure 4.27 – Test bench setup.

Therefore, the process starts by sending two UWB pulses U and V having the same width and at carrier frequencies f_1 and f_2, respectively, via the front-end antenna A_0. These pulses reach the AT and are transmitted back to the LBS via the antenna A_6 following the same steps as before. The received signals (U_1, V_1) and (U_2, V_2) by the two RX chains are then sampled with a sampling frequency of 20 GHz before being processed.

To improve distance resolution, the AT can take different positions on an axis orthogonal to $d_{baseline}$. This axis is located at a distance d from the center of $d_{baseline}$, chosen here equal to 29 cm. The AT can therefore take 51 different positions p_i with $i \in \{0, \cdots, 50\}$, as shown in Figure 4.28, by shifting it 2 cm each time in the same direction within the range [1 m ; 2 m].

This configuration is now used for the Matlab simulation bench, which again adopts the CM3 channel model of IEEE 802.15.4a. The two emitted pulses U and V correspond to the waveform defined in Eq.(4.1) and are given by

$$U(t) = A\cos\left(2\pi f_1 t\right) e^{-\left(\frac{t}{T_P}\right)^2} \tag{4.2}$$

$$V(t) = A\cos\left(2\pi f_2 (t - t_s)\right) e^{-\left(\frac{t-t_s}{T_P}\right)^2} \tag{4.3}$$

where $f_1 = 3.5$ GHz and $f_2 = 3.55$ GHz are the carrier frequencies of $U(t)$ and $V(t)$ respectively, and $t_s = 20$ ns the starting time of $V(t)$. t_s is chosen equal to the broadened pulse duration in order to prevent the interference between the two received signals.

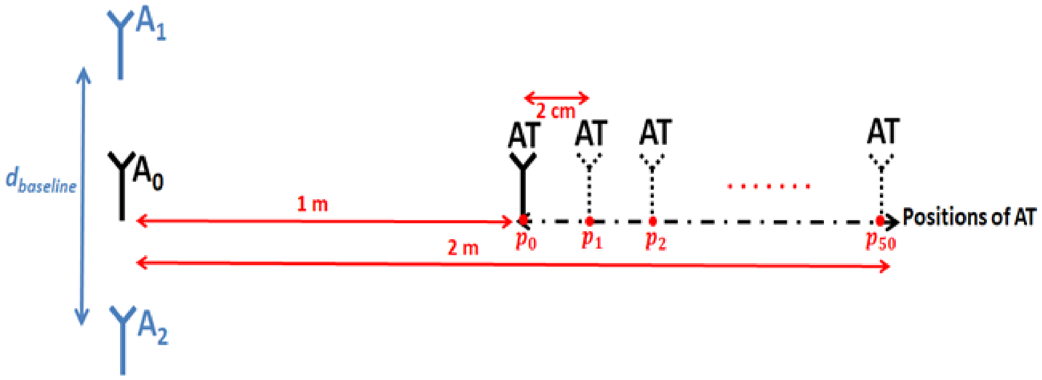

Figure 4.28 – Possible positions of the AT.

4.4.2 Simulated Results

In Figure 4.29 and Figure 4.30, the broadened received signals for the initial position of the AT are presented. As we can see, the deformation and distortion of these signals by the environment are the same for both center frequencies and on both RX-chains. Moreover, these received pulses, i.e. $U_1(t)$, $V_1(t)$, $U_2(t)$ and $V_2(t)$ takes the same time of flight to reach the respective RX-chain since the path difference between the received signals on both receiving chains is zero (the AT is placed at different positions on an orthogonal axis to $d_{baseline}$).

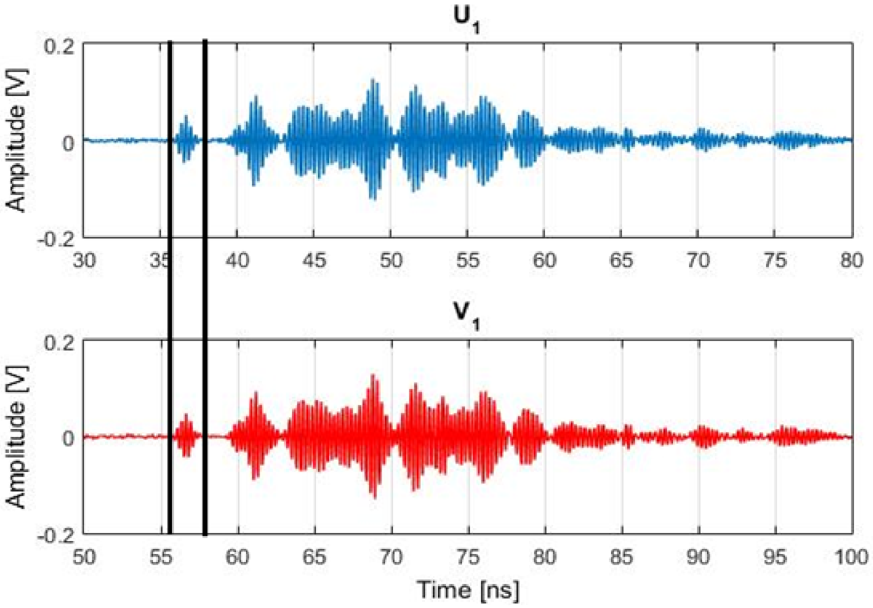

Figure 4.29 – Received signals at RX-chain 1 for the initial position p_0.

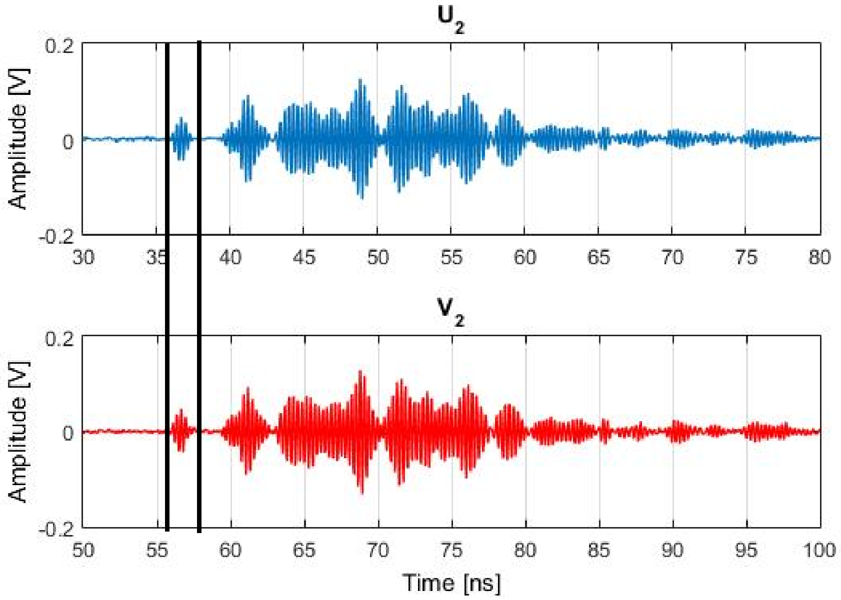

Figure 4.30 – Received signals at RX-chain 2 for the initial position p_0.

The distance between the LBS and the AT is estimated for each position p_i of the latter using the setup shown in Figure 4.27. To validate the proposed approach, the results of the simulated distance obtained by the duplex UWB method described in Section 2.6.1 are compared with two energy detection based methods. Namely, the ED method which consists in searching for the maximum energy and the TC method [2] which consists in searching for the excess of a pre-defined threshold ϵ given by

$$\epsilon = a.\sigma \tag{4.4}$$

with σ the standard deviation of the received noise and a the threshold factor. According to [3], the optimal threshold factor a is 2.5 for CM1, CM2, CM3 and CM4 channel models.

The frequency difference $\Delta f = f_2 - f_1$ is fixed to 50 MHz and the same parameters used before in the energy calculation are retained.

Among the entire signal (U_1, V_1, U_2 or V_2) shown in Figure 4.29 and Figure 4.30, we are interested in the part between the two black lines because it represents the first path of each signal. For this reason, we focus exclusively on these parts in Figure 4.31 and Figure 4.32.

Figure 4.33 compares the actual distance with that simulated by the ED, TC and duplex UWB methods, and Figure 4.34 shows the error in the simulated distance obtained by the abovementioned methods, for the 51 different positions of the AT.

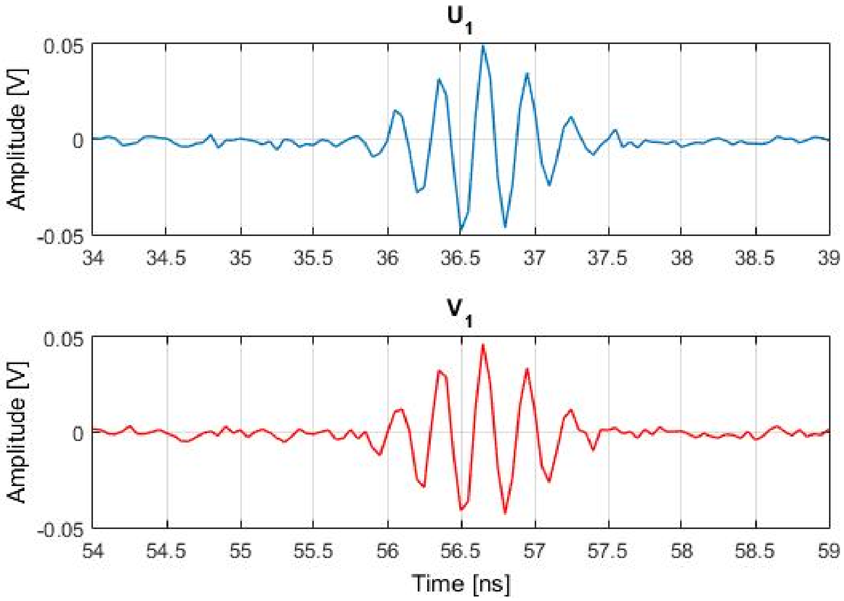

Figure 4.31 – Pulses of interest at RX-chain 1.

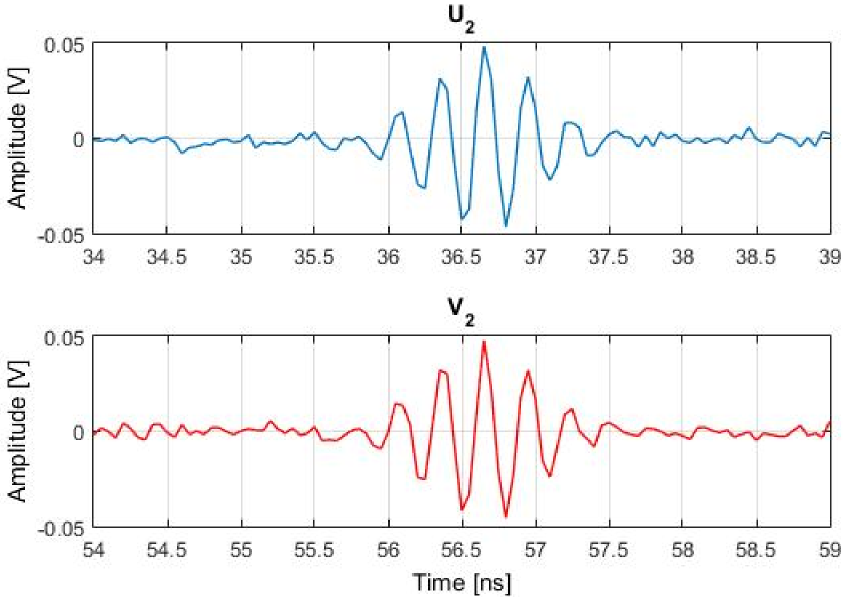

Figure 4.32 – Pulses of interest at RX-chain 2.

It is worth recalling that the ED method estimates the distance based on the detection of the maximum energy block. Therefore, the distance estimation error increases as the first path in our case is not always the one with the highest energy.

The distance resolution of the ED and TC methods depends on the chosen displacement

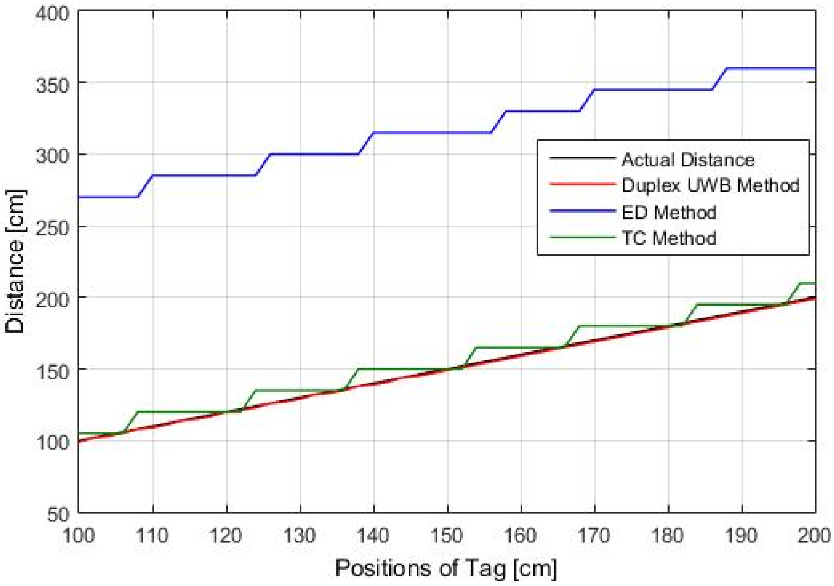

Figure 4.33 – Comparison of the distance estimation.

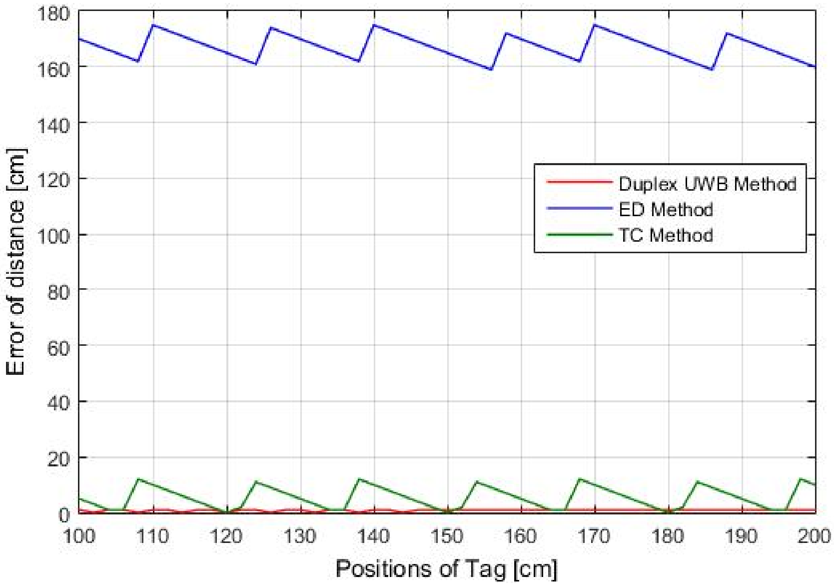

Figure 4.34 – Error in the distance.

step, while it depends on the sampling frequency for the duplex UWB method. In this configuration, the resolution of the ED and TC methods is 15 cm for a displacement step of 1 ns, whereas the resolution of the duplex UWB method is 0.8 cm for $F_e = 20$ GHz. Therefore, we can conclude that the ED and TC methods are unable to detect a distance offset of about 2 cm, whilst our proposed method can even detect a smaller offset.

This result is clearly reflected in Figure 4.34, where the average error in the estimated distance for the ED method is 167 cm (incorrect estimate of the first path) and 5.4 cm for the TC method. Moreover, the maximum error in the estimated distance with respect to its average is 8 cm for the ED method and 7 cm for the TC method, and decreases to 1 cm when the duplex UWB method is employed. This error provides an insight into the distance resolution offered by the used method. Therefore, we can argue that the TC method improves the distance accuracy but with the same distance resolution as the ED method. Our method remains much better than these two methods, since it improves distance accuracy and resolution at the same time.

4.5 Comparison with Trilateration Method in LoS Situation

This section is devoted to compare our results with those obtained by the famous trilateration method used in the literature for ILSs. The main difference between these two techniques is how the AT position is estimated: our technique is based on radial and angular measurements while the trilateration technique is based only on distance measurements using a constellation (multiple anchors). This comparison will highlight the significant improvement brought by our technique on the accuracy and resolution of the ILS.

4.5.1 Simulated Setup

Figure 4.35 shows the configuration considered for the MATLAB simulation bench with all the possible positions of the AT. On one hand, the LBS of our system consists of a transmitting antenna A_0 placed at the origin $(0, 0)$ between two receiving antennas A_1 and A_2 placed along the y-axis and separated by $d_{baseline} = 30$ cm. On the other hand, the constellation-based ILS consists of 3 anchors, with the first one being the same antenna A_0 of the LBS. The coordinates of each element are also shown in this figure.
To validate the improvement of the position resolution using our ILS, the AT can take 35 different positions p_i with $i \in \{0, \cdots, 34\}$. These positions can be divided into three different trajectories:

- **Trajectory 1:** The AT takes different positions on a straight line parallel to the y-axis at a distance $d = 1.5$ m from the center. It corresponds to positions p_0 to p_{12} in the range $[-30cm; 30cm]$ with a 5 cm offset between each two consecutive positions.
- **Trajectory 2:** The AT takes different positions along the x-axis in the range $[1.55m; 1.95m]$. It corresponds to positions p_{13} to p_{21} with the same offset of 5 cm between each two consecutive positions.
- **Trajectory 3:** The AT takes different positions again on a straight line parallel to the y-axis, but this time at a distance $d = 2$ m from the center. It corresponds to positions

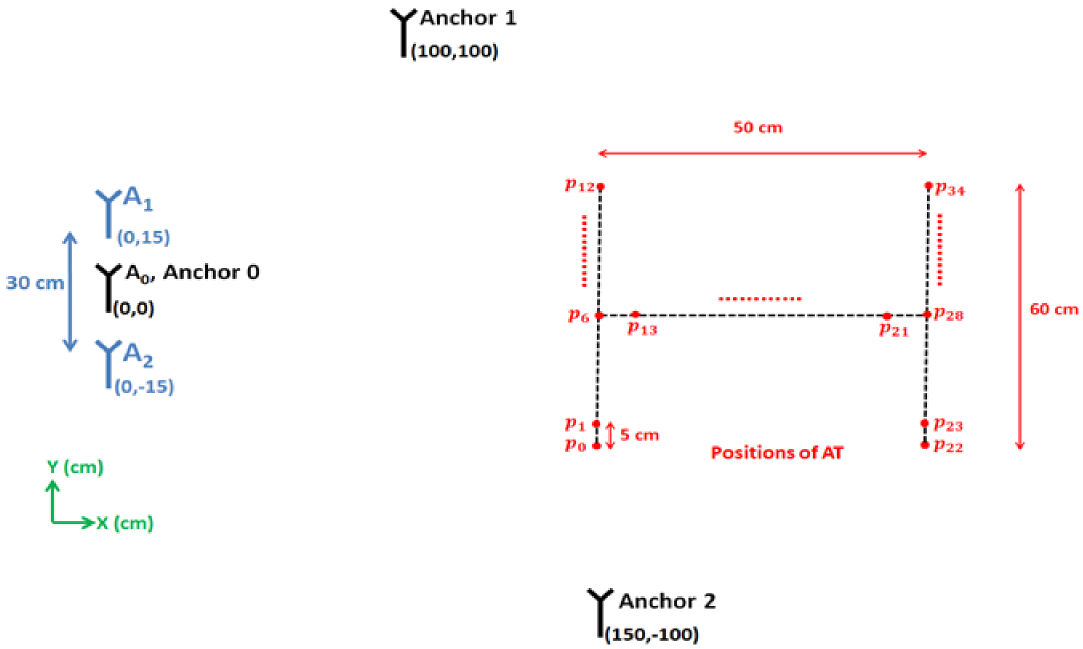

Figure 4.35 – Possible positions of the AT.

p_{22} to p_{34} covering the same range and using the same offset of the first trajectory.

Like in previous cases, the CM3 channel model of IEEE802.15.4a is adopted. A pulse U is emitted simultaneously by the 3 anchors with a center frequency $f_1 = 3.5$ GHz. After a delay $t_s = 20$ ns, A_0 (Anchor 0) emits a second pulse V with a center frequency $f_2 = 3.55$ GHz. U and V are already defined in Eq. (4.2) and Eq. (4.3), respectively. The sampling frequency used for processing is 20 GHz.

Figure 4.36 shows the methodology of the above-mentioned techniques in estimating the AT position. First, our ILS estimates the AT position in two steps:

1. Compute the radial distance d using the UWB duplex method.
2. Compute the Azimuth angle α using the PC method.

The position (x, y) of the AT is expressed in terms of d and α as follows

$$\begin{cases} x = d \sin \alpha \\ y = d \cos(180^\circ - \alpha) \end{cases} \tag{4.5}$$

In contrast, the constellation-based ILS estimates the AT position by applying the TC method over three estimated distances d_0, d_1 and d_2. These distances will then be used to estimate the AT position (x, y) as follows

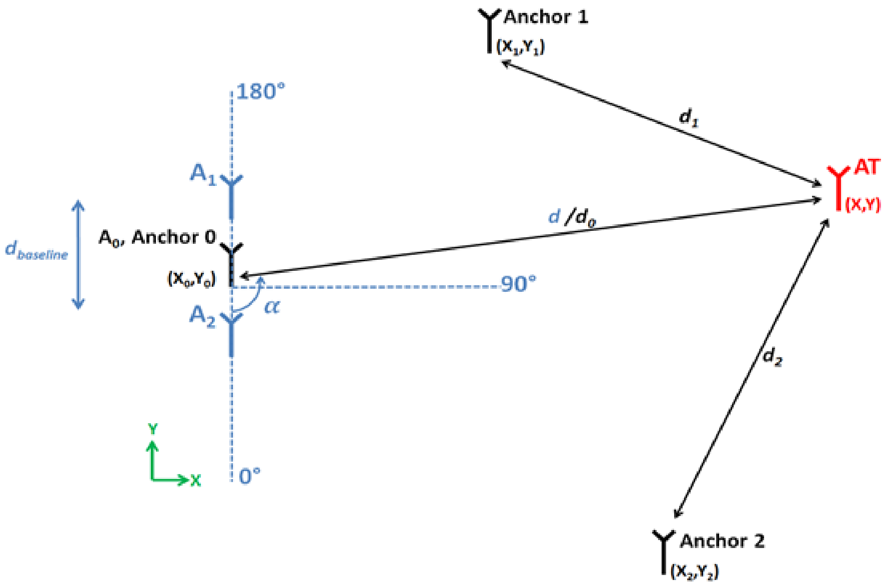

Figure 4.36 – AT position estimation methodology.

$$x = \frac{Ay_{21} + By_{02} + Cy_{10}}{2(x_0 y_{21} + x_1 y_{02} + x_2 y_{10})} \tag{4.6}$$

$$y = \frac{Ax_{21} + Bx_{02} + Cx_{10}}{2(y_0 x_{21} + y_1 x_{02} + y_2 x_{10})} \tag{4.7}$$

where

$$\begin{cases} A = {x_0}^2 + {y_0}^2 - {d_0}^2 \\ B = {x_1}^2 + {y_1}^2 - {d_1}^2 \\ C = {x_2}^2 + {y_2}^2 - {d_2}^2 \end{cases} \tag{4.8}$$

and

$$\begin{cases} x_{21} = x_2 - x_1 \\ x_{02} = x_0 - x_2 \\ x_{10} = x_1 - x_0 \end{cases} \tag{4.9}$$

$$\begin{cases} y_{21} = y_2 - y_1 \\ y_{02} = y_0 - y_2 \\ y_{10} = y_1 - y_0 \end{cases} \tag{4.10}$$

4.5.2 Simulated Results

Figure 4.37a, Figure 4.38a and Figure 4.39a show the actual distances d_0, d_1 and d_2 with those estimated by a constellation-based ILS, respectively. Figure 4.37b, Figure 4.38b and

Figure 4.39b show the error in estimating these distances for the 35 different positions of the AT. The accuracy is also indicated in terms of Root Mean Square Error (RMSE) measurement given by

$$RMSE = \sqrt{\frac{1}{N}\sum_{i=1}^{N}(\hat{\theta}_i - \theta_i)^2} \tag{4.11}$$

where N is the number of possible AT positions, θ_i and $\hat{\theta}_i$ are the actual and estimated values, respectively.

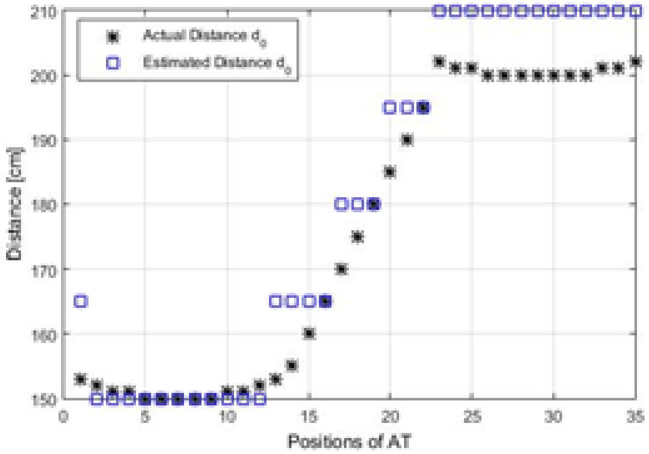

(a) Estimation.

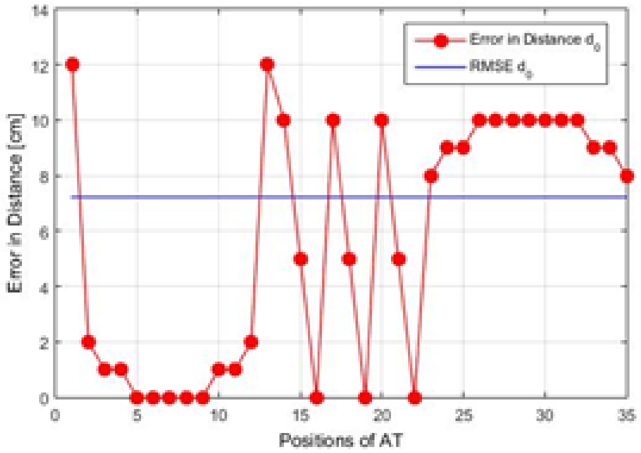

(b) Error.

Figure 4.37 – Distance d_0 Estimation and Error.

As we can see, the trilateration method estimates the same distances for different actual distances when the latter are too close to each other. Take the estimation of d_0 in Figure 4.37a as an example. The method considers the AT to be at the same distance 210 cm, when in reality it is changing slightly its position (from p_{21} to p_{34}). In terms of estimation

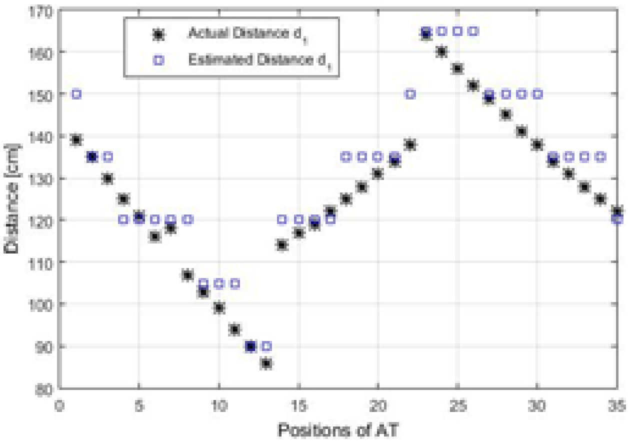

(a) Estimation.

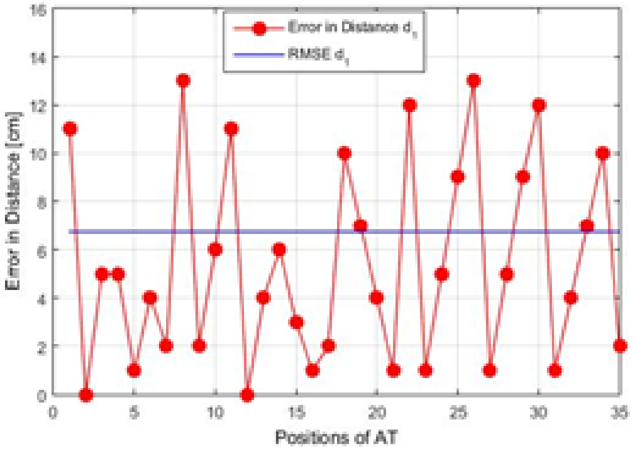

(b) Error.

Figure 4.38 – Distance d_1 Estimation and Error.

error, d_0 has a maximal error of 12 cm with an RMSE of 7.2 cm. Similarly, the maximal error in d_1 (reps. d_2) estimation is 13 cm (resp. 12 cm) with an RMSE of 6.7 cm (resp. 6.2 cm).

Figure 4.40a (resp. Figure 4.41a) shows the actual radial distance d (resp. the azimuth angle α) with that estimated by our ILS. Figure 4.40b (resp. Figure 4.41b) shows the error in this estimated distance (resp. angle) for the 35 different positions of the AT.

As we can see, our method can detect small changes in the AT position compared to the previous method which assumes that the AT is fixed if the positions are too close to each other. This conclusion is reflected in Figure 4.40a where there exists in most cases a different estimated distance for each actual distance, which demonstrates the significant improvement in the distance resolution. Moreover, in terms of estimation error, d has a

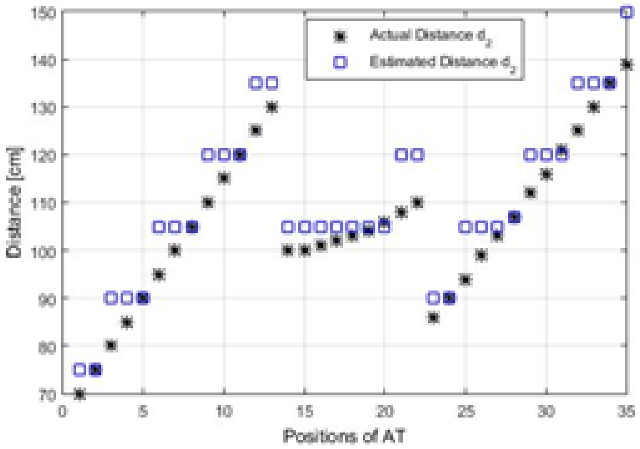

(a) Estimation.

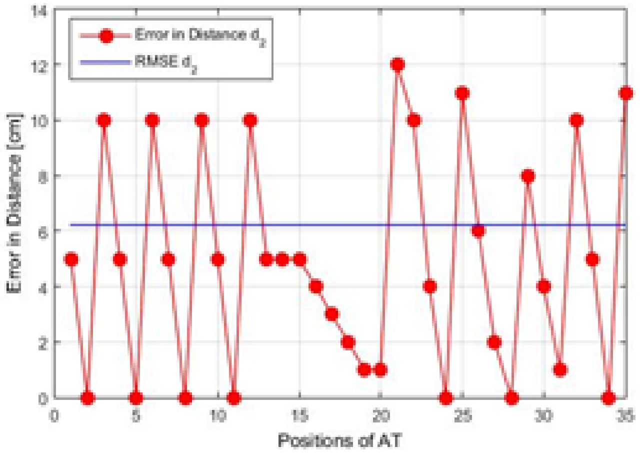

(b) Error.

Figure 4.39 – Distance d_2 Estimation and Error.

maximal error of 2 cm with an RMSE equal to 1.6 cm. This error is too small compared to the previous method, which in turn illustrates the improvement of the distance accuracy. On the other hand, we can see that the system can estimate the exact value of α when the AT is placed at different positions on Trajectory 2, and with some error when the AT takes different positions on the other two trajectories. The maximum error in the angle estimation is 1.5° with an RMSE equal to 0.8°. We can also notice that the maximal error increases with the distance: 1.5° for Trajectory 3 Vs. 1° for Trajectory 1.

Figure 4.42 compares the actual positions of the AT with those estimated by our proposed ILS and the constellation-based ILS. It is clear that our system can accurately estimate the position of the AT. The limitation of the trilateration system in detecting small variation in the distance results also in a limitation in estimating the overall position of the AT. In

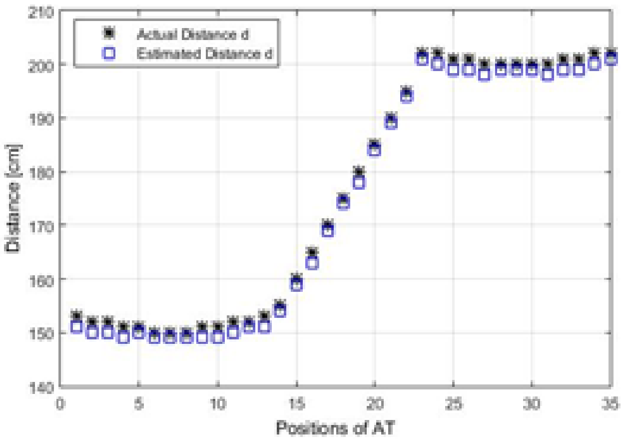

(a) Estimation.

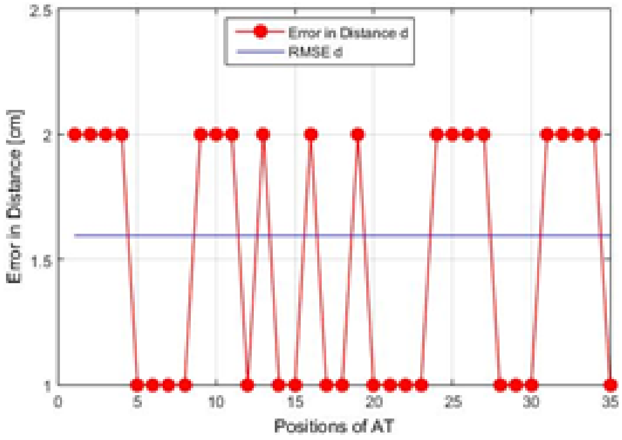

(b) Error.

Figure 4.40 – Distance *d* Estimation and Error.

other words, the same position is estimated for different AT actual positions (21 estimated positions Vs. 35 actual positions). We can therefore conclude that our system increases the accuracy and the resolution of the localization in an indoor environment.

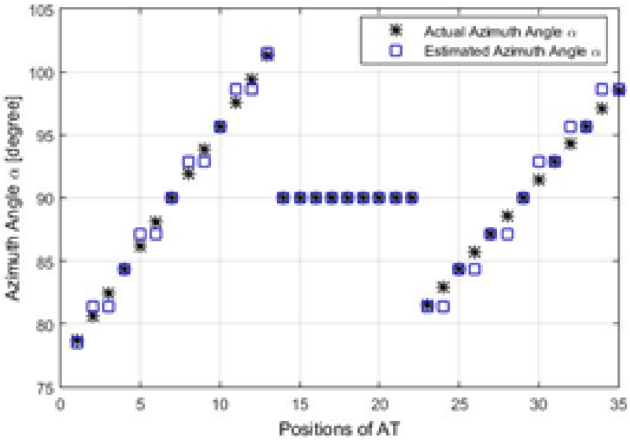

(a) Estimation.

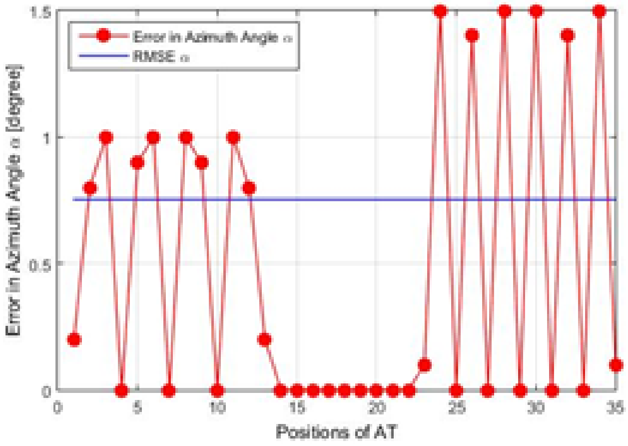

(b) Error.

Figure 4.41 – Azimuth angle α Estimation and Error.

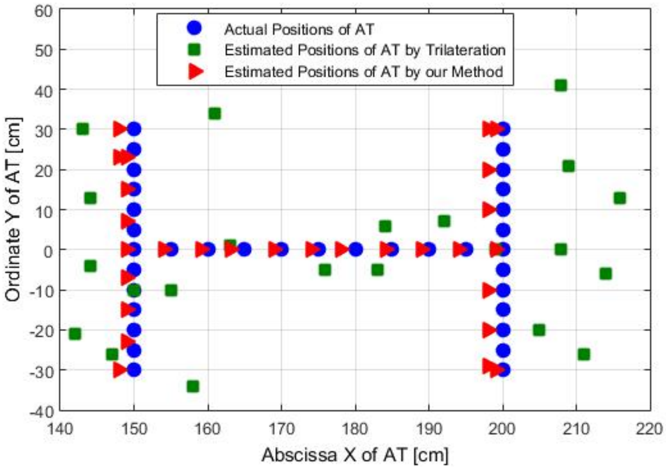

Figure 4.42 – Comparison of AT positions estimate.

4.6 Comparison with Trilateration Method in Obstructed LoS Case

In many real-life situations, the object to be located is not in the ILS line-of-site. This scenario can occur when there is a physical object or any obstruction in the propagation path, preventing a direct link between the transmitter and receiver. In this case, the radio transmission is mainly established by penetrating through the obstacle, which will further attenuate and delay the received signals. Therefore, this section extends the previous one to study the influence of an unexpected obstacle between the LBS and the AT. To this end, our technique is also compared to the trilateration method. The results prove that our technique is robust and remains effective even in obstructed LoS case.

4.6.1 Simulated Setup

The configuration adopted here and shown in Figure 4.43 is similar to that used in Section 4.5 with slight modifications:

- Anchors 1 and 2 are placed in different positions.
- The NLoS framework is created by adding a physical object at a distance $d = 30$ cm from the center.

In this configuration, we assume that $d_{baseline} = 10$ cm and the AT can take 7 different positions p_i with $i \in \{0, \cdots, 6\}$, such that the radial distances are kept in the range [1.5 m, 2.5 m] with respect to the fixed position of the LBS, and the angular positions remain in the angular zone [30°, 150°] as specified in Section 3.5.4.

In the simulations, the localization process of both techniques is carried out similarly to the LoS case, but with an additional delay of 0.5 ns to mimic the effect of the obstacle on signal propagation.

4.6.2 Simulated Results

Figure 4.44a, Figure 4.45a and Figure 4.46a show the actual distances d_0, d_1 and d_2 with those estimated by a constellation-based ILS, respectively. Figure 4.44b, Figure 4.45b and Figure 4.46b show the error in estimating these distances for the 7 different positions of the AT.

In terms of estimation error, d_0 has a maximal error of 40 cm with an RMSE of 36 cm. Similarly, the maximal error in d_1 (reps. d_2) estimation is 27 cm (resp. 24 cm) with an RMSE of 18 cm (resp. 18 cm). As we can see, d_0 has the largest RMSE because its Anchor

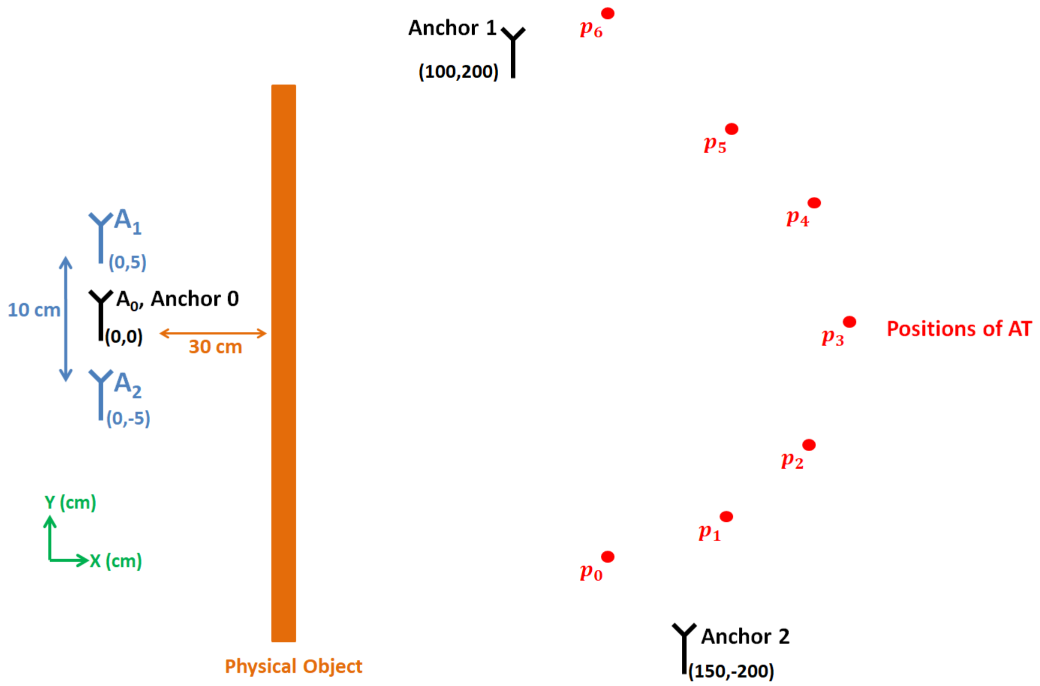

Figure 4.43 – Possible positions of the AT.

0 relies on obstructed LoS signals to estimate the distance, knowing that the obstacle adds an extra delay of 1 ns (30 cm round-trip) on the received signal.

Figure 4.47a (resp. Figure 4.48a) shows the actual radial distance d (resp. the azimuth angle α) with that estimated by our ILS. Figure 4.47b (resp. Figure 4.48b) shows the error in this estimated distance (resp. angle) for the 7 different positions of the AT.
In terms of estimation error, d has a maximal error of 14 cm with an RMSE equal to 13 cm. Compared to the previous method, this method offered a much smaller error illustrating thus the improvement of the distance accuracy. Moreover, a simple comparison of this result with the LoS case shows the high estimation error caused again by the extra 1 ns (30 cm round-trip) delay added to the received signal before reaching A_1 and A_2. This clearly shows the effect of the physical obstacle in estimating distance d.

On the other hand, the maximum error in the angle estimation is 4° with an RMSE equal to 3°. Compared to the LoS case, this error is also considered small because the two received signals are equally affected by the physical object.

Figure 4.49 compares the actual positions of the AT with those estimated by our proposed ILS and the constellation-based ILS. It is clear that our system can accurately estimate the position of the AT even in the obstructed LoS case. Our technique is less affected by the physical obstacle, since the Azimuth angle estimate is immune to it and only the distance

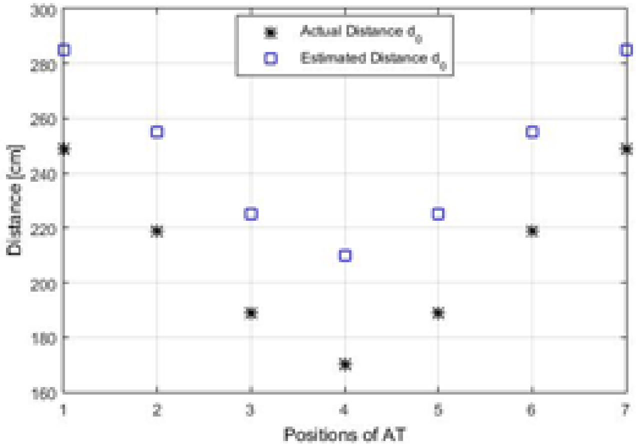

(a) Estimation.

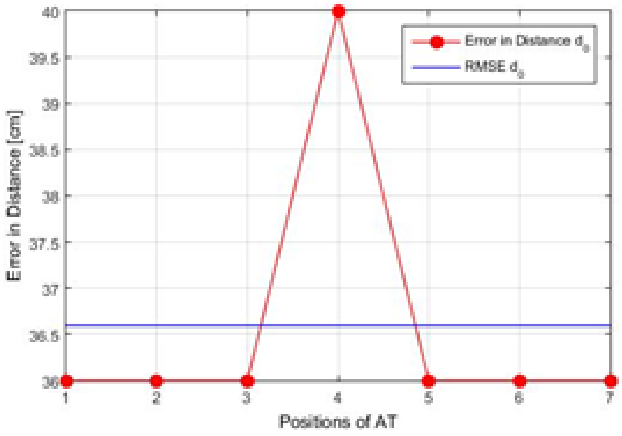

(b) Error.

Figure 4.44 – Distance d_0 Estimation and Error.

estimate is truly impacted. On the other hand, the trilateration method is badly affected, since it is based only on distance measurement which is influenced by the presence of the obstacle. We can therefore conclude that our system is more robust and increases the accuracy of the localization in an obstructed LoS situation of an indoor environment.

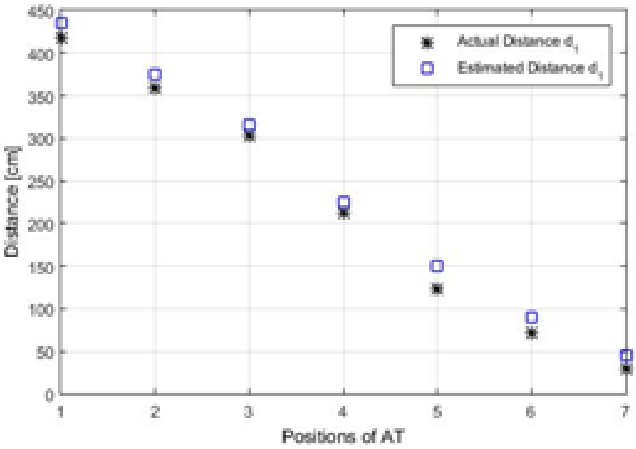

(a) Estimation.

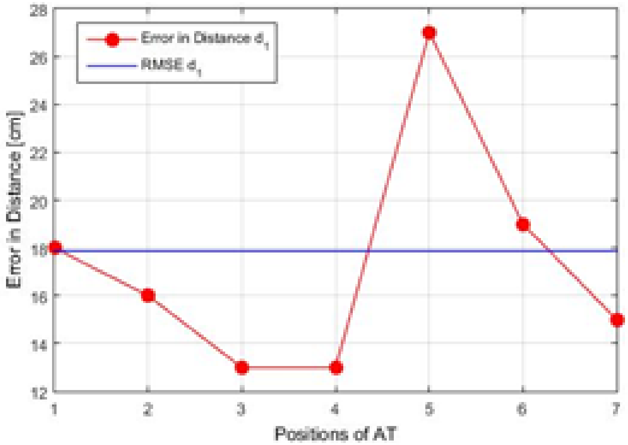

(b) Error.

Figure 4.45 – Distance d_1 Estimation and Error.

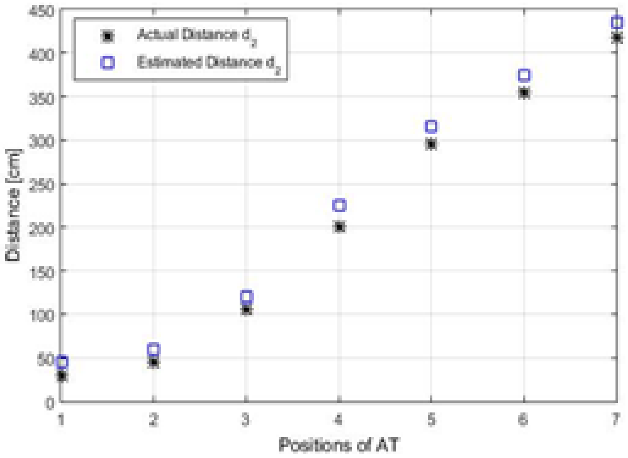

(a) Estimation.

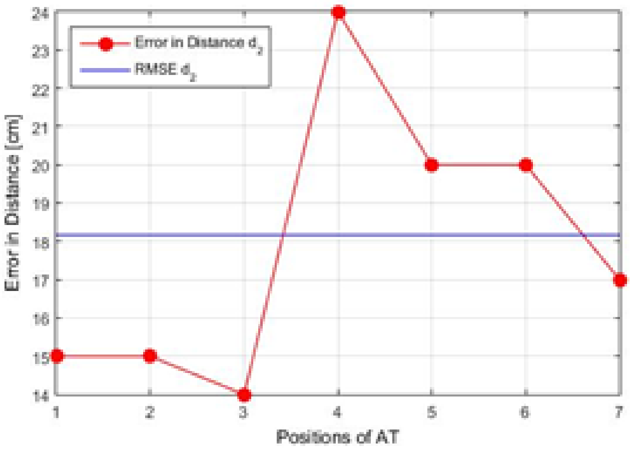

(b) Error.

Figure 4.46 – Distance d_2 Estimation and Error.

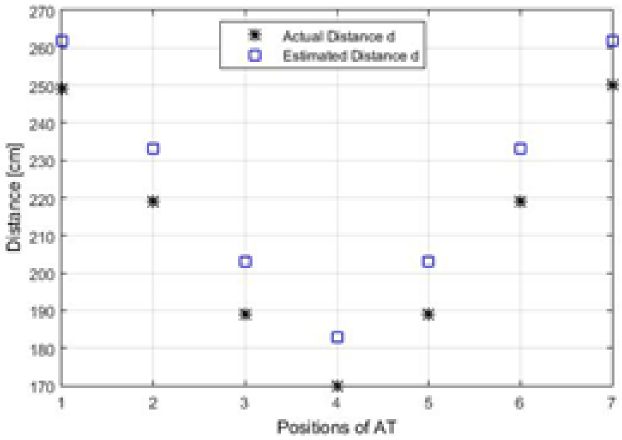

(a) Estimation.

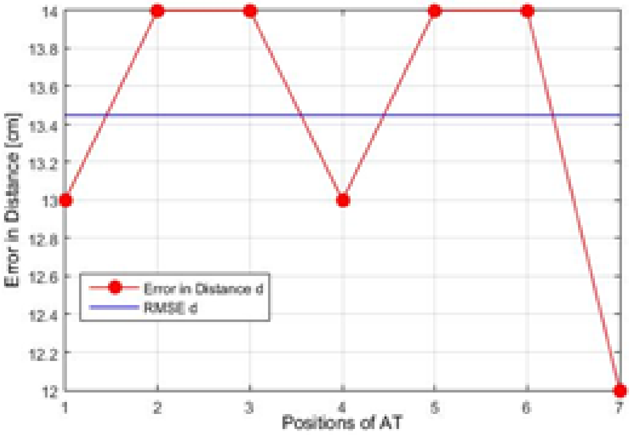

(b) Error.

Figure 4.47 – Distance *d* Estimation and Error.

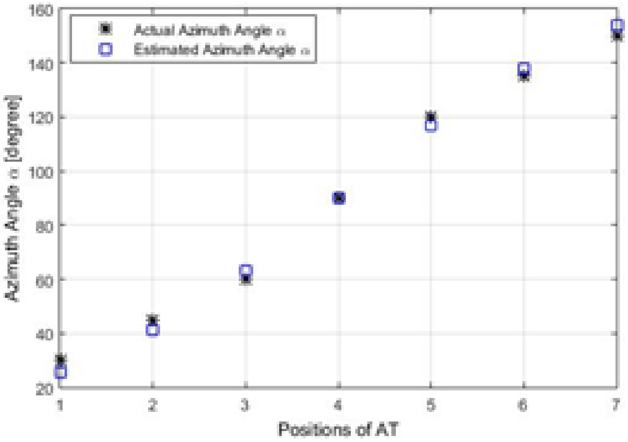

(a) Estimation.

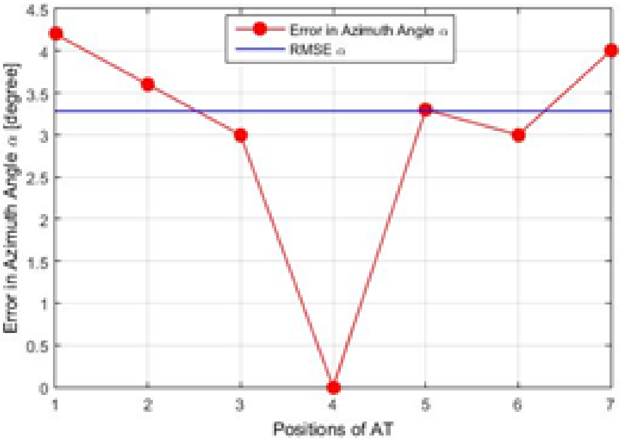

(b) Error.

Figure 4.48 – Azimuth angle α Estimation and Error.

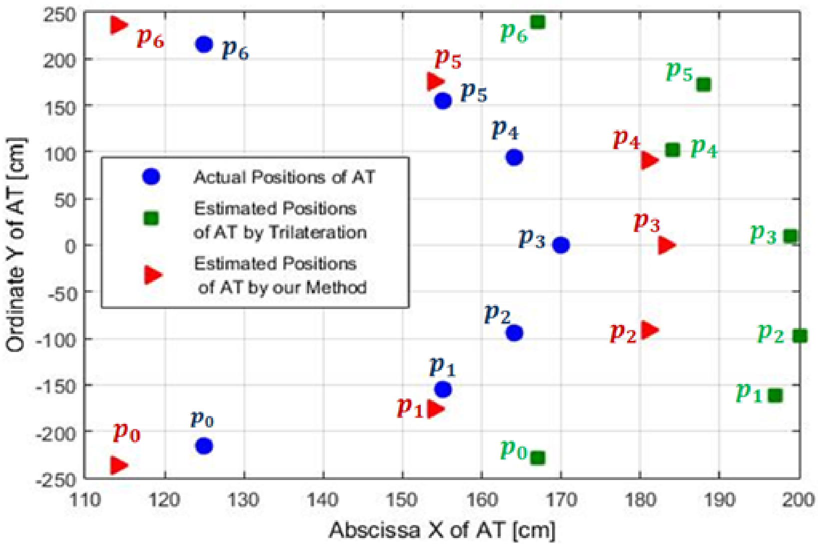

Figure 4.49 – Comparison of AT positions estimate.

4.7 Performance evaluation in NLoS situations

In this section, the performance of our hybrid technique combining the duplex UWB and the PC methods is studied in the NLoS situations.

4.7.1 Simulated Setup

In the NLoS scenario, the configuration adopted and presented in Figure 4.50 is similar to that used in Section 4.6, i.e. the LBS position is unchanged and the AT can take the same positions p_i, but without the obstacle and the three anchors of the trilateration method.

Figure 4.50 – Possible positions of the AT.

The localization process of our technique is evaluated through simulations using the CM4 channel model (office NLoS).

4.7.2 Simulated Results

Figure 4.51a (resp. Figure 4.52a) shows the actual radial distance d (resp. the Azimuth angle α) with that estimated by our ILS. Figure 4.51b (resp. Figure 4.52b) shows the error in the distance (resp. angle) estimate for the 7 different positions of the AT.

The main results are resumed in Table 4.3.

Compared to the obstructed LoS case, the RMSE of the distance estimation error has increased by 13 cm with the same angular error. Therefore, the angular estimation with our configuration is not significantly affected in an NLoS environment since the deformation of the received signals on the two receiving antennas A_1 and A_2 is the same, as shown in

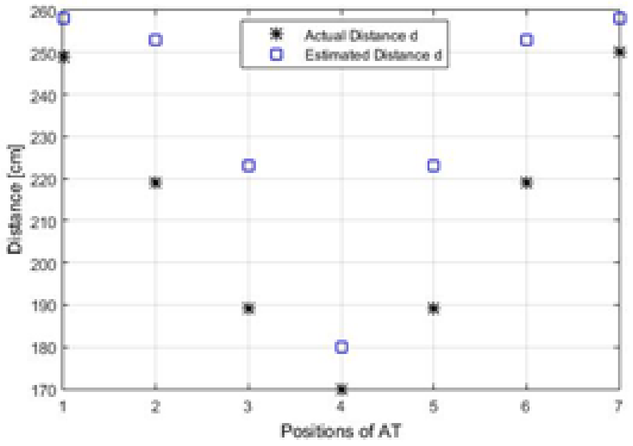

(a) Estimation.

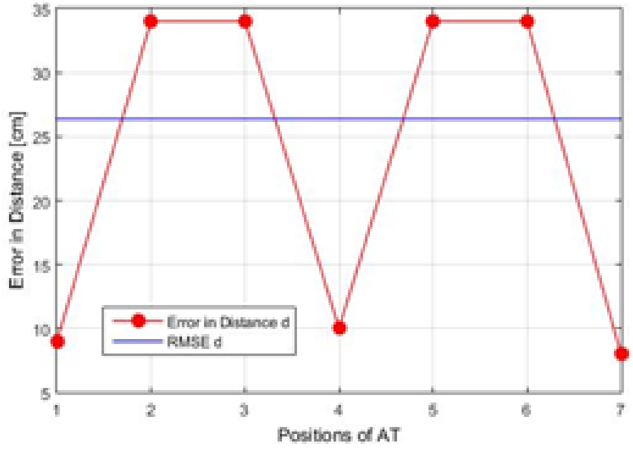

(b) Error.

Figure 4.51 – Distance *d* Estimation and Error.

Table 4.3 – Estimation Error

	Maximal Error	**RMSE**
Radial distance d [cm]	**34**	**26**
Azimuth angle α [°]	4	3

Figure 4.53.

Figure 4.54 compares the actual AT positions with those estimated by our proposed ILS. On one hand, the error in estimating the AT position increases considerably compared to LoS and obstructed LoS cases.

On the other hand, our system's performance is compared to that obtained in the state

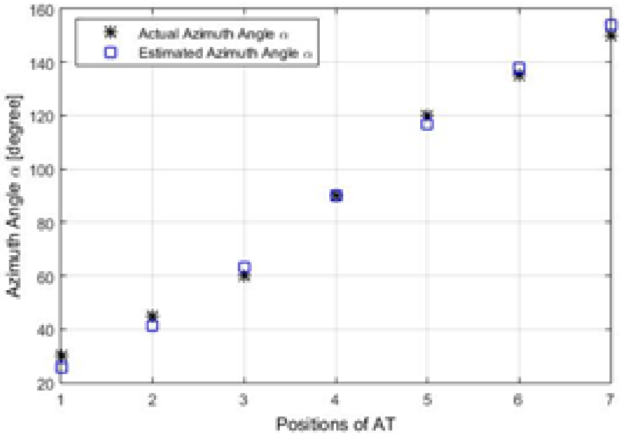

(a) Estimation.

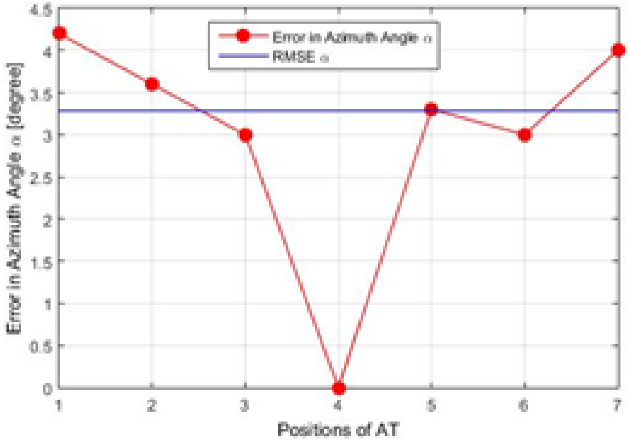

(b) Error.

Figure 4.52 – Azimuth angle α Estimation and Error.

of the art [4], in which the receiver position is computed using four beacons in an NLoS environment.

The main results are summarized in Table 4.4.

Table 4.4 – RMSE of the position error

	Abscissa X of AT	**Ordinate Y of AT**
state-of-the-art system [4]	142	85
Our proposed system	21	20

Based on this comparison, we can claim that our system performed well.

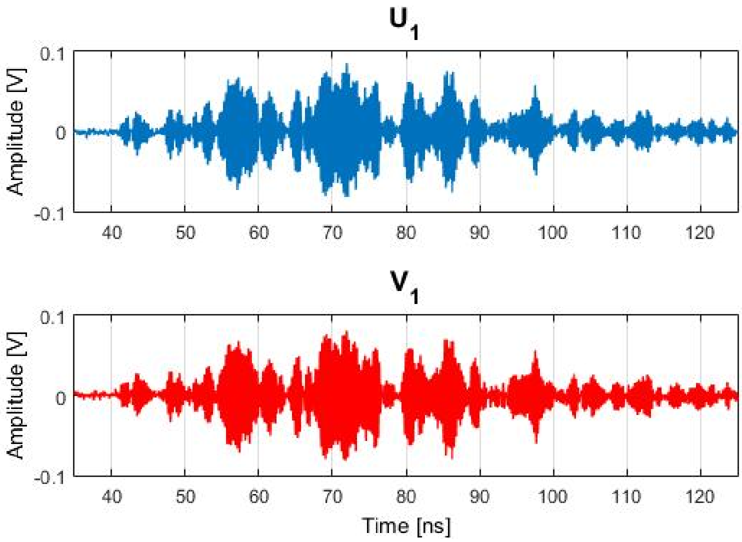

Figure 4.53 – Received signals on A_1 and A_2.

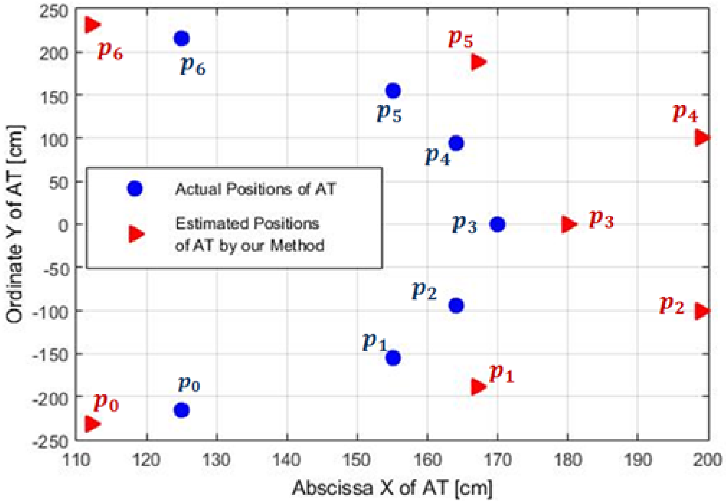

Figure 4.54 – Comparison of AT positions estimate.

4.8 Conclusion

In this chapter, the performance of the PC method is validated through a measurement and simulation campaign conducted first for a simplified ILS and then for our proposed ILS. The comparison between the ED and PC methods shows that the latter improves the angular resolution. More precisely, the ED method is unable to detect a small path difference, whereas the PC method is capable of doing so. For the simplified ILS, a maximum angular error of 1.6° and 1° is observed for sampling frequencies equal to 20 GHz and 160 GHz, respectively. For our proposed ILS, a maximum angular error of 1° and 1.4° is observed at $F_e = 40$ GHz for distances equal to 1 m and 1.5 m, respectively.

Moreover, the duplex UWB method used to estimate the distance is validated by a simulation campaign. The results show that the duplex UWB method improves the distance resolution with respect to the traditional ED and TC methods. In particular, the ED and TC methods fails to distinguish between two very close positions of the AT (in the order of 2 cm), whereas the duplex UWB method is able to do so with a maximum distance error of 1 cm for a sampling frequency equal to 20 GHz.

After improving the angular and distance resolution using our proposed methods, we moved on to show the direct effect of these methods on the resolution and accuracy of the AT position estimation. This validation is performed by comparing our ILS based on a joint measurement of range and angle with a traditional constellation-based ILS that predicts the position of the AT by calculating three distances using the trilateration method. The obtained results show that our ILS improve the resolution and can accurately estimate the position of the AT in LoS and obstructed LoS cases.

Finally, the performance of our ILS is studied in the NLoS situation. Our results reveal that our system outperform the one studied in [4].

Bibliography

[1] A.F. Molisch, D. Cassioli, C.C. Chong, S. Emami, A. Fort, B. Kannan, J. Karedal, J. Kunish, H.G. Schantz, K. Siwiak and M.Z. Win, “A Comprehensive Standardized Model for Ultrawideband Propagation Channels,” IEEE Transactions on Antennas and Propagation, vol. 54, no. 11, November 2006. Cited page 119

[2] I. Guvenc and Z. Sahinoglu, “Threshold-based ToA Estimation for Impulse Radio UWB Systems,” IEEE International Conference on Ultra-Wideband, September 2005. Cited pages 123 and 140

[3] Z. Yin, K. Cui, Z. Wu and L. Yin, “Entropy-Based ToA Estimation and SVM-Based Ranging Error Mitigation in UWB Ranging Systems,” Journal of Sensors, vol. 15, pp. 11701-11724, May 2015. Cited page 140

[4] E. Garcia, P. Poudereux, A. Hernandez, J. Urena and D. Gualda, “A Robust UWB Indoor Positioning System for Highly Complex Environments,” IEEE International Conference on Industrial Technology (ICIT), pp. 3386–3391, March 2015. Cited pages 161 and 163

Conclusions and future work

The main objective of this thesis was to develop a robust 2D indoor localization system capable of providing the position of an Active Tag (AT) with high accuracy and good resolution using a single anchor acting as the localization base station. The developed 2D Ultra Wide Band (UWB) indoor localization technique is based jointly on the measurement of radial distance (Duplex method) and Azimuth angle (Phase Correlation (PC) method).

In this framework, it was necessary to present the different technologies and their corresponding techniques used in indoor localization systems in order to choose the best one to meet our application requirements. This detailed state-of-the-art review led us to choose UWB technology as a promising solution for a more accurate Indoor Localization System (ILS) due to its large bandwidth and high temporal resolution. For this reason, a special focus was given to the definitions, characteristics and channel models of this technology. In addition, according to the Cramer-Rao lower bound (CRLB) analysis, UWB signals are highly suited for Time of Arrival (ToA) measurement.

To this end, UWB-based approaches that use ToA measurement to estimate the target position were illustrated. Most of these schemes are based on estimating the ToA of the strongest path. However, the strongest path is not necessarily the first arrival path in dense multipath channels, so their ToA accuracy is limited.

On the other hand, the famous Energy Detection (ED) approach suffers from the enhanced noise terms that become problematic in low/medium Signal-to-Nosie Ratio (SNR) regions. Moreover, we have seen that the resolution of this approach depends on the width of the energy block. For instance, for a pulse of 1 ns, the resulting distance resolution is 15 cm (path difference resolution of 30 cm). Furthermore, even if the Threshold Comparison (TC) method has slightly improved the accuracy of the ED method, they still have the same resolution.

To meet the requirements of future applications, our ILS must offer a higher resolution. For this reason, we have proposed a hybrid technique based on to locate the AT in an indoor environment:

- **Duplex UWB method:** used to estimate the distance based on ToA measurements.
- **PC method:** used to estimate the azimuth angle from Time Difference of Arrival (TDoA) measurements.

Afterwards, the architecture of the system used to implement and validate the proposed localization methods was presented. To locate an AT, this system uses two UWB pulses of 1 GHz bandwidth in the [3 − 4 GHz] band and at two different center frequencies f_1 and f_2. During the process, the AT adds a delay τ to the received signals before transmitting them back to the LBS in order to overcome the natural backscattering effects of the environment and eliminate the coupling between the transmitting and receiving antennas of the LBS.

Subsequently, the PC method was validated for two types of channels:

- **Wired channel:** This model is used as a proof of concept as it allows to eliminate the effect of the free space environment so that the performance and limitations of this method can be better understood.
- **Wireless channel:** This model is used to emulate a real indoor environment. The validation is done via experimental measurement and simulation using the CM3 channel (Office LoS) of IEEE.802.15.4a.

The experimental results showed that the PC method could achieve high accuracy and resolution in the angular measurement for a sampling frequency of 20 GHz (a maximum error of 1.6° Vs. an error of 11.3° for the traditional ED method).

Similarly, the Duplex UWB method was validated through a simulation campaign using the CM3 channel model. The results showed that this method was able to improve the distance resolution compared to the standard ED and TC methods. Notably, these two methods failed to distinguish between two very close positions of the AT (in the order of 2 cm), whereas the duplex UWB one was capable of doing so with a maximum distance error of 1 cm for a sampling frequency equal to 20 GHz.

Now that the angular and distance resolution have been significantly improved, we moved on to validate the resolution and accuracy of the AT position estimation. Our ILS based on a joint measurement of range and angle is then compared with a conventional constellation-based ILS. The results revealed that our system effectively improved the resolution and was able to accurately estimate the position of the AT even in the Non Line of Sight (NLoS) case.

Finally, some possible limitations of the proposed methods were presented:

- **Maximum radial distance:** For a frequency difference $\Delta f = 50$ MHz, the duplex UWB method can estimate radial distances up to $d_{max} = 3$ m.
- **Maximum angular zone:** This limitation in the PC method is imposed by the phase ambiguity and depends on the choice of $d_{baseline}$. For example, the angular area detection is [0°, 180°] for $d_{baseline} = 8.6$ cm, and decreases to [73.3°, 106.7°] when $d_{baseline}$ increases to 30 cm.

Perspectives

We provide in this section some future research proposals to further improve the proposed indoor localization system.

To begin with, we propose to validate the duplex UWB method and the estimation of the AT position in NLoS situation via a measurement campaign.

Another possible upgrade could be to extend the system to 3D positions by adding to the LBS two additional receiving chains connected to antennas A_3 and A_4, which are orthogonal to the previous ones, as shown in the following figure. The 3D UWB indoor positioning technique is based on the radial distance d, the Azimuth angle α and the elevation angle β measurements.

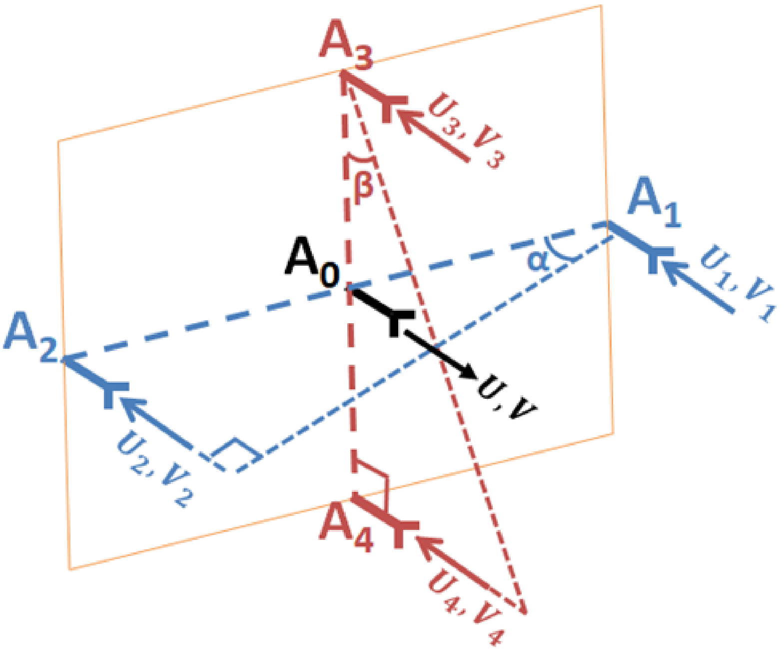

Architecture of the LBS in 3D.

Following the same procedure, the radial distances d_3 and d_4 are estimated by applying the duplex UWB method between the received pair of signals (U_i, V_i) and a delayed version (with the same delay τ) of the transmitted signals (U, V) for $i \in \{3, 4\}$.

$$d_i = \frac{c.T_i}{2} \qquad i \in \{3, 4\}$$

Where the times of flight T_i corresponds to the propagation time after removing τ.

The radial distance d, between A_0 and AT, is the average value of all calculated radial distances

$$d = \frac{1}{4}\sum_{i=1}^{4} d_i$$

The elevation angle β is estimated by applying the phase correlation method between the two received signals U_3 and U_4 on the two receiving chains. It can be expressed as follows

$$\beta = \cos^{-1}\left(\frac{c.\Delta t'}{d_{baseline}}\right)$$

Where $\Delta t'$ is the time difference of arrival between the two received signals U_3 and U_4.

A last area of investigation may be the generalization of the approach to multiple AT detection using different coding schemes such as Code Division Multiple Access (CDMA).

Publications

The work conducted during this thesis has led to the following publications.

Journals

J1. N. Awarkeh, J.C. Cousin, M. Muller and N. Samama, “Improvement of The Angle of Arrival Measurement Accuracy for Indoor UWB Localization,” submitted to Hindawi, Journal of Sensors, September 2019.

Conferences

C2. N. Awarkeh, J.C. Cousin, M. Muller and N. Samama, “Joint Distance and Azimuth Angle estimation using an UWB-based Indoor Localization System,” International Conference on Advances in Computing, Communication and Information Technology (CCIT), October 2019.

C1. N. Awarkeh, J.C. Cousin, M. Muller and N. Samama, “Improvement of The Angle Measurement Accuracy for Indoor UWB Localization,” European Microwave Week (EUMW), September 2018.

Appendix A

Multiple Hypothesis Testing System Model

The objective is to estimate the BP from the measurements $y = [y_0, \cdots, y_{L-1}]^T$ according to the optimal classification rule derived from the Neyman-Pearson criterion and extended to several assumptions. The null hypothesis H_0 indicates that there is no change while H_n is the hypothesis of having the BP in the n-th sample and it can be formally noted as

$$H_0 : y(i) \sim \mathcal{N}(0, R_0) \qquad i \in [0, L-1]$$

$$H(n) : \begin{cases} y(i) \sim \mathcal{N}(0, R_0), & \text{if } i \in [0, n-1] \\ y(i) \sim \mathcal{N}(0, R_1), & \text{if } i \in [n, L-1] \end{cases}$$

When the received UWB signals are modelled as time-correlated processes (correlation resulting from the transmitted waveform) with an exponentially decreasing PDP and a constant decay equal to the root mean square delay spread τ_{rms} of the CIR , R_0 is the covariance matrix of the time-correlated process before the BP and R_1 is the time-varying covariance matrix of the exponentially decreasing variables.

For each hypothesis H_n, the vector y is splitted into $y_0(n) = [y(0), \cdots, y(n-1)]^T$ and $y_1(n) = [y(n), \cdots, y(L-1)]^T$. The test statistics between alternative hypotheses are based on the inner product $\Phi_B = y_0(n)^T y_0(n)$ and $\Phi_F = y_1(n)^T y_1(n)$ for samples before (Backward) and after (Forward) the BP, respectively. So, the optimal estimator for the BP is

$$\hat{n}_0 = \arg\max_n [\gamma(n)]$$

where $\gamma(n)$ is the Probability Density Function (PDF) of $\Phi_B(n)$ and $\Phi_F(n)$ expressed in terms of $C(n)$ which is composed by all the independent terms from the samples of y, as follows

$$\gamma(n) = C(n) \times \left(\frac{\Phi_B(n)}{\Phi_F(n)}\right)^{\frac{n}{2}} \times \frac{1}{\Phi_B(n)} \times \left(\frac{\Phi_B(n)}{\Phi_F(n)} + 1\right)^{1-\frac{L}{2}} \tag{A.1}$$

Matched Filter

The algorithm proceeds as follows

1. Apply a matching filtering to the received UWB signal

$$\hat{y}(t) = y(t) \circledast g(t) \tag{A.2}$$

where $y(t)$ and $g(t)$ are the received and template signals respectively.

2. Determine the envelope of the match-filtered signal $\hat{y}(t)$, via modulus operation with low-pass filtering

$$e(t) = |\hat{y}(t)|_{LPF} \tag{A.3}$$

3. Determine the threshold value γ with respect to the peaks of the envelope signal $e(t)$

$$\gamma = \alpha.\max[e(t)] \tag{A.4}$$

where α is the dynamic threshold factor, generally chosen between 0.45 and 0.65 depending on the pulse repetition rate and environmental conditions.

4. Determine the first peak of the envelope exceeding the threshold

$$\hat{t} = \min\left[\arg_{t}(e(t) \geq \gamma)\right] \tag{A.5}$$

Two-step ToA estimators

First method

The coarse step relies on the sliding correlation over a symbol length to find a signal block where the direct path is enclosed. The coarse estimate $\hat{\tau}_{ToAc}$ is computed according to the following steps

1. The sliding correlation C_{Wck} is achieved by sampling and correlating K_c overlapping signal blocks along the duration T_s of a symbol. Each block has a duration T_{Wc} and is shifted from the previous one by the correlation step Δ_c.

2. The first derivative is computed over the K_c points of the resulting sliding correlation

$$\Delta C_{Wck} = C_{Wck} - C_{Wc(k-1)} \tag{A.6}$$

3. The position corresponding to the derived value above a threshold γ_c, denoted $\hat{K}_c$, is chosen to compute the coarse estimate $\hat{\tau}_{ToAc}$

$$\gamma_c = a_1.\max(\Delta C_{Wck}) \tag{A.7}$$

$$\hat{K}_c = \min\left[\arg_{k}(\Delta C_{Wck} \geq \gamma_c)\right] \tag{A.8}$$

$$\hat{\tau}_{ToAc} = \hat{K}_c.\Delta_c \tag{A.9}$$

where a_1 is a constant calculated experimentally in the simulations, ranging from 0.25 to 0.5 to produce the best results.

In the fine step, the sliding correlation C_{Wfk} is finely evaluated over the signal block obtained by the coarse step to accurately estimate the starting point of the pulse, following these steps

1. The fine sliding correlation C_{Wfk} is obtained by dividing the block contents into K_f sub-blocks, each with a time duration T_{Wf}. Here, the offset between two consecutive blocks is equal to Δ_f.
2. The derivative is computed over the K_f points of the resulting sliding correlation
$$\Delta C_{Wfk} = C_{Wfk} - C_{Wf(k-1)} \tag{A.10}$$
3. The position corresponding to the derived value above a threshold γ_f, denoted $\hat{K}_f$, is chosen to compute the fine estimate $\hat{\tau}_{ToAf}$
$$\gamma_f = a_1 . \max(\Delta C_{Wfk}) \tag{A.11}$$
$$\hat{K}_f = \min\left[\underset{k}{\arg}(\Delta C_{Wfk} \geq \gamma_f)\right] \tag{A.12}$$
$$\hat{\tau}_{ToAf} = \hat{K}_f . \Delta_f \tag{A.13}$$

Finally, the absolute ToA estimate is the sum of the coarse and fine estimates

$$\hat{\tau}_{ToA} = \hat{\tau}_{ToAc} + \hat{\tau}_{ToAf} \tag{A.14}$$

Second method

The estimation is performed in two steps. In the first one, the frame is analyzed to find the higher energy block, using an energy detector. To ensure reliable decision variables in this step, the energy for each block $y_{i,j}$ is combined from N_1 different frames of the received signal $r(t)$

$$y_i = \sum_{j=1}^{N_1} y_{i,j} \qquad i = 1, \cdots, N_b \tag{A.15}$$

$$y_{i,j} = \int_{jT_f + iT_b + C_jT_c}^{jT_f + (i+1)T_b + C_jT_c} |r(t)|^2 dt \tag{A.16}$$

where $C_j \in \{1, \cdots, N_c\}$ is the TH sequence.

The estimated block $\hat{k}_b$ with the highest signal energy is given by

$$\hat{k}_b = \arg\max_i [y_i] \tag{A.17}$$

In the second step, the estimated block $\hat{k}_b$ is analyzed to find the chip where the first signal path is located, by correlating the received signal with a shifted version of the template signal $s_{tmp}(t)$

$$z_i = \int_{iT_c}^{iT_c+N_2T_f} r(t).s_{tmp}(t - iT_c)dt \tag{A.18}$$

where N_2 is the number of frames over which the correlation output is obtained.

By choosing the block interval T_b appropriately, it is possible to assume that the block starts with a number of chips with noise components only (assumption H_0) followed by chips with signal plus noise components (assumption H_K). Thus, the arrival time of the first signal path is estimated through a hypothesis test approach. Therefore, the correlator outputs z_i are used to estimate the unknown parameters with the Method of Moments (MM). These are used to estimate the chip $\hat{k}_c$ containing the first signal path.

Finally, the ToA is obtained by

$$\hat{\tau}_{ToA} = \hat{k}_b T_b + \hat{k}_c T_c \tag{A.19}$$

Dirty Template

To acquire timing with frame-level resolution, the algorithm proceeds as follows

1. Define an observation interval T_o made up of M symbols

$$T_o = M.T_s \tag{A.20}$$

2. Compute the product of two received waveforms $x_{n,2m}(t)$ and $x_{n,2m+1}(t)$ for two adjacent symbols $2m$ and $2m+1$, $m \in \{0, \cdots, M-1\}$ in the n-th frame $n \in \{0, \cdots, N_f-1\}$

$$R_{x,x}(n,m) = \int_0^{T_s} x_{n,2m}(t)x_{n,2m+1}(t)dt \tag{A.21}$$

3. Estimate $R_{x,x}(n)$ of each frame n by averaging the absolute values of $R_{x,x}(n,m)$ across the $M/2$ pairs

$$R_{x,x}(n) = \frac{2}{M}\sum_{m=0}^{\frac{M}{2}-1} |R_{x,x}(n,m)| \tag{A.22}$$

4. Determine the estimated frame $\hat{n}_f$

$$\hat{n}_f = \arg\max_n [R_{x,x}(n)] \tag{A.23}$$

5. Finally, derive the estimated ToA using

$$\hat{\tau}_{ToA} = \hat{n}_f.T_f \tag{A.24}$$

université
PARIS-SACLAY

ÉCOLE DOCTORALE
Sciences et technologies
de l'information
et de la communication (STIC)

Titre: Sytème de Localisation 2D Indoor par Radar Multistatique UWB

Mots clés: Localisation, UWB, Radar, Télécommunications, Interférométrie, Goniométrie

Résumé: De nos jours, la capacité de suivre des objets et des personnes est cruciale pour un grand nombre d'applications, telles que les applications médicales (surveillance de patients) ou les applications indépendantes qui nécessitent une très grande précision et résolution dans le processus de positionnement. Par conséquent, l'objectif scientifique principal de cette thèse est de développer un système de suivi utilisant un système de radar multistatique UWB pour fournir une localisation 2D en temps réel de transpondeurs ou de balises actives. La localisation est réalisée en coordonnées polaires (distance et angle d'azimut) en fusionnant les principes d'interférométrie et de goniométrie, en supposant un canal de propagation à trajet direct, ou LoS entre la station et la cible. L'ILS conçu utilise une technique hybride en combinant les méthodes duplex UWB et de corrélation de phase pour les estimations de la distance radiale et de l'angle d'Azimut. L'ILS proposé comprend deux composants principaux, une station émettrice/réceptrice servant de LBS et un AT. Le LBS a une chaîne d'émission et deux chaîne de réception identiques et indépendantes. La localisation est effectuée en envoyant des impulsions UWB vers l'AT qui joue le rôle de transpondeur actif et retransmet le signal reų à son tour au LBS après l'avoir retardé. Cet ILS conų devrait offrir, dans les conditions LoS, une estimation de position avec une précision et une résolution élevées, tout en maintenant une faible complexité du système. Le système fonctionne avec une seule ancre et répond simultanément aux défis intérieurs tels que les trajets multiples, les fortes atténuations de signal, les réflexions, etc.

Title: 2D Indoor Localization System with an UWB Multistatic Radar

Keywords: Localization, UWB, Radar, Telecommunications, Interferometry, Goniometry

Abstract: Nowadays, the ability to track objects and people is crucial for a huge number of applications, such as medical applications (monitoring of patients) or independent applications that require a very high accuracy and resolution in the positioning process. Therefore, the main scientific objective of this thesis is to develop a tracking system using an UWB multistatic radar system to provide real-time 2D location of transponders or active tags. The localization is carried out in polar coordinates (distance and azimuth angle) by merging the interferometry and goniometry principles, assuming a propagation channel with a direct path, or LoS between the station and the target. The designed ILS incorporates a hybrid technique by combining the duplex UWB and the Phase Correlation methods for the radial-distance and the azimuth angle estimates. The proposed ILS consists of two main components, a transmitter /receiver (transceiver) station serving as a LBS and an AT. The LBS has one transmitting channel and two identical and independent receiving channels. The localization is performed by sending UWB pulses towards the AT which acts as an active transponder and retransmits in turn the received signal back to the LBS upon delaying it. This designed ILS is expected to offer, under LoS conditions, a position estimation with high accuracy and resolution while maintaining low system complexity. The system works with a single anchor, and simultaneously addresses indoor challenges such as multipaths, strong signal attenuations, reflections, etc.

Université Paris-Saclay
Télécom Paris
19 Place Marguerite Perey, 91120 Palaiseau, France